ABSTRACT

GODWIN, JR., JOE ENOCH. Study of Parameters Influencing LNAPL Extraction Using Cofra System. (Under the direction of Dr. Mohammed Gabr.)

This research consisted of a large scale laboratory experimentation program to evaluate the performance of a prototype, vacuum extraction, PVW system and numerical modeling of the experimentation. A large-scale (1.52 m x 1.52 m x 1.37 m) fine sand specimen was prepared and instrumented with a prototype PVW system and piezometers in the laboratory to investigate the fluid extraction phenomenon for a single PVW subject to a transient water table. Two key properties of the PVW system were varied during the study: the active length and the placement depth of the PVW within the subsurface. A transient water table was the result of the PVW fluid extraction with a no flow boundary around the specimen, which would be typical of field conditions for a single PVW in the middle of a network of PVWs. Experimental testing was divided into two phases. The first phase investigated the active lengths and placement depths of two PVWs for water extraction. A light Nonaqueous Phase Liquid (LNAPL) was placed in the sand sample during the second phase of testing, and the PVW active length and placement depth was again investigated for the extraction of B100 biodiesel, used as a model LNAPL. Two scenarios were conducted in each phase of testing and were described as Setups 1 through 4. After each set of tests were completed for both setups in Phase II of the experimentation, the distribution of the residual LNAPL within the testing domain was analyzed for mass balance of the LNAPL within the system.

The fluid extraction rates and hydraulic gradients were determined in each scenario and ranged from $1.2x10^{-3}$ m/s to $4.8x10^{-3}$ m/s, with the higher fluid extraction rates and higher gradients occurring in the scenarios with the greater depth of placement that remained below the water table elevation for longer periods (Setups 2 and 3). The greater LNAPL extraction was observed by the scenario with the shallowest placement depth and the shortest active length (Setup 4). The distribution analysis of the LNAPL within the system after testing was completed for Setups 3 and 4 indicated the shorter active length and shallow placement depth utilized in Setup 4 resulted in less smearing of the LNAPL within the sand, hence less volume of residual LNAPL. Mass balance of the LNAPL in Phase II also suggests that Setup 3, with greater water and air flow rates through the system, provided improved conditions for biodegradation and dissolution of the B100 biodiesel.

Numerical modeling was performed to simulate the results obtained in the laboratory testing in order to evaluate system performance, to better understand the extraction process of LNAPL using a single PVW, and to develop a strategy for field implementation. Two modeling programs were used to evaluate PVW system performance: i) SEEP/w was used to model the groundwater flow and water table depths, and ii) Bioslurp was used to model the LNAPL extraction and residual distribution. SEEP/w accurately modeled the water table drop with the rate of drop varying from 0.127 m (0.4 ft) per hour to 0.365 m (1.2 ft) per hour. The LNAPL transport modeling provided valuable prediction of LNAPL distribution and was compared with laboratory residual distribution results. The Bioslurp model yielded a more uniform distribution of residual LNAPL with specific volume ranges

from 0.0184 m (0.72”) to 0.0349 m (1.37”), while the experimental results yielded specific volumes ranging from 0.0043 m (0.17”) to 0.0263 m (1.04”).

Study of Parameters Influencing LNAPL Extraction Using Cofra System

by
Joe Enoch Godwin, Jr.

A thesis submitted to the Graduate Faculty of
North Carolina State University
in partial fulfillment of the
requirements for the Degree of
Master of Science

Civil Engineering

Raleigh, North Carolina

2008

APPROVED BY:

_____	_____
Mohammed A. Gabr, PhD. Committee Chair	Robert C. Borden, PhD.
_____	
Roy H. Borden, PhD	

DEDICATION

I dedicate this work to my wife, my two daughters, and my son, for their support and understanding while I pursued my research and graduate work.

BIOGRAPHY

Joe Enoch Godwin, Jr. attended Meadow Elementary School, and he graduated from South Johnston High School in 1994. He subsequently enrolled in North Carolina State University, in Civil Engineering. Upon graduating in 1998 with a B.S. in Civil Engineering, Joe began working with Enoch Engineers in Benson, NC. While working at Enoch Engineers, he obtained professional licensure in North Carolina as an engineer and a surveyor in 2003 and 2005, respectively. He began his graduate studies at North Carolina State University in the fall of 2006.

ACKNOWLEDGEMENTS

First and foremost, I am most grateful and privileged to have had the support, guidance, and encouragement of my advisor, Dr. Mohammed A. Gabr. I would also like to express my sincere thanks to Dr. Roy H. Borden and Dr. Robert C. Borden for reviewing this thesis and providing helpful support and advice. I am fortunate to have worked for and studied under Dr. Gabr, Dr. Roy Borden, and Dr. Robert Borden, and I am grateful for the knowledge and experience that they have passed to me.

I am also thankful for the assistance and help of Nadia Sharmin, who provided valuable help with many of my research endeavors.

I also thank Michael Higgs, Charles Herring, Coleman Dargerhardt, Benjamin Cote, and Brent Robinson for their assistance with the project.

I would like to thank the Army Corps of Engineers for their support. The research presented herein was partially sponsored by the Army Corps of Engineers, and their support was greatly appreciated.

I would like to thank Dr. Keith Esch, with RTI International, for his in kind support, providing a portion of the B100 biodiesel for experimentation in this research.

TABLE OF CONTENTS

LIST OF TABLES

LIST OF FIGURES

1. INTRODUCTION

1.1 Overview

Groundwater is the largest source of readily available drinking water for most of the world (Schwartz and Zhang, 2003). Underground storage tanks (USTs), leaking pipelines, and other potential sources of release of gasoline and other petroleum-based products constitute a major source of contamination in the U.S. and the world. Borden and Kao (1992) estimated that greater than 10 percent of the existing 1.4 million USTs used for gasoline in 1984 have leaked, or greater than 140 000 UST-related spills have occurred, contaminating groundwater aquifers. EPA (2004) indicates that more than 439,000 aquifer contamination cases were reported. Therefore, contamination of this vital water resource is a major problem that will continue to occur for the foreseeable future and remediation of existing contaminated groundwater aquifers has been a serious concern for decades.

Remedying contaminated aquifers is very expensive and time consuming, even for the slightest contamination situations. The EPA (2004) cites that a major reason for the increased expense in groundwater remediation is that treatment technology is commonly not appropriately selected or optimally designed for the site-specific situation. Costs to remediate contaminated subsurface soils can range from $10,000 to more than $125,000, but to remediate contaminated groundwater, the costs can range from one to more than three orders of magnitude more, or $100,000 to more than $1 million (EPA, 2004).

Release of gasoline, jet fuel, kerosene, diesel, and other petroleum products constitute the largest percentage of LNAPL related groundwater contamination in the United States (Newell, et al., 1995). Once in the subsurface soil, petroleum based fuels behave as a nonaqueous phase liquids (NAPL), where they become trapped within the vadose zone and seep into groundwater aquifers. NAPL can be classified as either light (LNAPL) or dense (DNAPL), depending on the density, or specific gravity, of the particular liquid. Generally, the transport and fate of LNAPL and DNAPL are different; therefore, different approaches are often used to remediate LNAPL and DNAPL contaminated subsurface soil and aquifers. This research is focused on the remediation of LNAPL.

1.2 Problem Description

LNAPLs are typically found in unconfined aquifers due to the chemical and physical properties of the fluids and the transport mechanisms. LNAPL has a density less than that of water; therefore, accumulated volumes of LNAPL typically float on the surface of the water table and are encountered in the unsaturated zone above the water table, or vadose zone.

There are various methods used for the remediation of LNAPL in unconfined aquifers. These include, but are not limited to, conventional pump and treat, soil vapor extraction (SVE), bioventing, bioremediation, and dual phase extraction, implemented, for example, by an in-situ soil flushing approach termed well injection depth extraction (WIDE.) Each

method has advantages and disadvantages which vary depending on the site and situation. For example, past remediation efforts attempted to extract volatile LNAPL mostly in the vapor phase. Though positive results are obtained, this approach incurred higher costs for the treatment of the contaminated vapors to be discharged into the open atmosphere as mandated by state Environmental Protection Agencies (EPA). On the other hand, extracting LNAPL in the liquid phase does not require such treatment and on petroleum release sites the extracted fuel can potentially be used to run the compressor connected to the vacuum system. Furthermore, there are several difficulties encountered when attempting to remediate LNAPL contaminated sites, which include but are not limited to the following:

1) LNAPL can exist in any of 4 phases: free, aqueous, gaseous, or solid phases (Newell, et al., 1995). This property of LNAPL complicates remediation efforts which should be designed to address all phases.
2) Contaminated sites can vary in geology, soil types and heterogeneity, chemical contaminants and concentrations, and hydrogeologic conditions (EPA, 2004). These factors, and more, influence the remediation technology selection.
3) Seasonal fluctuations of the water table, with or without confining layers in the subsoil, affect the accumulated portion of the LNAPL by trapping it in the soil pores and causing smearing (Newell, et al., 1995).

1.3 Research Objectives

There has been much advancement in remediation technologies and contaminant characterization over the last decade, particularly with remediation technologies implementing the prefabricated vertical well (PVW), which has historically been limited to geotechnical applications. Gabr and Bowders (1995) and Gabr et al. (1995) introduced significant advancements to the existing application of the PVW for liquid and vapor extraction. More recent advancements have been made in developing the well injection depth extraction (WIDE) technology as an innovative remediation method.

In an effort to develop a better methodology for the WIDE technology implementation, this research specifically seeks to characterize a prototype PVW extraction system and to perform the following:

1) To measure the fluid extraction rates and hydraulic gradients at different PVW active lengths and placement depths.
2) To evaluate the hydraulic gradient over time with transient water table conditions.
3) To investigate the effects of PVW active length and placement depth on the distribution of a LNAPL within a homogeneous sand.
4) To investigate the most efficient depth of placement and active depth of a PVW that maximizes the efficiency and extraction volume of a LNAPL and of groundwater.
5) To measure or determine any mass lost within the system due to biodegradation or dissolution of the LNAPL.

Laboratory experimentation was designed to evaluate the performance characteristics of the prototype PVW by measuring the water and LNAPL extraction rates under vacuum while varying the depth of placement and the active length of the PVW with a transient water table. The large scale test preparation and implementation is herein described. Modeling is performed to simulate the results obtained in the laboratory testing and to understand the removal process of LNAPL using PVWs and develop a strategy for field implementation.

1.4 Thesis Organization

This thesis is organized as follows, with the pertinent tables, equations and figures included within the text of each chapter:

- ***Literature Review***

  The literature review includes a summary of information on the contaminant of concern, LNAPL, on biodiesel as a "laboratory test" fluid to substitute for diesel fuel, on the prefabricated vertical well, and on several remediation technologies.

- ***Laboratory Experimentation Program***

  The laboratory experimentation program is outlined, defining the test sand characteristics and physical properties, the test box preparation, the PVW and

piezometer configurations, and the four setups, or scenarios, which were implemented to investigate extraction characteristics of LNAPL using PVWs.

- ***Model Development***

Modeling of the laboratory experimentation was performed using finite element analysis. Analyses of the groundwater flow, solely, and of the groundwater and LNAPL transport was performed using SEEP/W and Bioslurp, respectively. The results of the modeling are presented.

- ***Results and Conclusions***

The test data from the laboratory experimentation program, the results from the modeling and analysis, and the literature review are combined and presented. The contributions of this research are compared to the original objectives.

- ***Future Research***

Suggestions for further research are provided.

- ***Appendix***

All ancillary test data and tables are included in the appendix.

2. LITERATURE REVIEW

The purpose of this literature review is to summarize applications of the prefabricated vertical wells in subsurface remediation, to present information pertaining to the contaminant of concern (LNAPL) in this research, to present information on the use biodiesel as a LNAPL for laboratory testing, to present pertinent research regarding the WIDE remediation technology and to summarize several current remediation technologies.

2.1 Background

Active and passive remediation technologies for LNAPLs can be classified into in-situ and ex-situ approaches. A defining characteristic of active remediation technologies is that active methods seek to mobilize the contaminant fluid, in the form of liquid or vapor, toward an extraction well. Also, a main objective of an active remediation system is to expeditiously reduce the amount of free products (LNAPL in the case of this research) within the subsurface to the greatest extent possible. This is desirable because LNAPL, also called free product or mobile LNAPL, acts as a continuous contamination source. Both active and passive methods are presented herein, including conventional pump and treat, soil vapor extraction and bioventing, and well injection depth extraction (WIDE). This research work has specific implications to the WIDE method which utilizes prefabricated vertical wells.

The prefabricated vertical well (PVW), also called the prefabricated vertical drain (PVD), is an innovative technology developed originally for geotechnical applications. The PVD has been used to expedite the consolidation of fine grained soils since as early as the late 1930's; however, over approximately the past two decades, PVW systems have seen advancements in subsurface contaminant remediation applications which are presented in literature by Bowders and Gabr (1995), Gabr et al. (1995, 1996, 1997, 1999), Warren and Gabr (2005), Quaranta et al. (1997), and Quaranta and Gabr (2000).

2.2 Nonaqueous Phase Liquids

Nonaqueous phase liquids (NAPL) are hydrocarbon liquids that are considered immiscible with water in their pure state due to the differences in the physical and chemical properties between the NAPL and air or water; however, often the NAPLs or different additives to the NAPLs are soluble with water to various degrees (Newell, et al., 1995). NAPL can be generally categorized as being either light (LNAPL) or dense (DNAPL) based on their densities, or more specifically, their specific gravities, which is the ratio of the mass of a given volume of fluid at a specified temperature to the mass of the same volume of water at the same temperature. This research focuses on the extraction of LNAPL, alternatively termed by Charbeneau (2006) as organic immiscible liquid (OIL), using a prefabricated vertical well (PVW).

2.2.1 Light Nonaqueous Phase Liquids

There are difficulties with remediating sites contaminated with LNAPL. Firstly, LNAPL may exist in or partition to any of the four following phases: (1) the free or liquid phase, (2) the aqueous or dissolved phase, (3) the gaseous or vapor phase, and (4) the solid phase where the NAPL adsorbs to the soil. The LNAPL contaminants may exist in the free, aqueous, and solid phases in the saturated zone, and may exist in the free, aqueous, solid, and vapor phases in the unsaturated zone.

The term free product is colloquially used to describe the mobile liquid portions of LNAPL. Typical LNAPLs include Ethyl Benzene, Benzene, Styrene, Toluene, and petroleum based fuels, which are the most predominant on contaminated sites (Newell, et al., 1995). Table 1 presents several of the most common LNAPL contaminants found on superfund sites with their respective densities and dynamic viscosities.

Table 1. Density and Viscosity of Select Common LNAPL Chemicals (Newell, et al., 1995)

Chemical	Density (g/cm3)	Dynamic Viscosity (cp)
Methyl Ethyl Ketone	0.805	0.40
4-Methyl-2-Pentanone	0.8017	0.5848
Tetrahydrofuran	0.8892	0.55
Benzene	0.8765	0.6468
Ethyl Benzene	0.867	0.678
Styrene	0.9060	0.751
Toluene	0.8669	0.58
m-Xylene	0.8642	0.608
o-Xylene	0.880	0.802
p-Xylene	0.8610	0.635
Automotive gasoline (@ 15.6° C)	0.72 - 0.76	0.36 - 0.49
#2 fuel oil (@ 21° C)	0.87 - 0.95	1.15 - 1.97
#6 fuel oil (@ 38° C)	0.87 - 0.96	14.5 - 493.5
Jet Fuel (JP-4) (@ 21° C)	~0.75	~0.83
water (@ 20° C)	0.998	1.00

2.2.2 LNAPL Transport and Hysteretical Effects on LNAPL Remediation

The field scale transport and migration processes of LNAPL are complicated. Charbeneau (2000), Hunt et al. (1998a) and Newell et al. (1995) provide detailed insight regarding LNAPL transport phenomena. The LNAPL transport process is complex, because mobile LNAPL is affected by factors such as capillary forces in the subsurface soil, the degree of saturation, the relative permeability, the density, and the viscosity of the LNAPL.

To summarize the transport process, LNAPL contamination typically occurs due to a point source release, or multiple point source releases over an area. The LNAPL migrates downward through the vadose zone, due to gravity, with portions of the LNAPL retained in the soil pores as residual LNAPL due to capillary forces. If a significant volume was released, the mobile portion continues downward and reaches the water table, where the LNAPL ponds (Charbeneau, 2006). Heterogeneous soil with intermittent fine and coarse lenses further distribute the LNAPL. Additional migration of the LNAPL can occur laterally, but only occurs in the liquid, dissolved, and vapor phases, not in the solid phase.

Charbeneau (2006) also states that flow between the different fluids practically occurs independent of each other. One can observe the effects of several of the aforementioned parameters by applying Darcy's Law to the flow of the separate phases of LNAPL and other fluids through the soil pores as expressed in Equation 1.

Equation 1

$$v = -\frac{k \cdot \rho \cdot g}{\mu}\left(\frac{\delta h}{\delta L}\right)$$

Where:
δh = change in hydraulic head
δL = length of flow path
$\delta h/\delta L$ = hydraulic gradient of LNAPL
k = intrinsic permeability
g = force of gravity
ρ = density of LNAPL
μ = dynamic viscosity of LNAPL
v = velocity of LNAPL flow

As the density of the fluid increases, the viscosity decreases, or the intrinsic permeability increases, the flow velocity will increase. However, the permeability, viscosity, and density defined above are that of the particular fluid or phase.

A fluctuating water table has a negative effect on remediation efforts due to hysteretical trapping, or smearing, of the LNAPL in the contaminated zone. However, water table fluctuations in an unconfined aquifer are generally inevitable, and occur as a result of variations in natural and induced, recharge and discharge of groundwater within the aquifer system. Water table oscillations entrap LNAPL and air in the soil pores, creating occluded residual globules or ganglia, partly due to the hysteretical behavior of the soil characteristics (Hunt et al, 1988a). As a result of a transient water table, soil-water characteristics, more specifically volumetric water content (θ), hydraulic conductivity (k), and capillary pressure (p_c) or capillary head (ψ), vary as the subsurface is drained or wetted (Topp and Miller, 1966). The fluid saturation, as a percentage, is also used in lieu of volumetric water content. Soil undergoing wetting and drying cycles does not always exhibit the same soil-water characteristic curve during both processes. Hysteresis is observed, particularly with the $p_c(\theta)$ and $p_c(k)$ relationships, as presented in experimental results by Topp and Miller (1966), which demonstrate the influence of capillary forces on the behavior of water movement in a porous medium. Typical soil-water characteristic curves demonstrating hysteresis of the saturation versus capillary pressure relationship for wetting and drying of monotonically dispersed glass beads is shown in Figure 1. The

significance of hysteresis to liquid flow in soil has long been recognized, and the theory is beyond the scope of this literature review. Literature by Topp and Miller (1966) and Mualem (1986) is suggested for a more thorough review of the theoretical aspects of hysteresis.

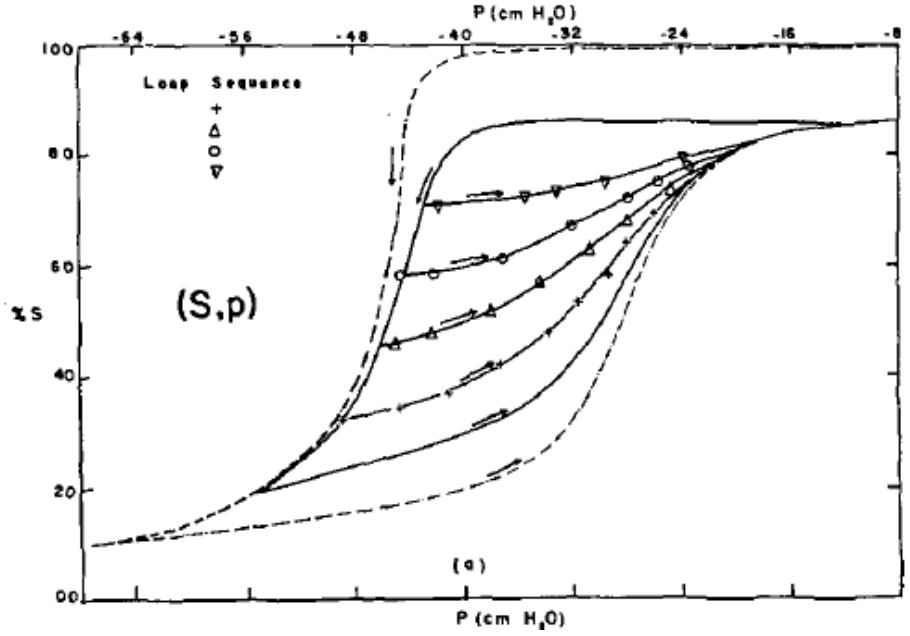

(a)

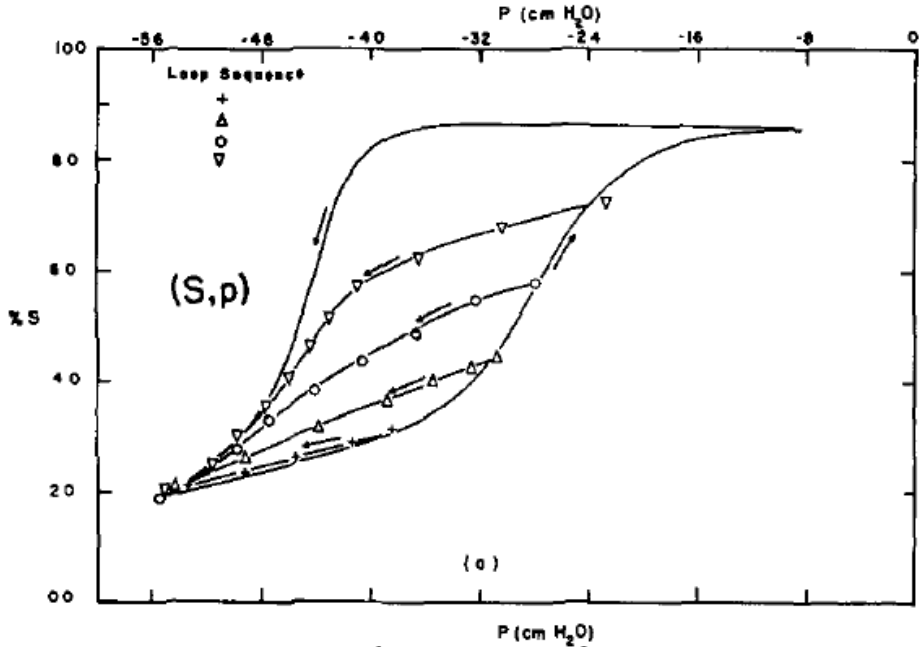

(b)

Figure 1. Soil-Water Characteristic Loops for Percent Saturation versus Capillary Pressure (a) Re-wetting and (b) Re-drying (Topp and Miller, 1966)

2.2.3 Laboratory LNAPL Remediation Case Studies

Cognizant of the transport, migration, and smearing of LNAPL, remediation efforts must address all of the contaminant phases to be effective. Most importantly, remediation efforts should primarily seek to remove the mobile free product and the residual LNAPL, which can serve as a continuing source of contamination. Past research has primarily focused on the removal of mobile LNAPL liquids and vapors, often accounting for remaining residual LNAPL as immobile while utilizing active remediation technologies. The following case studies were reviewed pertaining to research aimed at active remediation of residual LNAPL:

1) Hunt et al. (1988a) predicted that dissolution of trapped LNAPL by flushing volumes of water is limited by mass transfer as calculated from dissolution rates, and proposed the use of steam and hot liquid water to displace residual LNAPL contamination. Hunt et al (1988b) conducted laboratory-scale experiments using instrumented horizontal sand columns to analyze the displacement of residual NAPL using steam for three different NAPL chemicals. Ottawa sand with particle sizes ranging from 160 to 200 μm and a porosity of 0.385 was used as the test soil. Trichloroethylene (TCE), a 50/50 mixture by volume of Benzene and Toluene, and commercial gasoline were used as test NAPL fluids. Though TCE is a DNAPL, the binary mixture and commercial gasoline were LNAPL contaminants. Each test consisted of injecting 18 mL of each respective NAPL midstream and approximately 1/3 the length of the water saturated sand column, downstream of

the inlet. Initial LNAPL saturations averaged 2.5%. Water was initially flushed at flow rates as high as 15 m/d in attempts to remove the NAPL, until recovered effluent showed insignificant concentrations of the NAPL contaminants upon which the flow rates were decreased. In each case residual contaminant volumes remained and steam was injected as a single pulse in the samples to mobilize the residual NAPL. Then additional hot water was flushed through the samples. During steam injection, the sand columns were insulated and heated to maintain heat flow. For the TCE tests, flushing of 12.5 pore volumes of water recovered approximately 43% (7.7 mL) of the DNAPL through dissolution in the effluent, leaving a residual amount of 10.3 mL. An additional 9.3 mL was recovered by flooding the column with steam, for a total recovery of 17 mL or 94%. For the binary mixture tests, 11.2 pore volumes of water were flushed through the sample to recover 9 mL of the LNAPL mixture. The mass balance of the total LNAPL mixture indicates a loss of benzene possibly due to volatilization of the recovered effluent. However, 98% of the less volatile toluene was recovered through both the water and steam flushing processes. The water flushing process removed approximately two thirds of the total toluene during the initial flushing process. For the commercial gasoline tests, low hydrocarbon concentrations were observed and no separate phase gasoline was displaced during the first 5.6 pore volumes of flushed water. However, just ahead of the steam front at approximately 5.6 pore volumes, 13.3 mL of separate phase gasoline was recovered. Differing from the tests with the other NAPLs, 0.1 mL of separate phase gasoline was obtained from

the recovered condensed steam. Also, the recovered liquids exhibited the presence of emulsified hydrocarbons as evidenced by their cloudy appearance.

2) Borden and Kao (1992) demonstrated that pumping large volumes of water appreciably reduced the BTEX residual concentrations in the test soil due to mass transfer of the residual LNAPL globules. Laboratory-scale leaching column tests were performed on sand to evaluate the soil flushing technology on the removal of residual BTEX. Results indicated that between 70 and 84% of the residual BTEX chemicals were recovered in the effluent during the flushing process. Based on analysis of samples obtained from the column material after testing, approximately 9 to 10% of the original residual chemicals remained. Though significant results were obtained, some residual BTEX chemicals remained in the aquifer material. Borden and Kao (1992) concluded the volume of water passed through the aquifer material, 880 pore volumes, may not be feasible to reproduce in a field scale PT system, due to the slow transfer rate of the aromatic hydrocarbon from the free to the aqueous phase, which concurs with theoretical postulations by Hunt et al. (1989a) and experimental results by Hunt et al. (1989b).

3) Fortin et al. (1997) conducted enhanced soil flushing experiments using low concentration surfactant solutions. The column experiments were performed on water saturated sieved coarse sand using ethoxylated alcohol surfactant to remove trapped the LNAPL and DNAPL, o-xylene and o-dichlorobenzene, respectively. To distribute the NAPL in the sand, excess water was drained from the column and NAPL was flushed through the bottom until it reached the top. To obtain residual

saturation of the NAPL, all excess chemicals were flushed through the columns using two to four pore volumes of water. Residual saturation of the LNAPL ranged from 10.6 to 15.7%. The surfactant was flushed in both downward and upward directions, simulating transient conditions. LNAPL recovery percentages ranged from 13 to 98.7%, with the number of pore volumes flushed through the samples, using the surfactant, ranged from 1.9 to 33.6. As expected, the greater number of pore volumes produced the greatest percentage of LNAPL extraction.

2.2.4 Biodiesel

This research focuses on characterizing the extraction of LNAPL while varying the active depth and PVW placement in homogeneous sand. Based on the desired objectives of the planned research and due to the toxic nature of most typical LNAPLs, the experimentation portion of this research utilized B100, or 100% biodiesel fuel, as a substitute for petroleum-based diesel fuel. The benefits of using biodiesel to model LNAPL transport and extraction is that biodiesel has similar physical properties to petroleum based diesel fuel, it poses much less of a hazard in a laboratory environment, and it is easily degraded in the proper environment for disposal purposes (Leung, et al., 2006, and Zhang, et al., 1998). Biodiesel produced according to industry standards has a density and viscosity similar to that of petroleum diesel fuel. Table 2 compares the viscosity and specific gravity ranges of four types of biodiesel to the viscosity and specific gravity of standard Phillips 2-D diesel fuel (Zhang, et al., 1998).

Table 2. Property Comparison of B100 Biodiesel and D-2 Diesel Fuel (Zhang, et al., 1998)

Property description	Property Value		
	Biodiesel*	Diesel (Phillips 2-D)	Water
Specific gravity	0.88 - 0.89	0.8466	0.998
Kinematic Viscosity (cSt @ 40°C)	3.89 - 6.17	2.7	0.658
Flash point (°C)	124 - 274	74	NA

* Values for rapeseed and soyate methyl and ethyl esters.

However, due to the chemistry of biodiesel, it is less volatile than diesel and as such will not behave as a true multiphase contaminant. To put the volatility of biodiesel, gasoline and diesel into perspective, biodiesel is less volatile than diesel, and diesel is less volatile than gasoline (Leung, et al., 2006, and Schwartz and Zhang, 2003).

Pure bio-fuel products degrade more easily because they are produced from raw materials that are fully biodegradable, like vegetables. Zhang, Peterson, Reece, Haws, and Moller (1998) suggest that one of the reasons biodiesel degrades much more rapidly than petroleum diesel is that the enzymes needed to assist microorganisms in the biodegradation naturally exist in the fatty acids used as a raw material for biodiesel production.

Leung, Koo, and Guo (2006) evaluated the biodegradation of biodiesel under different storage conditions as follows: 1) in a sealed environment, 2) in contact with air, 3) sealed with water present, 4) in contact with air and water. These experiments were conducted

over a period of 52 weeks and at temperatures of 0°, 20°, and 40° C. The biodegradation of the samples were measured by performing purity tests and acid value tests. The testing concluded that air and high temperature (40° C), or air, water and high temperature exposure, combined, caused higher biodegradation rates than the other storage conditions. These conditions resulted in biodegradation to a purity of approximately 60% after 52 weeks, from an initial purity of approximately 99.7%. Also, biodiesel with higher water content condition did not degrade as significantly as with the combination of air and high temperature, though air and high temperature as separate conditions did not biodegrade the biodiesel as much as the conditions combined. Figure 2 illustrates the effects of the different temperatures on the four storage conditions. The exposure to air and high temperature and air, water and high temperature, as shown in (ii) and (iv) of Figure 2 respectively, indicates significant biodegradation beginning at approximately 10 to 12 weeks. However, total biodegradation over 52 weeks for all of the conditions at temperatures of 20° C and 0° C resulted in a loss of purity from 99.7% to no less than approximately 92%.

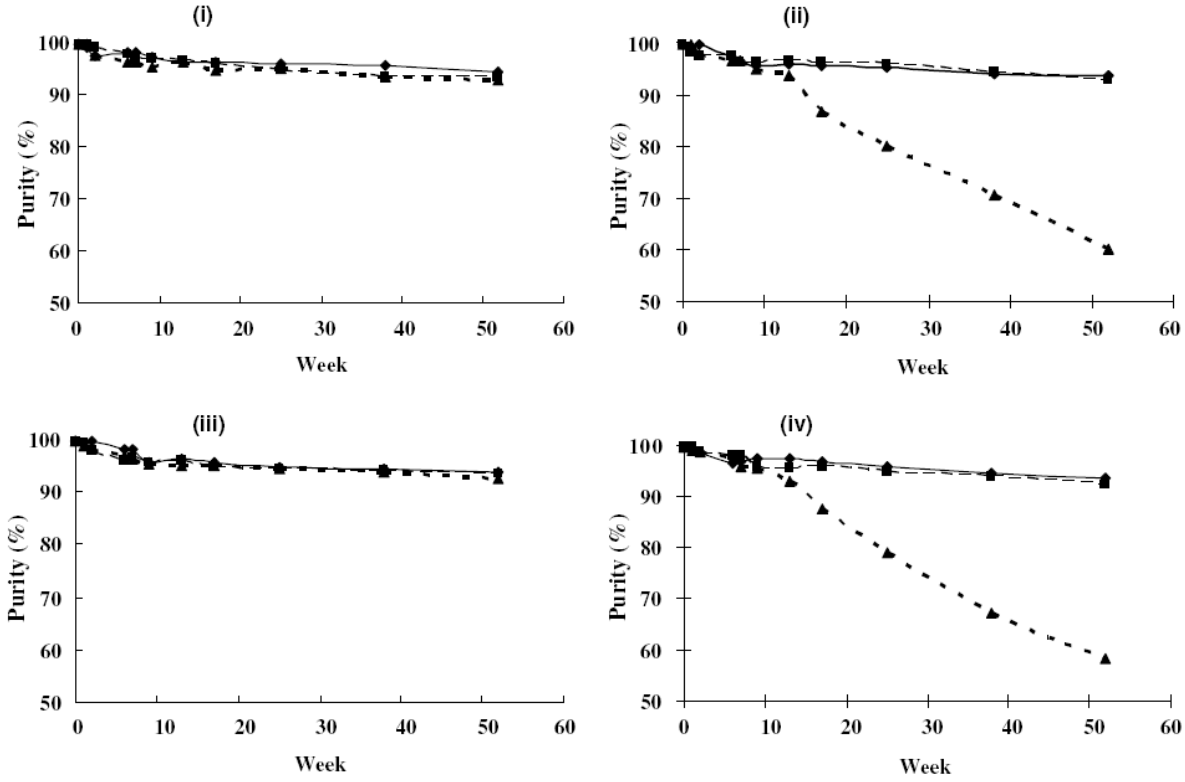

Figure 2. Purities of Biodiesel at Different Temperatures (i) Sealed, (ii) With Air Exposure, (iii) Sealed with Water Presence, (iv) With Air Exposure and Water Presence; (♦) 0° C; (■) 20° C; (▲) 40° C (Leung, et al., 2006)

Coulibaly and Borden (2003) studied the effects of edible oils injection on the permeability of sands and clayey sands. The focus of their research is in development of enhanced anaerobic bioremediation to treat groundwater contamination. Soybean oil is used as a NAPL and as an oil-in-water emulsion to inject into laboratory prepared sand columns. The sand samples are saturated with deaired tap water, then injected with the NAPL or oil-in-water emulsion, and then flushed with multiple pore volumes of deaired water. The residual oil saturation was then determined. A volatile solids (VS) analysis was used to

determine the final moisture content and final oil residual saturation or oil content of the sand. The process determined the moisture content by mass loss after drying at 105° C for 24 hours, and determined the VS content by mass loss after ignition at 550° C for 1 hour.

Coulibaly and Borden (2003) indicate the injection of the neat soybean oil as a NAPL presented difficulties for the specimens with clay. For the sand specimens, residual saturation of the NAPL was the highest for the well graded sands and lower for the uniform graded sands (i.e. Ottawa 20-30), and ranged from 54% to 22%. They conclude after testing with the NAPL that the final permeability was observed to decrease to approximately half of the initial permeability, after flushing approximately 20 pore volumes of water through the sand to displace the oil. However, problems were encountered using the NAPL due to a significant difference in the viscosities of the NAPL and water. Coulibaly and Borden (2003) also state the NAPL had a viscosity of approximately 60 to 70 times that of the water at typical groundwater temperatures. An approximate 2 orders of magnitude increase in the hydraulic conductivity was observed during the NAPL injection, and it was difficult for the NAPL to migrate any significant distance through the soil specimen from its point of injection.

2.3 The Prefabricated Vertical Well (PVW)

The prefabricated vertical drain (PVD), also called the prefabricated vertical well (PVW) when used in environmental remediation applications, has been used in geotechnical

engineering applications since the late 1930's. Kjellman (1948) first patented the cardboard vertical "wick" drain and a method to install the drain in 1939 as an alternative to the vertical sand drain. Both the wick and sand drains were used to expedite the consolidation of fine grained soils by decreasing the drainage path for the removal of the pore fluids. The theory, design, and implementation of PVD systems for soil consolidation purposes is presented in literature by, among others, Kjellman (1948), Hansbo (1979), and Barron (1948).

A method used to install PVWs, patented by Nilex Corporation (Denver, Colorado), uses a hollow steel mandrel mounted to an excavator's arm. The mandrel is 120 mm wide by 30 mm deep and exceeds 30 m in length. The mandrel uses hydraulic forces to install the PVW to the specified depth. If compressed or dense soils are encountered, a dynamic installation method utilizing a vibratory hammer is used to drive the mandrel and install the PVW. A self-locking steel anchor plate is attached to the bottom of the PVW to anchor the PVW as the mandrel is withdrawn. Once the mandrel is retrieved, the PVW is cut and the equipment proceeds to the next well location. Kjellman (1948) reports a maximum installation rate of approximately 0.3 m/s was measured, using the installation equipment designed, patented, and constructed by Kjellman. Quaranta et al. (2000) indicate an installation rate of between 1 to 3 m/s in a clay, using the aforementioned Nilex equipment and process, once setup is complete at the intended installation location. Figure 3 presents two photographs of typical PVW installation equipment.

Figure 3. (a) Installation of PVWs Using Mandrels Mounted to Two Large Cranes and Excavators (Courtesy Cofra). (b) Installation of PVW Using Mandrel Mounted Excavators (Courtesy Nilex)

A typical PVW consists of a band shaped geocomposite system, comprised of a flexible inner core and a non-woven polypropylene geotextile outer jacket. Prefabricated vertical wells used in this research have a rectangular cross section with an approximate width and thickness of 100 mm and 4 mm, respectively. The inner core is typically made of extruded polypropylene with formed flow channels on both sides along its length. The outer jacket is tightly wrapped around the inner core, with a sewn seam, and serves as a filter. The purpose of this filter is threefold: (1) to maintain the cross-sectional profile to allow fluid

to flow through the channels in the inner core, (2) to allow water to pass through the filter, and (3) to prevent fines from passing through the filter which may clog the flow channels and prevent the system from functioning. Both the inner core and the outer filter jacket are designed to withstand biological and chemical degradation. A typical 100 mm by 4 mm PVD, with an impermeable sleeve, is illustrated in Figure 4. The prototype Mebradrain™ PVW outfitted with sheathing as proposed by Cofra is illustrated in Figure 5. The Mebradrain™ sheathing allows for depth specific extraction and injection features like the impermeable sleeve; however, the adaptor delivers fluids to an HDPE tube, reducing the length of PVW at each well location. Also, the HDPE tubing is easily connected to the extraction/injection system manifold with quick connect tees at the surface, expediting the system installation process.

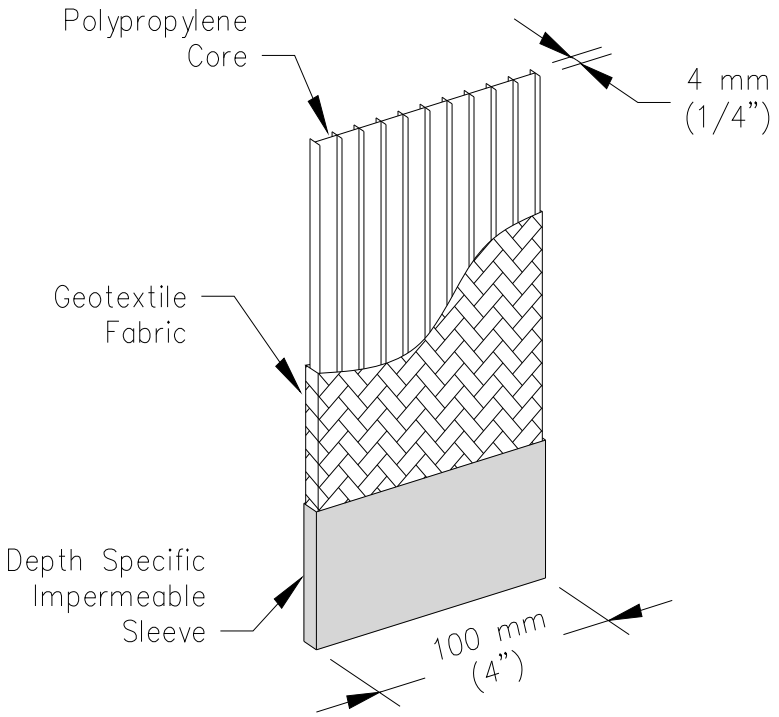

Figure 4. Typical Prefabricated Vertical Well Components (Inverted)

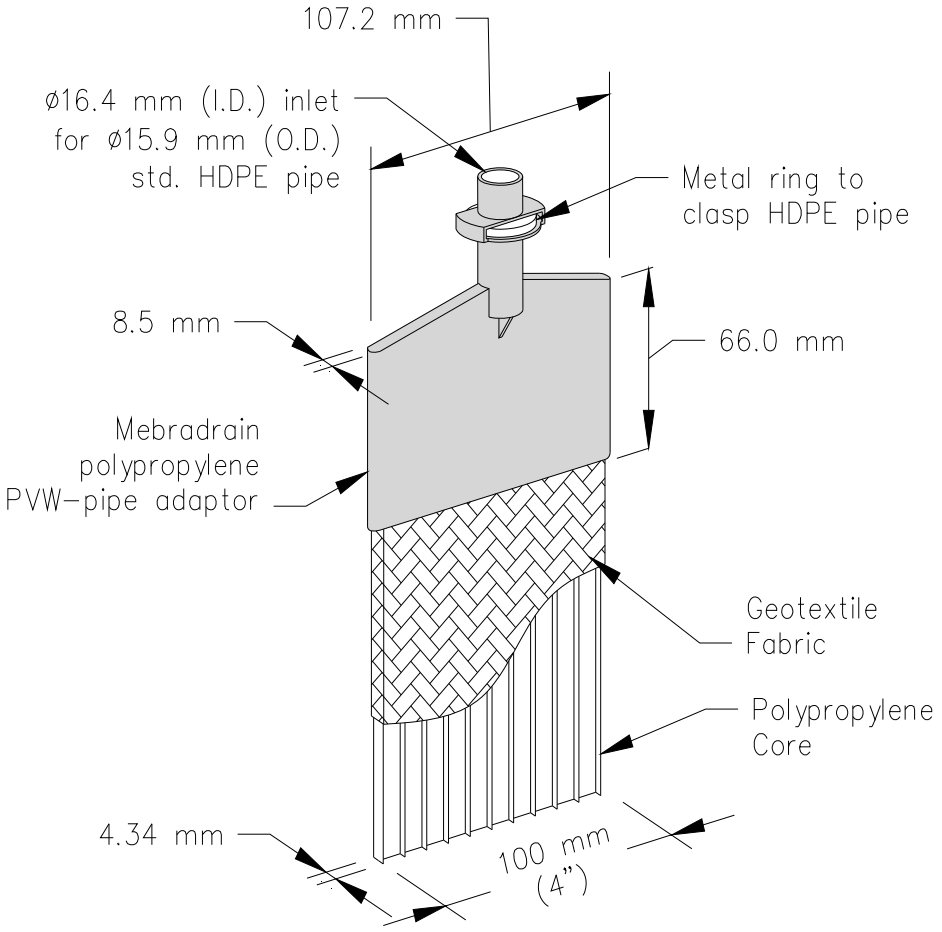

Figure 5. PVW with Mebradrain PVW to HDPE Pipe Adaptor as Developed by Cofra

The equivalent well diameter concept was developed since the PVW has a rectangular cross section and because design and analysis of the band-shaped wells is based on radial consolidation theory. Kjellman (1948) and Hansbo (1979) indicate the cross sectional area of the drain was not as critical as the contact of the surface of the drain with the soil,

specifically the circumference of the drain. Therefore, it is more appropriate in theory and for design to use the equivalent well diameter, $d_{e,}$ as shown in Equation 2:

Equation 2

$$d_e = \frac{2(b+t)}{\pi}$$

Where;
d_e = Equivalent well diameter
b = PVD width
t = PVD thickness

Therefore, for a typical PVD with thickness of 100 mm and width of 4 mm as shown in Figure 4, the equivalent well diameter is 66 mm. Also, Hansbo (1979) and Gabr, et al. (1997) suggest the equivalent diameter be reduced if the effects of smear, due to mandrel installation, are to be accounted. The effects of smear reduce the permeability of the soil surrounding the well, especially in varved clays.

Closely spaced PVWs are used to expedite pore fluid removal by shortening the path the fluids must travel. In current practice, a surface surcharge is placed on the soil, which creates positive pore pressures, or a vacuum is applied to the PVW, which creates a negative pressure zone around the PVW, to induce a hydraulic gradient. Also, these methods to increase the head potential can be used separately or in conjunction. However, geotechnical applications attempting to consolidate compressible soils utilizing PVDs more typically use a surcharge to remove pore fluids. For environmental applications where fluids are flushed through the soil pores, applying a surcharge is usually undesirable.

This is because the additional stress applied to the soil decreases the pore spaces in the soil by rearranging the soil fabric, which decreases the permeability and increases the duration of the remediation process (Bowders and Gabr, 1995).

As presented in Quaranta, et al. (2000), a significant distinction between a PVW and a PVD is in the application, being environmental or geotechnical in nature with the possibility of injection through a PVW. The active depth of a PVW, or the screened depth as in the application of conventional wells, is controlled by using an impermeable sleeve as shown in Figure 4. When used in conjunction with a surcharge for geotechnical applications, the active depth of the PVD is the full depth of placement. The impermeable sleeve is unique to the PVW and provides control to select the appropriate injection and extraction depth for contaminant removal.

2.4 Well Injection Depth Extraction (WIDE)

2.4.1 WIDE Overview

Well injection depth extraction (WIDE) is a dual phase, vacuum enhanced, pump and treat technology that is utilized for contaminant liquid and vapor recovery. WIDE efficiently combines several of the features of pump and treat, in-situ soil flushing, and soil vapor extraction (SVE) methods. This enhanced remediation technology is considered more effective than pump and treat because of its relatively close spacing of wells and the redundancy inherit in the system due to the installation of many wells. WIDE essentially

withdraws accumulated free product, soil vapors, and groundwater in the same process stream by applying a vacuum to a PVW or a system of PVWs.

The system components typically include multiple PVWs connected to manifolds for injection and extraction, a fluid and vapor extraction system, a fluid injection system, and treatment equipment. The extraction/injection PVWs typically have active depths across the contaminated portion of the aquifer and portions of the vadose zone. Upon installation of the system of PVWs and piping, negative pressures are applied to the system using a vacuum pump. A cone of depression is created around the extraction wells by the negative vacuum pressures and a mound of fluid is created around the injection wells, creating a hydraulic gradient toward the extraction wells. Figure 6 illustrates the surface features of a typical WIDE system installation.

Figure 6. Photograph of Surface of Typical WIDE System Implementation on Contaminated Site

A significant difference between vacuum enhanced extraction using WIDE and traditional pump and treat is that during traditional pumping methods, the hydraulic gradient is created by gravity only. With vacuum enhanced recovery methods, the hydraulic gradient is greater due to forces of gravity and the additional head created by negative vacuum pressures at the well.

Field and laboratory scale studies by Gabr et al. (1999), Quaranta et al. (2000), Quaranta et al. (2005), and Warren and Gabr (2005) have demonstrated the effectiveness of WIDE technology in fine grained soils and have demonstrated WIDE as a versatile and effective remediation technology for LNAPL and DNAPL. Some benefits of the WIDE remediation technology that can be concluded from past research include the following:

1) Injection and extraction flow rates can be balanced in a controlled system so that consolidation does not occur (Bowders and Gabr, 1995).
2) The Mebradrain™ prototype PVW system is a unique feature to the PVW which provides additional control in the active length and depth of placement. Furthermore, no drilling is required for PVW installation.
3) The wide coverage and the close spacing of the extraction and injection PVWs ensure accurate contaminant detection and coverage, and expedite the soil flushing process which reduces remediation durations (Warren, 2002).
4) The system of PVWs can be installed rapidly and inexpensively in a tightly arranged pattern (Quaranta et al., 2000).
5) The negative pressures created by the vacuum in the subsoil overcome the capillary attraction of the soil particles to the groundwater and LNAPL in the subsoil, within the zone of influence.
6) WIDE promotes interphase mass transfer, meaning LNAPL and contaminated groundwater and vapor are removed in the same process stream, which benefits remediation efforts due to increased mobilization and mass extraction (Gabr et al., 2007).

7) WIDE can be conducted under multiple modes of operation as warranted by the site specific needs. These modes of operation include vapor extraction only (as an enhanced soil vapor extraction system), soil vapor and fluid extraction only, and concurrent extraction and injection (as a vacuum enhanced soil flushing system) (Warren, 2002).

2.4.2 WIDE Field and Laboratory Studies

Gabr, et al. (1999) demonstrated the application of PVWs as enhanced vacuum extraction wells during a pilot scale test to remediate soils contaminated with benzene, toluene, ethyl benzene, and Xylene (BTEX). The subsurface soil was classified as CL with a permeability of $3x10^{-9}$m/s. A row of 5 PVWs were installed linearly approximately 0.9 m apart, and the row was placed between two on-site monitoring wells, which were used to monitor the drawdown in the water table and to observe the extent of the vacuum. An impermeable sleeve, approximately 1.5 m in length, was installed on each PVW, from the PVW attachment to the manifold pipe at the surface down to the water table. The active depth of the PVWs is extended approximately an additional 3.0m below the water table, for a total depth of approximately 4.5 m.

The pilot scale test conducted by Gabr, et al. (1999) yielded positive results while operating at intervals during a 2 day period. BTEX concentrations in the monitoring wells increased during the test, which indicated contaminant mobilization toward the PVWs. An

interesting observation was that the extraction flow rate decreased from 23 mL/s initially to 16.7 mL/s, possibly due to partial clogging of the PVW's geotextile filter.

2.5 Alternative Remediation Methods

Many of the following remediation methods are used in conjunction with other methods, integrated sequentially or simultaneously. Also for each technology, vacuum enhanced PVW systems can be used in lieu of conventional wells to enhance the remediation efficiency.

2.5.1 Conventional Pump and Treat

Conventional pump and treat (PT) systems are one of the predominant technologies used for soil and groundwater remediation and containment (Cohen et al., 1997). For this method, contaminated groundwater is pumped using extraction wells, then treated, either on or off site, and discharged or injected in the subsurface soils. There are different design requirements and system configurations of this method used to remediate or prevent the migration of contaminated groundwater. A typical PT system is illustrated in Figure 7 (EPA 1997)

Borden and Kao (1992) indicate that conventional PT systems are effective at removal of the contaminated groundwater, but are ineffective at complete remediation of the contamination. Warren and Gabr (2005), Borden and Kao (1992), and (Cohen et al., 1997)

describe the tailing and rebounding effects observed over long periods of pumping, referring to the progressive decrease in contaminant concentrations upon commencing the pumping program which eventually level off asymptotically and the prompt increase in contaminant levels after pumping is ceased.

Warren and Gabr (2005) and Cohen et al. (1997) also indicate that PT systems are effective at, and often utilized for, containment of the groundwater contamination where complete remediation is not possible. A common pump and treat strategy utilizes advantageously placed wells to implement hydraulic control over an area to contain the groundwater contamination and to maintain the water table to reduce smearing effects. Cohen et al. (1997) suggest that many of the failures of PT systems can be attributed to an insufficient number of injection and extraction wells, inadequate pumping rates, poor system adaptation to the physical and chemical properties of the contaminant, and poor system implementation and optimization.

Because of these issues, conventional pump and treat systems are not a suitable complete remediation technology on many contaminated sites primarily due to the heterogeneous nature of the subsurface soils, the nature of the transport and fate of many NAPLs, and because this method can be very expensive if performed over long periods of time for containment, for instance in the case of most superfund sites (Cohen et al., 1997).

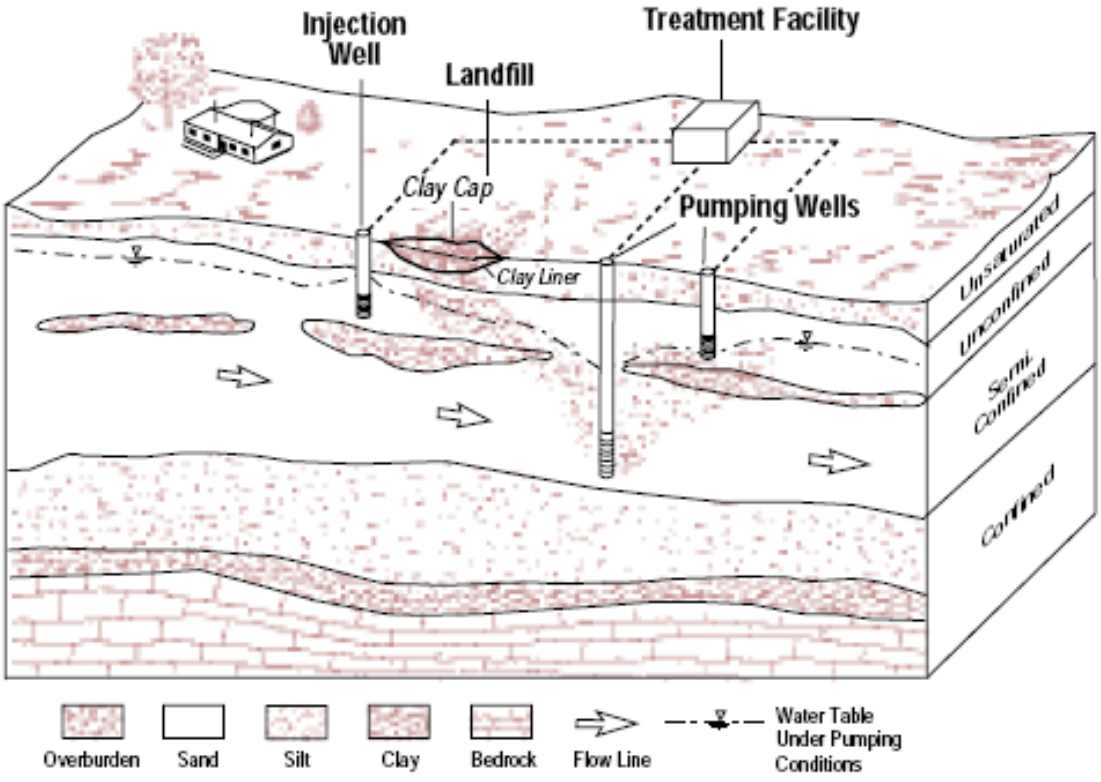

Figure 7. Typical Pump and Treat System (EPA, 1997)

2.5.2 In-Situ Soil Flushing

In-situ soil flushing, considered a variation to the pump and treat technology, is an innovative process that utilizes extraction and injection wells on a site to remove contaminants from subsurface soils and other aquifer materials. This technology can use water as the flushing solution, though surfactants are typically used to assist in contaminant removal (U. S. EPA, 2006). The treatment process can be designed to meet the conditions of the site and the type of contaminant by strategically placing the wells and selecting the appropriate flushing solution. However, this technology, using conventional

wells, is not well suited for sites with subsurface soils that contain a high fine fraction, have low permeabilities, extremely heterogeneous soils, or sites with mixed contaminants (U. S. EPA, 2006).

2.5.3 Bioremediation

According to Norris, et al. (1994), bioremediation is often incorporated, either sequentially or simultaneously, with other remediation methods. For bioremediation to be feasible, the contaminant must be biodegradable, or capable of being converted to a less toxic material or fluid with the aid of nutrients and microorganisms. Bioremediation can be performed ex-situ or in-situ, below the water table, above the water table in the vadose zone, or on excavated soil. Examples of bioremediation technologies include but are not limited to bioventing, air sparging, and natural bioremediation (Norris, et al., 1994). Bioremediation systems typically involve extraction and injection wells to provide oxygen and nutrients to the contaminated zone. A critical factor when implementing a bioremediation system is the hydraulic conductivity of the soil in the contaminated zone. Norris, et al. (1994) suggest a conductivity of 10^{-4} cm/s or greater for bioremediation systems to be effective.

2.5.4 Soil Vapor Extraction (SVE) and Bioventing

Soil vapor extraction (SVE) and Bioventing are similar processes where air is drawn through the soil pores toward vapor extraction wells using a vacuum pumps and blowers attached to conventional wells. Generally, SVE involves flushing air through the vadose

zone to volatilize the LNAPL or volatile organic compounds (VOC's) (EPA, 2004). This process is only suitable if the contaminants in the subsurface soil can volatilized at temperatures within the soil, unless heat is applied to the system (Bowders, et al., 2005).

The key difference between SVE and bioventing is that SVE seeks to remove the contaminants through volatilization, and bioventing promotes biodegradation of the contaminants while minimizing volatilization (EPA, 2004). As the mass removal and volitization rates decline and smaller residual amounts of contaminants remain while implementing SVE, bioventing can be implemented to encourage bioremediation. With bioventing, air is slowly flushed through the vadose zone to provide nutrients and to introduce oxygen to aid in aerobic biodegradation of the residual constituents (Norris, et al., 1994). Figure 8 illustrates a typical bioventing system.

However, because SVE relies on the volatile nature of the contaminant and bioventing relies on biodegradation of the contaminant, these methods are not recommended to be used as the sole methods for removing significant volumes of LNAPL, especially when time is a factor in deciding appropriate remediation methods (EPA, 2004, and Bowders, et al., 2005).

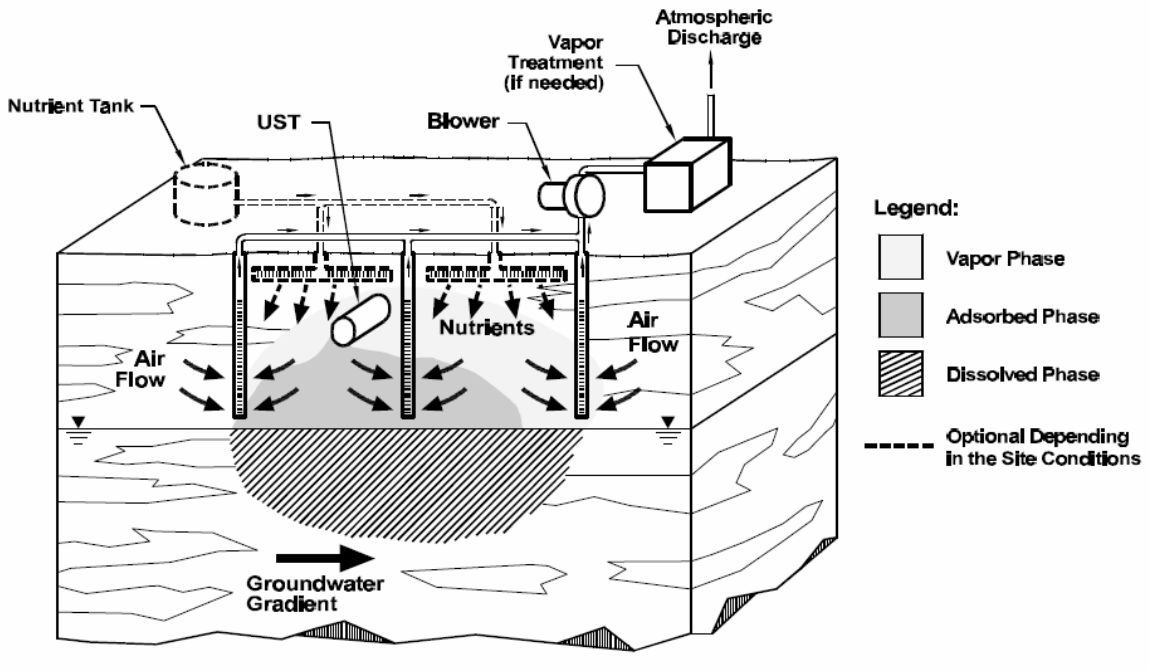

Figure 8. Typical Bioventing System Utilizing Vapor Extraction (EPA, 2004)

3. LABORATORY EXPERIMENTATION PROGRAM

3.1 Introduction

The laboratory experimentation component of this research was conducted in two phases. The objective of the Phase I was to investigate the Cofra PVW system performance while varying the active depth of the PVW and PVW depth of placement. The first phase extracted water only. Phase II of experimentation included the placement of biodiesel LNAPL on the sand surface. Again, the liquid extraction and system performance was investigated while varying the active depth of the PVW and the PVW depth of placement. Both phases of experimentation for this project consisted of conducting several tests comprised of applying vacuum pressure to the PVW system while monitoring flow rates and head distribution. The PVW system consisted of a single prototype PVW fitted with the quick connect pipe components developed by Cofra. Particularly, the influence of the active PVW depth and the depth of placement on the water outflow rates and biodiesel extraction was evaluated, as well as the head distribution around the PVW with flow rate are investigated.

The experiments were conducted by applying a 16.9 kPa (5”Hg) vacuum to a prototype PVW installed in fine homogeneous sand. The sand was placed in a 1.52 m (5 ft) by 1.52 m (5 ft) by 1.37 m (4.5 ft) high, waterproofed steel test box. A barrel-mounted venturi vacuum was used to apply vacuum and extract air, water, and biodiesel through the PVW and piping. A vacuum gauge was installed at the tee connection of the HDPE piping to the PVW for both phases of testing, and vacuum gauges were installed along the PVW during

Phase I of testing involving only water extraction. Piezometers were installed in one quadrant of the sample and used to measure the hydraulic head distribution. The surface of the water in each piezometer was measured using copper wires and a multi-meter.

The test soil was homogeneous, poorly graded fine sand (SP) obtained from a sand distributor located in Columbia, South Carolina. The maximum and minimum index unit weights, in kilonewtons per square meter (kN/m^3) were 17.08 kN/m^3 (108.7 pcf) and 14.03 kN/m^3 (89.3 pcf), respectively. The permeability of the sand was determined at two void ratios, 0.65 and 0.67.

Using the general configuration described, seven tests were conducted during Phase I using two different sample preparation approaches and test configurations (Setups 1 and 2), and fourteen tests were conducted during Phase II using the sample preparation approach and test configuration utilized in Setup 2. The depth of the sand sample inside the test box was 1.06 m (3.48 ft), 1.18 m (3.87 ft), 1.18 m (3.87 ft), and 1.22 m (4.00 ft) for the first, second, third and fourth experimental setups, respectively.

3.2 Test Soil Characteristics

The test soil was a homogeneous, poorly graded fine sand obtained from the Columbia, SC plant of U.S. Silica Company. The sand is designated as GS #40 and is classified as SP according to the Unified Soil Classification System (USCS). The sand is classified as A-3

according to the AASHTO Soil Classification System. Typical properties of the test sand are provided in Table 3. Typical grain size distribution (GSD) of the test sand is provided in Table 4. A chart of the GSD is illustrated in Figure 9. Also, a picture of the test sand is shown in Figure 10, magnified at 60x.

Table 3. Sand (GS 40) Properties

Specific Gravity:	2.65
Shape:	angular
pH:	5.5-6.8
Color:	White
Mineral:	Quartz
C_c^*:	1.9
C_u^*:	1.0

* Cu and Cc Determined from GSD provided by US Silica Co.

Table 4. Grain Size Distribution Curve for GS #40 Sand

USA Standard Sieve Size	Sieve Size (mm)	Individual % Retained	Cumulative % Passing
30	0.600	<1	>99
40	0.425	20	80
50	0.300	31	49
70	0.212	28	21
100	0.150	14	7
140	0.106	5	2
200	0.075	1	<1
270	0.053	<1	0
(Provided by US Silica Co., P.O. Box 187, Berkeley Springs, WV 25411-0187)			

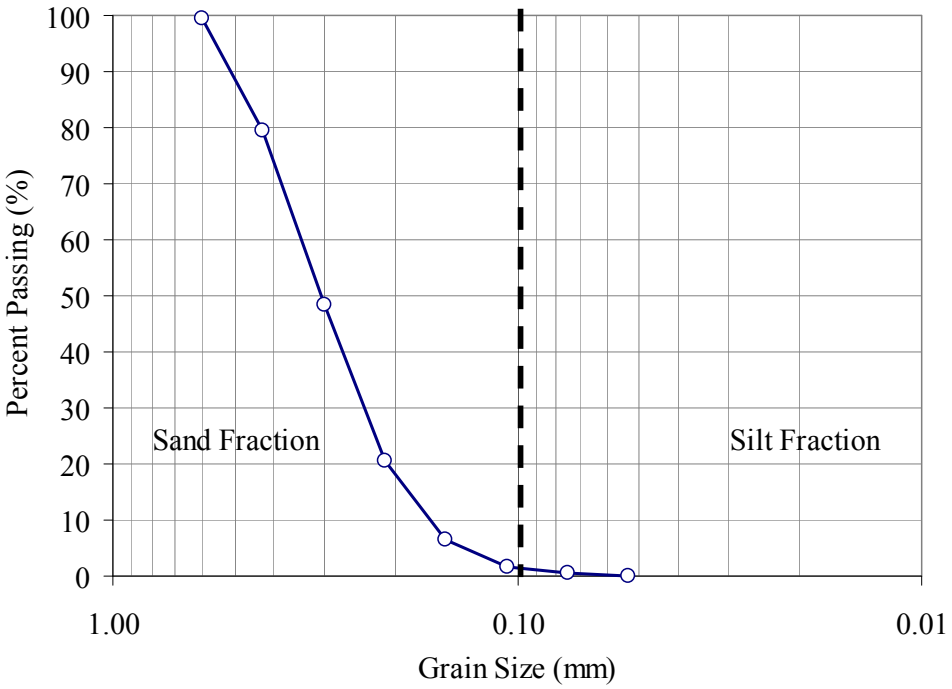

Figure 9. Test Sand GSD Curve

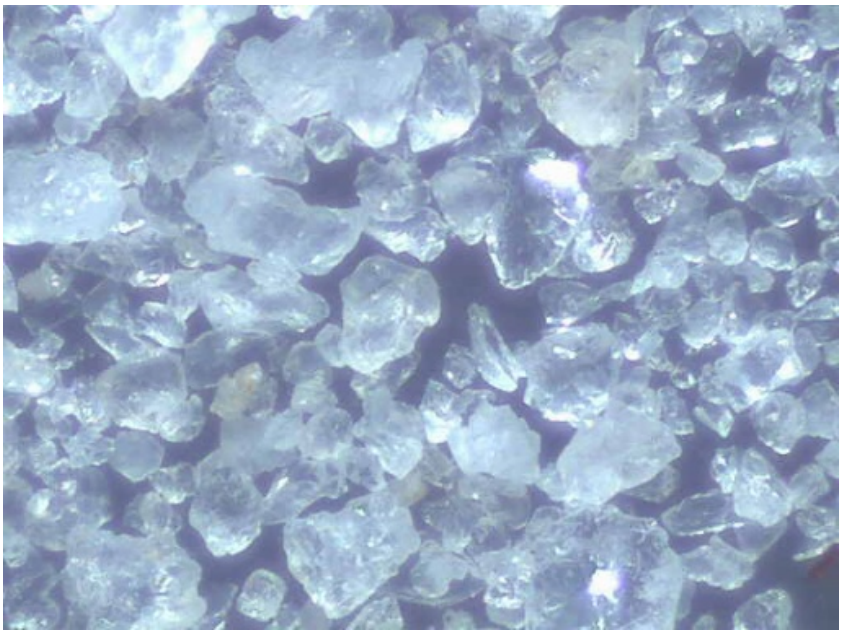

Figure 10. Manufactured Sand Used in Testing (60x Magnification)

The maximum index density and unit weight of the test sand were determined according to ASTM D 4253-00, and the minimum index density and unit weight were determined according to ASTM D 4254-00. The maximum unit weight of the test sand was determined to be 17.08 kN/m^3 (108.7 pcf), the average of four tests with a standard deviation of 0.055 kN/m^3 (0.35 pcf). The maximum index unit weight corresponds to a minimum void ratio of 0.522, with a standard deviation of 0.005. The minimum unit weight of the test sand was determined to be 14.03 kN/m^3 (89.3 pcf), the average of five tests with a standard deviation of 0.053 kN/m^3 (0.34 pcf). The minimum index unit weight corresponds to a maximum void ratio of 0.853, with a standard deviation of 0.007. A chart of the relationship between the unit weight and the void ratio for the test sand is shown in Figure 11.

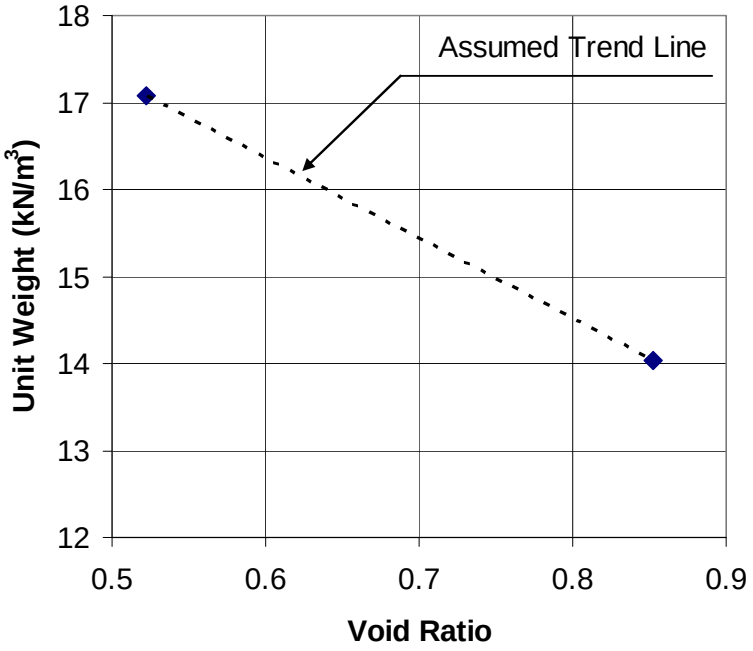

Figure 11. Relationship between Unit Weight and Void Ratio for Test Sand

The hydraulic conductivity of the test sand was measured using a flexible walled permeameter according to ASTM D 5084-03. Hydraulic conductivity tests were conducted on two specimens with void ratios of 0.67 and 0.65, or in terms of unit weights, 15.57 kN/m^3 (99.1 pcf) and 15.76 kN/m^3 (100.3 pcf), respectively. The hydraulic conductivities of the test specimens, corrected to 20° C, are 5.8x10^{-5} m/s (1.9x10^{-4} ft/s) and 8.0x10^{-5} m/s (2.6x10^{-4} ft/s), respectively.

3.3 LNAPL (Biodiesel) Properties and Testing

Biodiesel was the LNAPL used in this research. The biodiesel was obtained commercially from a third party vendor. The vendor produced the biodiesel by performing a batching

process: transesterification of vegetable oil using sodium hydroxide as a catalyst and methanol. The biodiesel used in this experimentation was produced more specifically from waste vegetable oil (WHO). A typical batch analysis report presenting the physical and fuel use related properties of the biodiesel used in this experimentation is presented in Table 5.

Several lab tests were conducted using the biodiesel. First, the specific gravity of the biodiesel was determined using a graduated cylinder and a specific gravity hydrometer (Bellwether), calibrated to measure fluid specific gravities ranging from 0.800 to 0.910. The specific gravity of the biodiesel was measured in triplicate, and was determined to be 0.885 at 20° C with no observed variation.

Table 5. Typical Fuel Properties of B100 Biodiesel Used During Testing (Determined From Analysis Report of Batch*)

Property	Method	Units	Limits	Actual
Free Glycerin	D-6584	Mass %	0.02 max.	<0.005
Total Glycerin	D-6584	Mass %	0.24 max.	0.169
Moisture	D-1796	PPM	Report	<1000
Water & Sediment	D-2709	Volume %	0.05 max.	<0.010
Acid Number	D-664	mg KOH/g	0.80 max.	<0.001
Cloud Point	D-2500	Degrees C	Report	5
Soap	Cc-17-79	PPM	Report	<15
Flash Point	D-93	Degrees C	130 min.	134
Corrosiveness to copper	D-130	ASTM Std.	3 max.	1B
Sulfated Ash	D-874	Mass %	0.02 max.	0.001
Particulate Free	D-100	Visual App	Yes	Yes
Kinematic Viscosity 40C	D-445	mm2/s	1.9-6.0	3.36
Sulfur - Non Petroleum	D-4294	PPM	15 max.	9
Cetane	D-613		47 min.	52
Carbon Residue 100% sample	D-4530	Mass %	0.050 max.	0.012
Phosphorous Content	D-4951	Mass %	0.001 max.	<0.001
Distillation Temp., AET, 90% Recovered	D-1160	Degrees C	360 max.	319
Oxidation Stability	EN-14112	Hours	3 min.	3' 55"
Calcium/Magnesium	EN-14538	PPM	5 max.	<0.001
Sodium/Potassium	EN-14538	PPM	5 max., combined	<0.001

*Courtesy of and Piedmont Biofuels, Inc.

A test was conducted on the biodiesel to evaluate the volatility of the biodiesel and other constituents in the fluid. This test was performed by measuring the mass loss after 24 hours in an oven at 104° C. Five samples were tested with a mean mass loss of 5.7%, and a standard deviation of 1.1%. As reported in the batch analysis, the biodiesel had a flash point, the lowest temperature which the substance can produce an ignitable vapor, of 135° C. However, excess methanol or water used in the batching process to produce the biodiesel, can vaporize at the lower temperature used during this lab test.

Another test was conducted to evaluate the miscibility of the biodiesel with water. The purpose of the test was to determine if any of the constituents of the biodiesel could be dissolved in tap water by agitation within a graduated cylinder. The test consisted of placing 10 grams of biodiesel in a 100 mL graduated cylinder. The remainder of the cylinder was filled with tap water to 100 mL. The volume of the biodiesel was measured as 12 mL. The cylinder and contents were shaken for two minutes, and then remained undisturbed for two hours. The volume of the biodiesel was again measured as 12 mL, which indicated no noticeable dissolution.

A second test was conducted to evaluate the miscibility of the biodiesel with water under vacuum. The small scale lab test was performed using a 2L Erlenmeyer flask, 500 mL of biodiesel and 1000 mL of water. The Erlenmeyer flask was sealed with two tubes installed through the seal. One 6.35 mm (1/4”) tube was provided to apply a vacuum and one 3.18

mm (1/8”) tube was provided to allow air to vent through and mix with the fluids from the bottom of the flask. The configuration is illustrated in Figure 12.

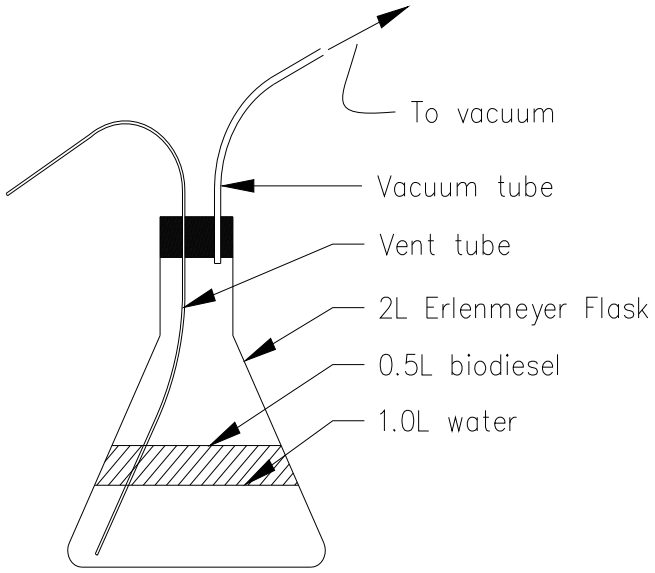

Figure 12. Flask and Tubing Configuration

A negative pressure of 54.2 kPa (16 inHg) was applied to the biodiesel and water within the flask using a vacuum pump, and the fluids mixed vigorously for 1 hour. Figure 13 presents two pictures of the process while it occurred. Figure 14 is a photograph of the Erlenmeyer flask 24 hours after the lab experiment, which illustrates the end result of the mixed fluids. The tap water was clear prior to commencing the test. As shown in Figure 14 after the test was complete, the water was a cloudy white, indicating noticeable mixing or dissolution of the biodiesel.

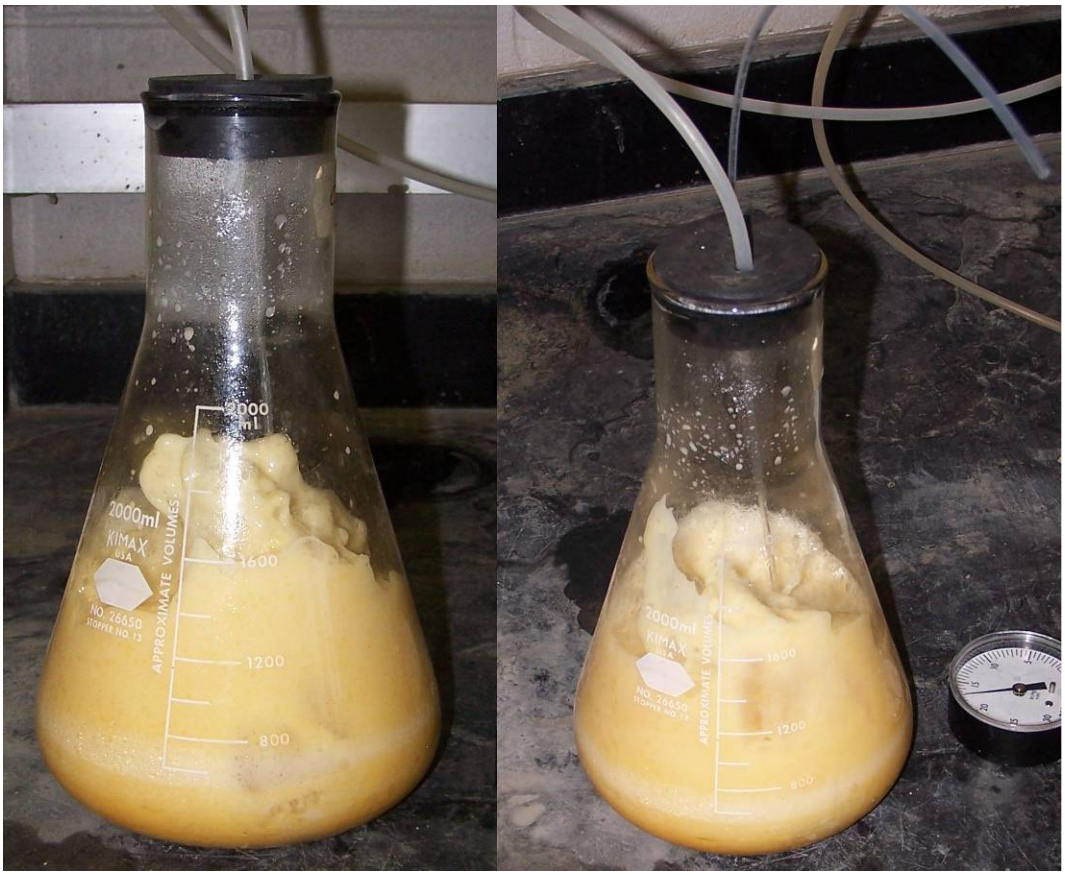

Figure 13. Mixing of 500 mL of Biodiesel and 1000 mL of Water by Applying 54.2 kPa Vacuum Pressure

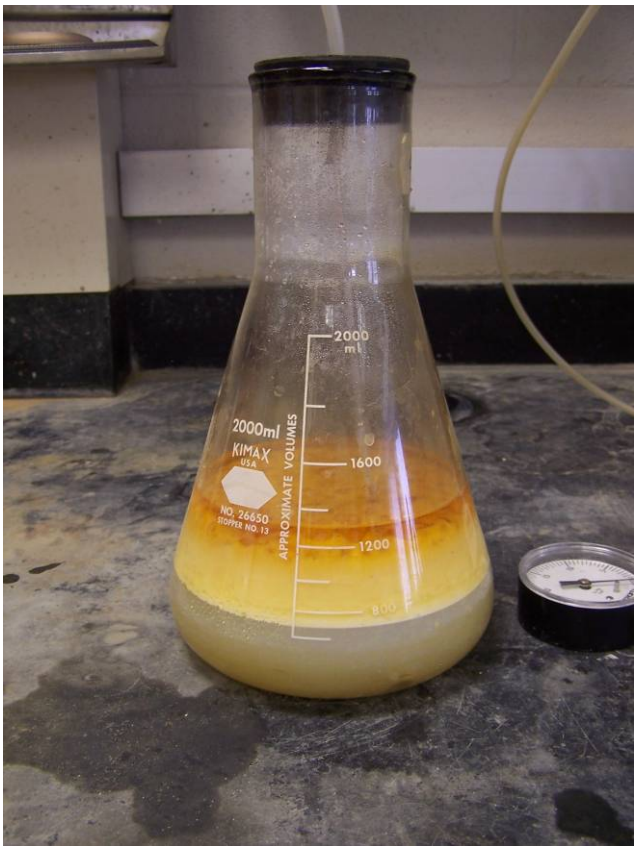

Figure 14. Erlenmeyer Flask Containing Biodiesel and Water After Equilibrated for 24 Hours, After 1 Hour Test

3.4 Test Configuration and Sample Preparation

For each sample, the sand was placed in a 1.52 m (5 ft) by 1.52 m (5 ft) by 1.37 m (4.5 ft) high test box. The sides and floor of the box are comprised of 1.27 cm (1/2") steel plates. The test box was waterproofed using 40 mil PVC liner and silicone caulking along the joints of the 1.3 cm (1/2") thick steel plates used to form the test box, as shown in Figure 15.

Figure 15. Test Box with Waterproofing

The sample for the first setup was prepared by placing the sand into the test box in 7 lifts to a depth of 1.06 m (3.48 ft). Each lift was compacted using a vibratory tamper, consisting of an electric jack hammer with a modified plate attachment, as shown in Figure 16. Each lift was placed so that its final compacted depth would be approximately 15.2 cm (6”). The weight of sand placed into the test box was 40.033 kN (9 kip). The volume of the test sand, as prepared, was determined to be 2.467 m^3 (87.1 ft^3). The average dry unit weight

of the sand, after completing all lifts, was 16.23 kN/m^3 (103.3 pcf), corresponding to a void ratio (e) of 0.60 and a porosity (n) of 0.375.

Figure 16. Sample Preparation (Setup 1)

The first sample preparation method made instrumentation and PVW placement in the sand difficult due to the high density. A second sample preparation method was developed as a means of obtaining a lower sand density. In this case, the sand was saturated and the water level was raised to approximately 5 cm (2") above the sand surface. The sand was

then thoroughly mixed and agitated to an approximate depth of 76.2 cm (30”) using a motorized 20.3 cm (8”) auger, as shown in Figure 17.

Figure 17. Sample Preparation and Equipment (Setup 2)

The sample was then completely drained. Density and water contents were observed at four locations on three separate lifts, using a Troxler nuclear density gauge. A relative frequency histogram of the densities observed is illustrated in Figure 18. The densities ranged from 14.77 kN/m^3 (94 pcf) to 15.55 kN/m^3 (99 pcf), with mean, median, and standard deviation, 15.21 kN/m^3 (96.8 pcf), 15.24 kN/m^3 (97 pcf), and 0.251 kN/m^3 (1.6

pcf), respectively. The sand was replaced in the test box, and the aforementioned sample preparation method was repeated for Setups 2, 3 and 4.

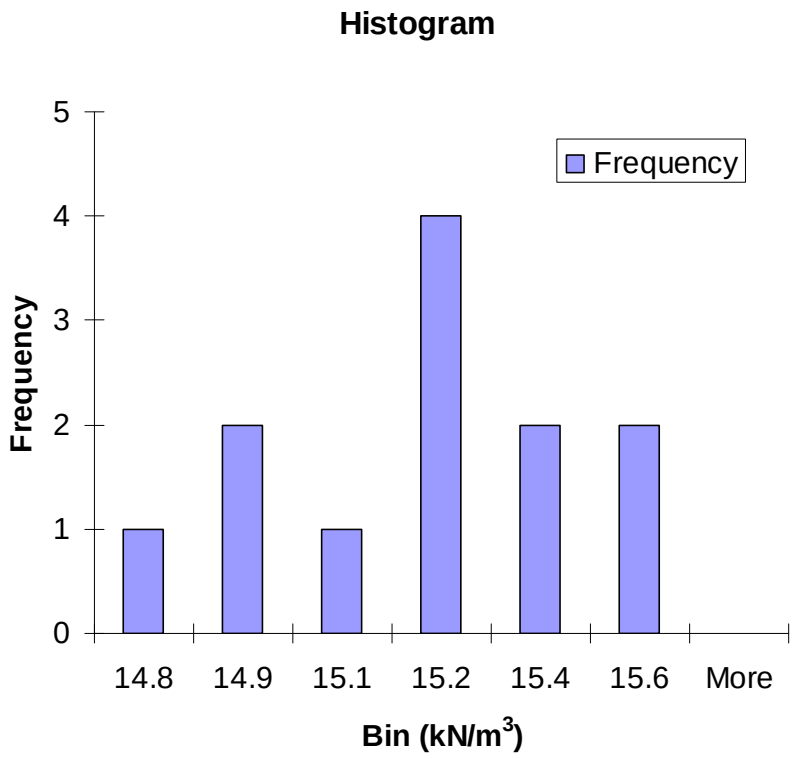

Figure 18. Frequency Histogram of Observed Densities of Test Sand During Trial Sample Preparation Prior to Setup 2

Several tests were conducted during the laboratory experimentation using two described methods of sample preparation. Figure 19 shows the unit weights and the void ratios of the sand samples as prepared in the setup methods.

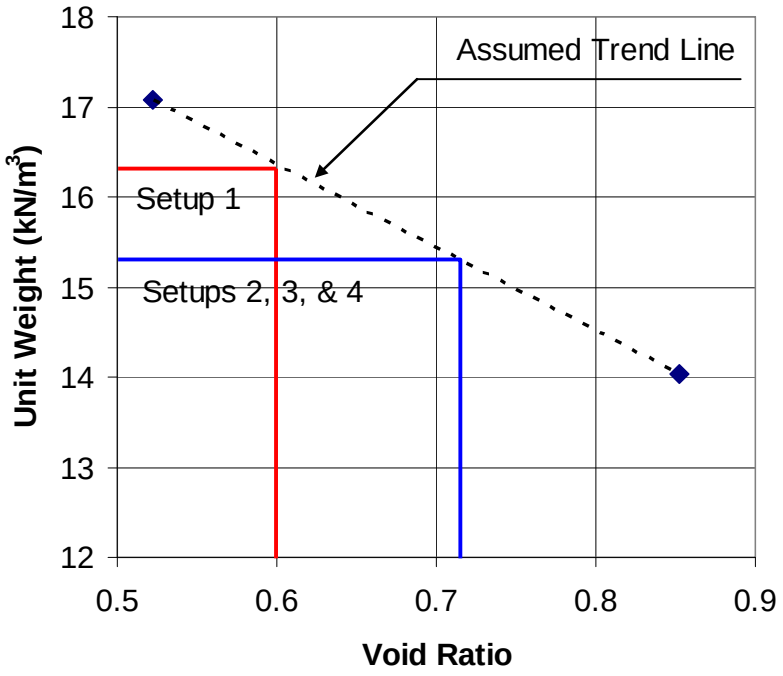

Figure 19. Unit Weights and Void Ratios of Test Sand for Experiments Conducted for All Setups

3.5 Instrumentation and Testing Procedures

3.5.1 Piezometer Configuration

Three rows of piezometers were installed in each sand sample to determine the head distribution. Upon completion of the sand placement and preparation, the piezometers were installed. The piezometers installed in the samples for Setups 1 through 3 were composed of acrylic, and were 1.37 m (4.5 ft) in length, with an inside diameter of 0.95 cm (3/8") and an outside diameter of 1.27 cm (1/2"). Degradation of the acrylic piezometers occurred after tests were completed for Setup 3. Therefore, nine 1.27 cm (1/2") inside diameter polyvinyl chloride (PVC) piezometers, 1.0 m (3.3 ft) in length, were placed in the

sample for Setup 4. A plan view of the typical piezometers layout for all four setups is illustrated in Figure 20. For Setups 1, 2, and 3, the open ends of the acrylic piezometers were covered with a geotextile fabric and secured as shown in Figure 21. For Setup 4, eight 3.2 mm holes were drilled at the ends of the PVC piezometers in the side wall of the pipes. A geotextile fabric was secured over the holes and the end of the PVC piezometers was plugged. Figure 22 illustrates the finished construction of the PVC piezometers for Setup 4.

For Setup 1, the piezometers were installed approximately 0.76 m (2.5 ft) into the samples, or 0.30 m (1 ft) from the bottom of the sample box. Due to the dense sand specimen prepared for Setup 1, a unique piezometer installation procedure was utilized. Each piezometer was installed by driving a 2.5 cm (1") diameter steel conduit pipe into the sample to approximately 0.76 m (2.5 ft). The sand inside the pipe was removed using a vacuum tube. The piezometer was installed inside the pipe, and the pipe was removed from the sand.

The sample preparation method used in Setups 2, 3 and 4 produced a sand sample with a higher void ratio, and manual insertion of the piezometers was performed. A 0.94 cm (0.37") diameter steel rod was inserted inside each acrylic piezometer to stiffen the piezometer, and each was manually inserted into the sand sample approximately 0.76 m (2.5 ft). The PVC piezometers used in Setup 4 were manually inserted approximately 0.70 m (2.3 ft) without the stiffening rod.

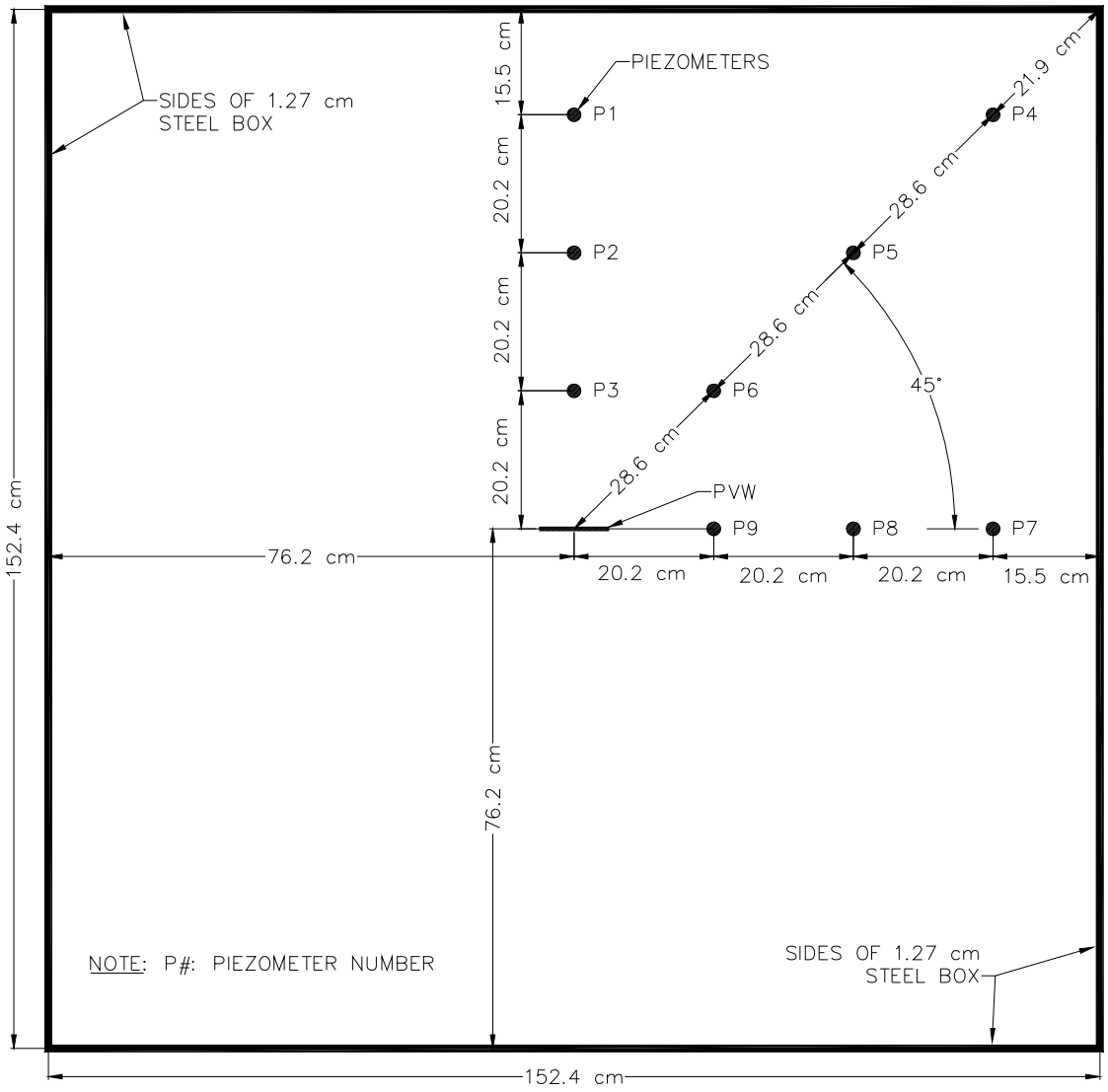

Figure 20. Plan View of Typical PVW and Piezometer Installation

Figure 21. End Construction of Laboratory Piezometers for Setups 1 Through 3

Figure 22. End Construction of Piezometers for Setup 4

3.5.2 PVW System Configuration

A Mebra drain wick system (manufactured by Nilex Corporation) was used during the laboratory testing. The physical and mechanical properties of the PVW are shown in Table 6. A single PVW was installed in the center of each sand sample for all experimental setups. The PVW adaptor connected each PVW to 1.6 cm (5/8") O.D. HDPE pipe. The HDPE pipe was connected to a quick connect tee which remained above the surface of the

sample during testing. A vacuum gauge was installed at the end of the 1.6 cm (5/8") O.D. HDPE pipe that extended beyond the tee using 1.6 cm (5/8") I.D. reinforced clear rubber pipe. The assembled PVW configuration was attached to the suction of a venturi vacuum device using 1.6 cm (5/8") I.D. reinforced clear rubber tubing.

A barrel-mounted venturi vacuum (Nortech Vacuum System model 551 B by Nortech Corporation, Midland Park, NJ) was used to extract air and water through the PVW. The venturi vacuum was powered by a 15 hp electric air compressor pump. A 220 L (58 gal) barrel was used to store the fluid extracted during each test. The vacuum and storage tank components of the PVW system are presented in Figure 23.

Table 6. Mebra Drain Specifications for MD-88*

Physical Properties	**Test Method**	**Units**	**MD-88**
Drain Material			Polypropylene
Filter Material			Polypropylene
Weight	ASTM-D 1777	g/m	85
Width		mm	100
Thickness	ASTM-D 5199	mm	4.34
Mass of Filter	ASTM-D 1777	g/mm^2	154
Equivalent Diameter		mm	65
Mechanical Properties	**Test Method**	**Units**	**MD-88**
Core Grab Tensile Strength	ASTM-D 638	kN	0.996
Filter Grab Tensile Strength	ASTM-D 4632	kN	0.710
Filter Grab Elongation	ASTM-D 4632	%	90
Filter Strength @ 10% Elongation	ASTM-D 4632	kN	0.230
Tear Resistance	ASTM-D 4533	kN	0.390
Puncture Strength	ASTM-D 4833	kN	0.267
Discharge Capacity @ 10 kN/m^2	ASTM-D 4716	m^3/s	$180x10^{-6}$
Discharge Capacity @ 300 kN/m^3	ASTM-D 4716	m^3/s	$140x10^{-7}$
Pore Size Opening	NEN 5168	mm	0.075
Pore Size Opening	ASTM-D 4751	mm	0.110
AOS	ASTM-D 4751	#	120/140
Flux	ASTM-D 4491	$l/min/m^2$	1360
Filter Permeability	ASTM-D 4491	mm/s	0.171
Permittivity	ASTM-D 491	l/s	0.45

* Data provided by Nilex Corporation, 15171 E. Fremont Drive, Centennial, CO 80112

Figure 23. Vacuum Pump and Storage Tank Components of PVW Extraction System

Prior to PVW installation in Setup 1, three vacuum gauges were connected to rigid tubing and were inserted into the PVW at 2 cm, 44 cm, and 83 cm from the bottom of the PVW. Silicone caulking was used to seal all openings. An illustration of the assembled components of the PVW configuration for Setup 1 is shown in Figure 24. The PVW was installed to a depth of 65 cm (25.6”) using a 3.2 mm (1/8”) thick steel plate, a fabricated steel driving cap, and a hammer. A 9 cm (3”) depth fold was placed in the bottom of the PVW which allowed for the 9 cm (3”) wide steel plate to be inserted into the fold, allowing

the PVW to be driven into the dense sand. The PVW was driven with care to avoid damaging the fold in the PVW. The wick was installed 41.19 cm (16.2”) from the bottom of the test box and a portion of the PVW extended above the sand surface. The remaining 34 cm (13.4”) of the wick was enclosed in an impermeable plastic membrane, similar to current field installation procedures, to a depth of 4 cm (1.6”) below the surface of the sand. The membrane was sealed using vacuum grease and extended into the sand sample to ensure a closed system for proper PVW performance. The active length was 61 cm (24”), and the depth of placement was 65 cm (25.6”) for Setup 1.

Figure 24. PVW Instrumented with Vacuum Gauges for Setup 1

Also for Setup 1, A 40 mil PVC liner was constructed to cover the sand sample to minimize air infiltration while allowing the instrumentation to extend above the sand surface. The constructed and instrumented setup is shown in Figure 25 for Setup 1. Figure 26 shows the exposed PVW after the test is completed. No significant damage was observed of the PVW after testing due to the aforementioned installation method. The moisture content of the saturated portion of soil during the three trials for this setup was

determined to be an average of 22%, with a standard deviation of 0.2%. A detailed cross-section of the PVW installation is illustrated in Figure 27.

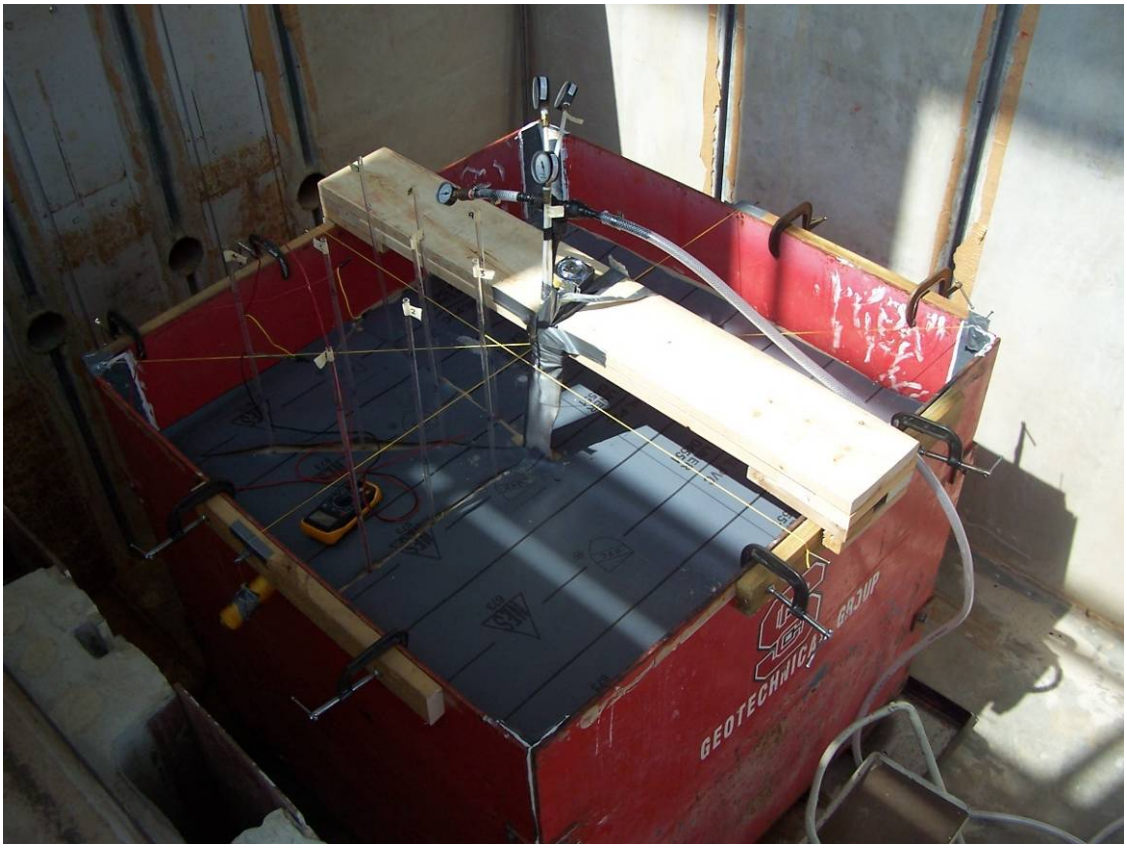

Figure 25. Constructed Test Sample and Instrumentation for Setup 1

Figure 26. PVW in Sand Sample After Test Completion (Setup 1)

SET UP 1

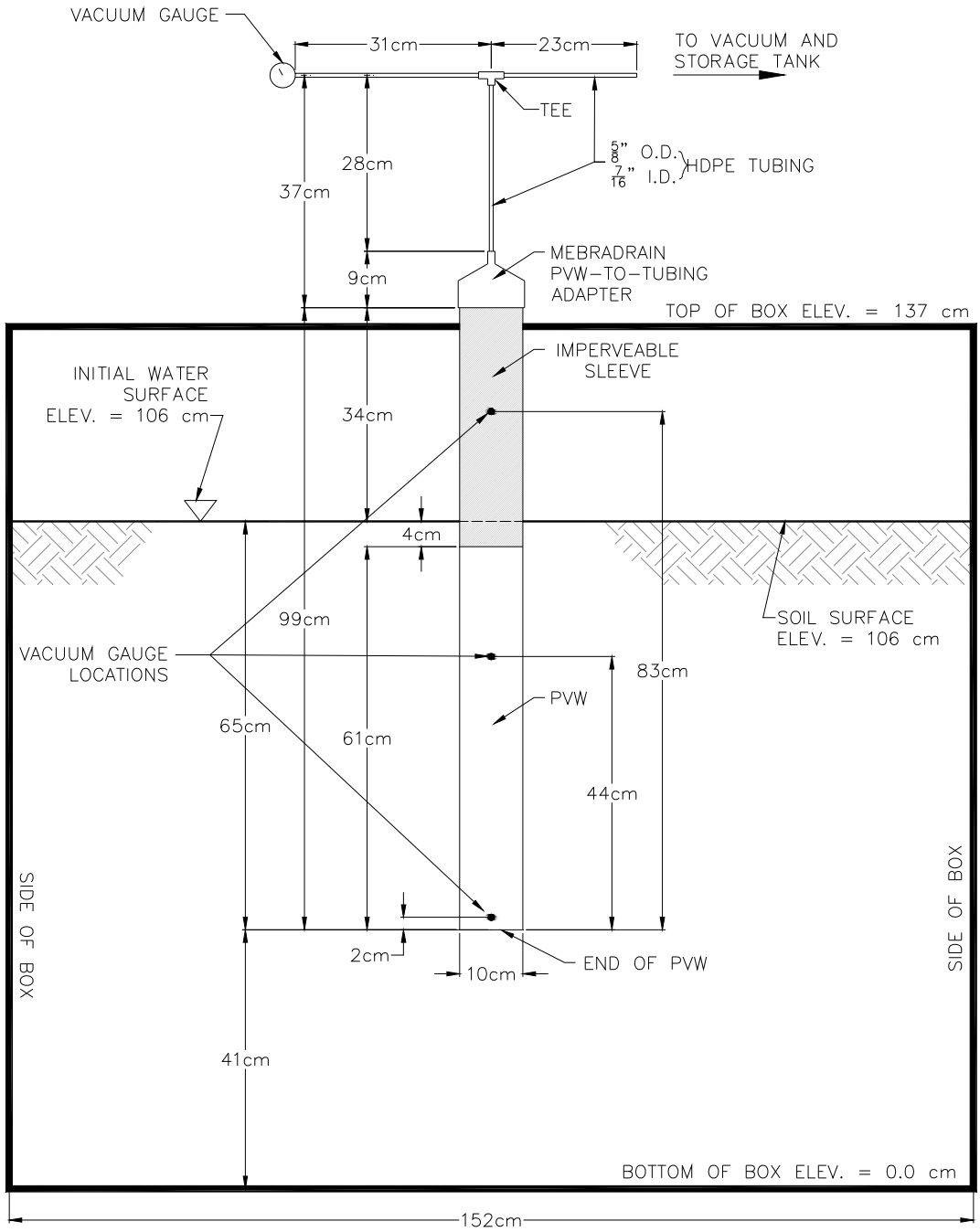

Figure 27. Cross-Section Detail of PVW Installation (Setup 1)

For the second setup, the active length of the PVW was 31 cm (12.2”), or approximately 1/2 the active length used in the first setup, and the depth of placement was 65 cm (25.6”), approximately the same depth used in the first setup. Prior to PVW installation, two vacuum gauges, connected to rigid tubing, were inserted into the PVW, at 2 cm and 29 cm from the bottom of the PVW. The HDPE pipe from the adapter to the tee was lengthened to place the bottom of the PVW at the same depth as the first setup. The PVW was inserted into the sand with less effort than that used in the PVW insertion for Setup 1, using the same steel plate but without the hammer. The remaining components of the second setup, including the placement and orientation of the piezometers, the PVW, and the PVC liner were the same as the first setup. A detailed cross-section of the PVW installation is illustrated in Figure 28.

The PVW configuration for Setup 3 was similar to that of Setup 2. The PVW was manually inserted into the sand using the 3.2 mm (1/8”) thick steel plate. The active length of the PVW was 31 cm (12.2”), the same length used in the second setup, and the depth of placement was 65 cm (25.6”), the same depth used in the second setup. Vacuum gauges were also inserted into the PVW for Setup 3, in the same manner and locations as in Setup 2. The PVC liner was not placed on the sand surface during testing due to the placement of the LNAPL. The remaining components of the third setup, including the placement and orientation of the piezometers, were the same as the previous setups. A detailed cross-section of the PVW installation is illustrated in Figure 29.

The configuration for Setup 4 exhibited the shortest active length PVW and the shallowest placement depth. The PVW was again manually inserted into the sand using the 3.2 mm (1/8") thick steel plate. The active length of the PVW was 15 cm (6"), or approximately 1/2 the length used in Setup 3. The placement depth, 19 cm (7.5"), was also much less than that used in Setup 3, with the top portion of the PVW only 4 cm (1.6") from the sand surface. Vacuum gauges were not inserted into the PVW, and the PVC liner was not placed on the sand surface during testing, for Setup 4. The remaining components of the fourth setup, including the placement and orientation of the piezometers, were the same as the previous setups. A detailed cross-section of the PVW installation is illustrated in Figure 30.

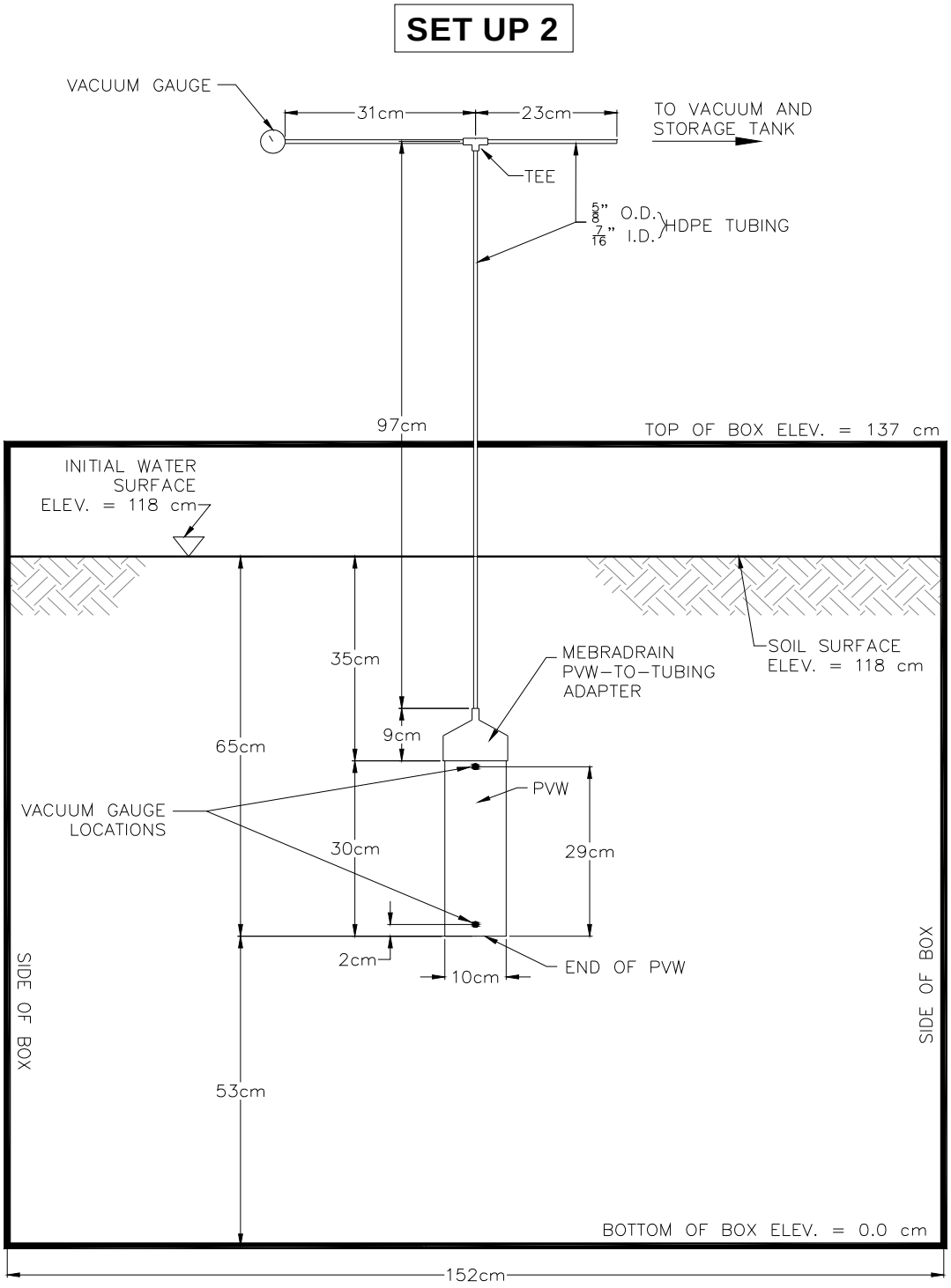

Figure 28. Cross-Section Detail of PVW Installation (Setup 2)

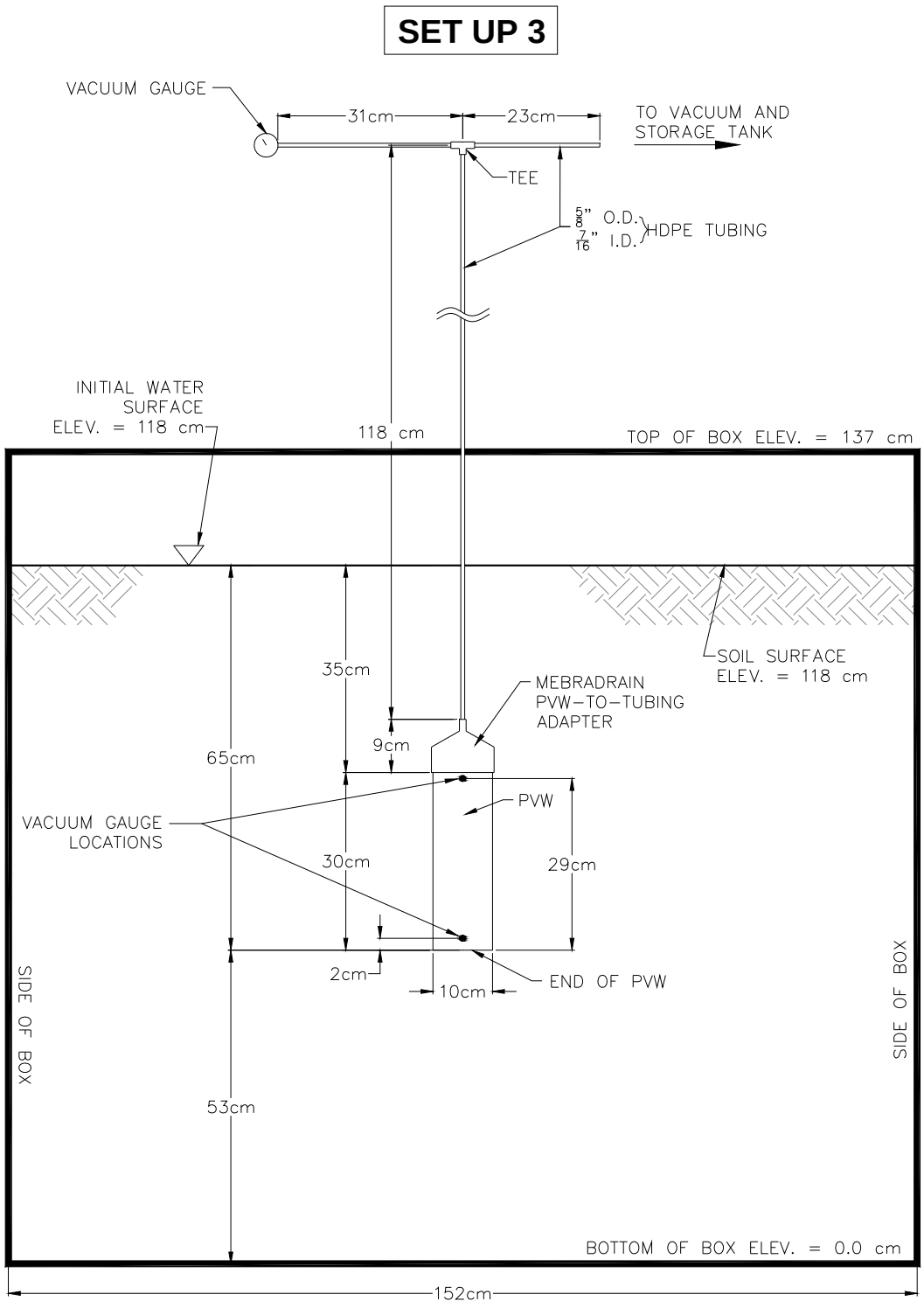

Figure 29. Cross-Section Detail of PVW Installation (Setup 3)

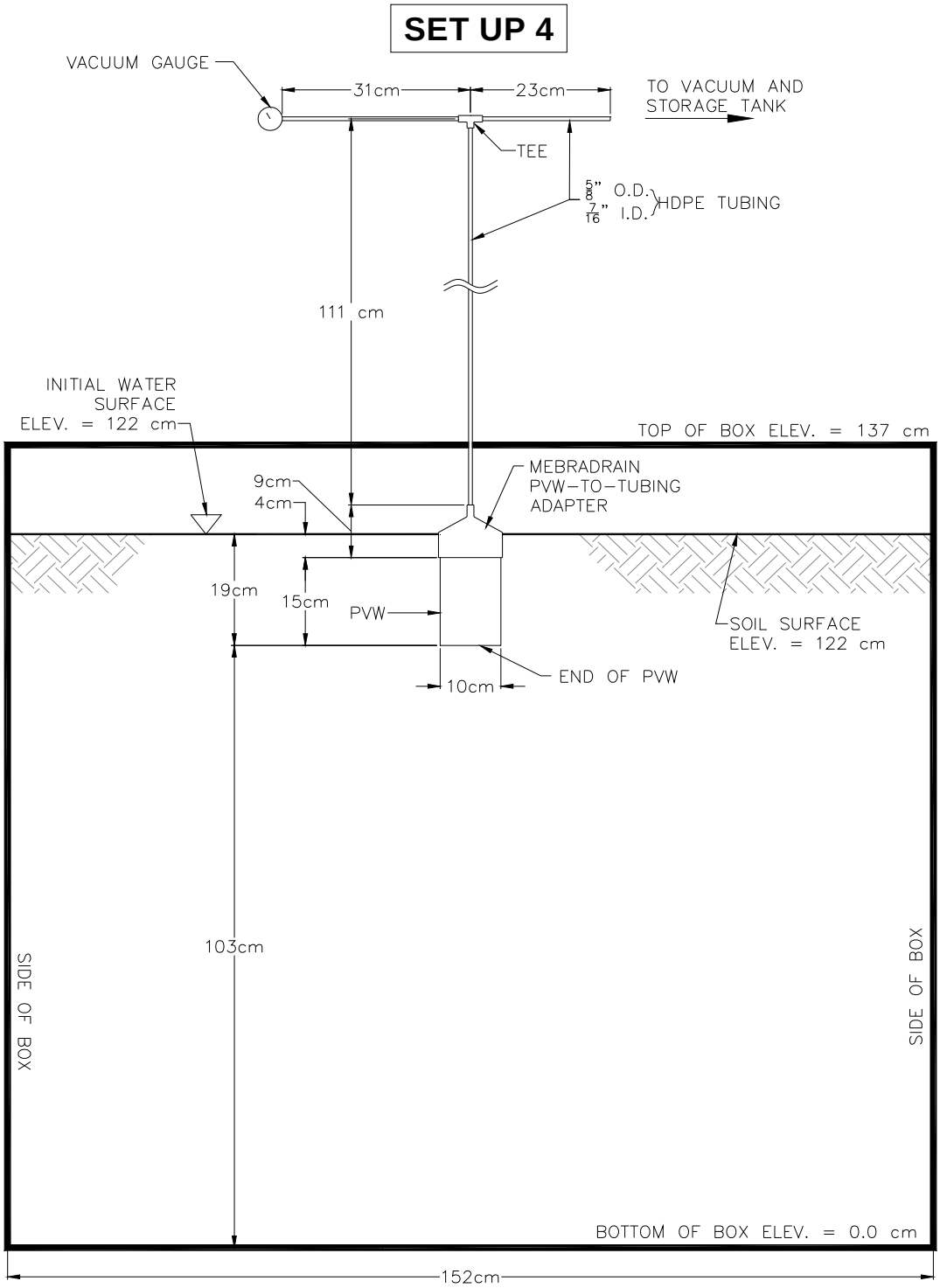

Figure 30. Cross-Section Detail of PVW Installation (Setup 4)

3.5.3 Testing Procedure

Upon completing the sample preparation and instrumentation installation, the sand was saturated with tap water and the system was allowed to equilibrate for 24 hours or greater for Phase I testing; however, the saturation period and the equilibration period varied during Phase II testing. The saturation and system equilibration periods for Setups 3 and 4 are presented in Table 7.

Table 7. Sample Saturation and LNAPL Equilibrium Periods for Setups 3 and 4

Setup	Test	Saturation Time (hr)	System Equilibration Time (hr)
3	1	2	24
3	2	2	36
4	1	2	24
4	2	5	17
4	3	18	0
4	4	48	72
4	5	72	48
4	6	4	68
4	7	3	72
4	8	8	96
4	9	24	110
4	10	24	72
4	11	8	48
4	12	72	96

The tests were conducted with the following flow conditions: (i) inflow and outflow and (ii) outflow only. Inflow to the sample was applied to the samples in an evenly distributed manner, through a commercial 1.6 cm (5/8") hose, similar to surface recharge. The flow from the hose was measured and timed to determine the flow into the sample. To

determine the outflow through the PVW for each test, the test was halted at various times, and the water and LNAPL fluid levels were measured within the venturi vacuum storage tank. The total head was measured in the system through the piezometers at various times, also.

The water surface in the piezometers was determined using a battery-powered digital multi-meter and copper wires. One copper wire was attached to one of the two multi-meter leads and inserted into the saturated portion of the sand. Another copper wire used for measuring the distances was attached to the other lead. A hole, with diameter smaller than the diameter of the copper wire, was bored in a rubber stopper and was placed on the measuring copper wire to mark the location of the measurement along the copper wire and reduce measurement error. The measuring copper was slowly lowered into the piezometer until the multi-meter indicated a closed circuit condition, meaning the copper wire had contacted the water surface. The length of the copper wire from the surface of the water to the top of the piezometer was then measured and recorded in reference to the datum, the bottom of the test box. String lines were installed along the top edge of the test box adjacent to the piezometers to relate the top of each piezometer to the bottom of the test box. For quality control purposes, data repeatability and user error was verified using a section of a piezometer placed inside a graduated cylinder filled with water. One copper wire attached to a multi-meter lead was placed on the outside of the piezometer, in the water. The measuring copper wire attached to the other lead was slowly lowered into the piezometer until the multi-meter indicated a closed circuit condition. Using the described

measurement method and control setup, five trials were performed with an average distance of 15.78 cm and a standard deviation of 0.066 cm.

The biodiesel and water interface in the storage tank was determined using the same method as described to detect the water surface. One copper wire was attached to one of the two multi-meter leads and inserted into the bottom portion of the tank in the water. The measuring copper wire was attached to the other lead and slowly lowered vertically along the edge of the tank into the biodiesel until the multi-meter indicated a closed circuit condition, meaning the copper wire had contacted the water and biodiesel interface. The length of the copper wire from the surface of the water to the top of the tank was then measured and recorded in reference to the datum, the top of the tank. The top of the biodiesel was determined using a similar process measuring the same lead wire. The lead wire was lowered vertically until visual contact with the biodiesel was observed. The length of the copper wire from the surface of the biodiesel to the top of the tank was then measured and recorded in reference to the datum. The measurements were performed in triplicate and the average measurement was recorded.

This process was suitable to determine the interface depth because of the significant difference in electrical conductivities of biodiesel and water. Biodiesel has an electrical conductivity of approximately 10^{-12} S/m and typical tap water has an electrical conductivity that ranges from 10^{-2} to 10^{-4} S/m (Anonymous). The conductivity of the biodiesel was not measurable using the multimeter. Again, for quality control purposes,

this process was verified for data repeatability using a graduated cylinder filled with 800 mL of water and 100 mL of biodiesel. One copper wire attached to a multi-meter lead was placed into the water inside the graduated cylinder. The measuring copper wire and lead was slowly lowered into the graduate until the multi-meter showed a closed circuit condition, indicating the detection of the water and biodiesel interface. Another measurement was made using the same lead wire to visually determine the depth to the surface of the biodiesel. Five trials were performed to determine the water and biodiesel interface and the top of the biodiesel. The average distance to the water and biodiesel interface was 14.60 cm with a standard deviation of 0.055 cm. The average distance to the top of the biodiesel was 10.81 cm with a standard deviation of 0.069 cm. The diameter of the graduated cylinder was also measured in triplicate. Using the average diameter of the graduated cylinder and the average measurements of the water and biodiesel interface and the top of the biodiesel, the volume of the biodiesel was determined to be 102 mL.

3.4 Performance Results

3.4.1 Phase I Extraction Results

Three tests were conducted using the Setup 1, and four tests were conducted using the Setup 2. Flow rates were measured to compare the efficiency of the PVW at two active lengths for Phase I of the laboratory tests. The extraction data, the measured inflow and outflow rates, and the system operation times are presented in Table 8. Measured inflow and outflow rates are shown in Figure 31 and in Figure 32 as a function of time. Figure 31

displays the flow rate as a function of time for the various described cases, and Figure 54 displays the flow rate, normalized by dividing it by the active depth of the PVW, as a function of time for the various cases.

Table 8. Phase I Laboratory Extraction Flow Rate Results

Case	Runtime (min)	Outflow rate (L/min)	Inflow Rate (L/min)	Net Outflow (+) or Inflow (-) Rate (L/min)	Active Depth (m)	Outflow rate per length of active depth (L/min/m)
Case 1a, 1b	39	1.39	0.96	0.43	0.61	2.28
Case 2a, 2b	39	1.96	2.33	-0.37	0.61	3.22
Case 3	116	0.97	0	0.97	0.61	1.59
Case 4	10	5.36	0	5.36	0.31	17.30
Case 4	20	4.85	0	4.85	0.31	15.66
Case 4	30	4.60	0	4.60	0.31	14.83
Case 4	40	4.24	0	4.24	0.31	13.68

Cases 1 through 3 were conducted using Setup1. Case 4 was conducted using Setup 2. For Case 1 and Case 2, the (a) and (b) designation distinguishes between the outflow vs. time and the net outflow vs. time, respectively, in Figure 31 and Figure 32. The inflow for Case 1 and Case 2 was 0.96 L/min (0.25 gpm) and 2.33 L/min (0.62 gpm), respectively. The inflow for Case 2 was more than twice as much as the inflow for Case 1.

The outflow rate of Case 2 decreased with time by approximately 20% over the 40 minutes of testing. Comparing the two Setups, the outflow rates for Setup 2, where the active length was half the active length of Setup 1, are greater than the outflow rates for Setup 1. In Cases 1 and 2 (Setup 1), the outflow rates for the 39 minute runtime are less than half

the flow rate for Case 4, 40 minute runtime. This is mainly due to the ability to sustain vacuum head as desaturation occurs around the PVW with system operation.

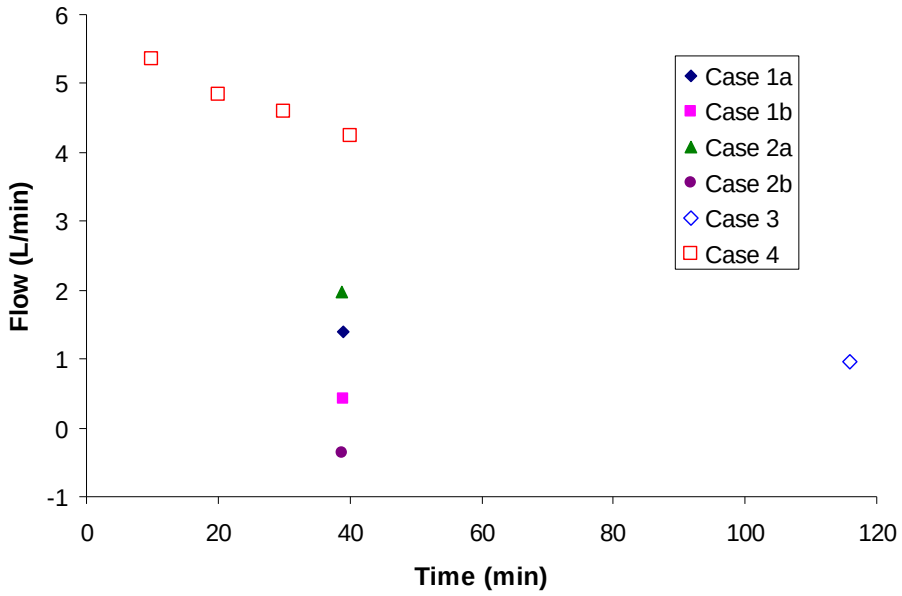

Figure 31. Laboratory Outflow Rate vs. Time (Setups 1 and 2)

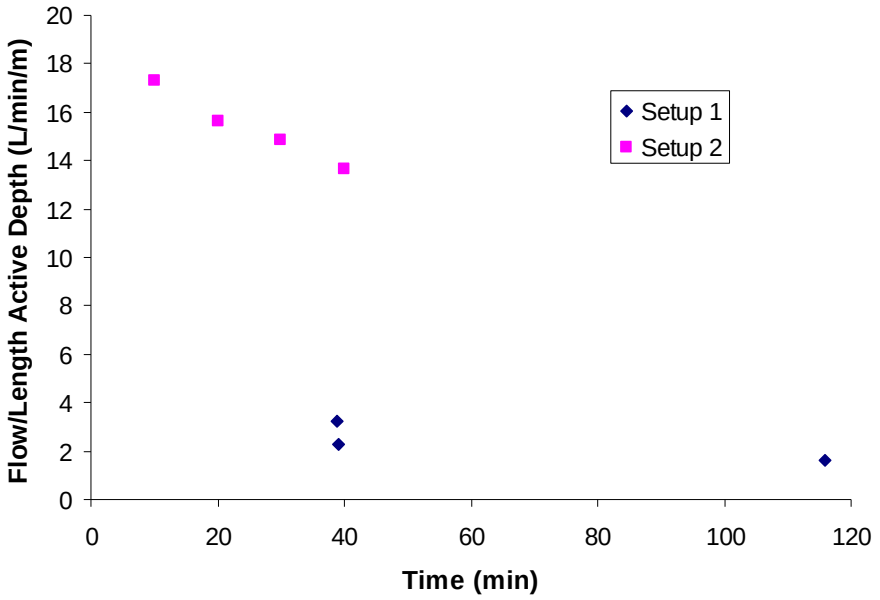

Figure 32. Laboratory Outflow Rate per Length Active Depth vs. Time (Setups 1 and 2)

3.4.2 Phase II Extraction Results

For Phase II testing, once the sand was initially saturated, 76 L (20 gal.) of LNAPL biodiesel was placed on the water table surface prior to the two initial tests using Setups 3 and 4. After each test was completed, and prior to commencing the next test, the water table was gradually raised over a period of time to simulate actual field conditions. The system was then allowed to equilibrate for a period to allow the free product adequate time to rise to the surface above the water table and to minimize air and LNAPL entrapment. A total of two tests were conducted with Setup 3, and twelve tests were conducted using Setup 4.

The total volume of LNAPL biodiesel extracted was 1.5 L (0.40 gal) and 27.3 L (7.22 gal) for Setup 3 and Setup 4, respectively. In terms of percentages, Setup 3 extracted 2.0 % and Setup 4 extracted 36.0% of the total LNAPL placed within the system. The extraction results data are presented in Table 9 and Table 10 for Setup 3 and Setup 4, respectively. The cumulative water and LNAPL biodiesel extraction results are plotted in Figure 33, for Setup 4, and the cumulative LNAPL biodiesel extraction results are plotted separately in Figure 34. For Setup 4, the cumulative water and LNAPL biodiesel extraction results are plotted in Figure 35 and the cumulative LNAPL biodiesel extraction results are plotted separately in Figure 36. Figure 37 presents the extraction results per test, over the entire period of testing. The significant drop in LNAPL extraction on the third and fourth test is possibly due to the water table not being raised as high as the previous and following tests. Nonetheless, a downtrend or tailing effect was observed in the LNAPL extraction overall. There is also a notable difference in the water extraction rates between Setups 3 and 4. A volume of 957 L of water was extracted during the 220 minutes of operation for Setup 3, compared to the 856.5 L of water extracted during the 720 minutes of operation for Setup 4, resulting in overall average water extraction rates of 4.35 L/min and 1.19 L/min for Setups 3 and 4, respectively.

Table 9. Fluid Extraction Results for Setup 3

Test 1	Time (min)	*30*	*60*	*90*	*120*
	Cumulative LNAPL Extraction (L)	0.51	0.77	0.77	0.77
	Cumulative Water Extraction (L)	149.6	264.8	361.3	446.1
Test 2	Time (min)	*20*	*40*	*70*	*100*
	Cumulative LNAPL Extraction (L)	0.00	0.00	0.77	0.77
	Cumulative Water Extraction (L)	122.1	237.6	382.9	510.9

Table 10. Fluid Extraction Results for Setup 4

	LNAPL Extracted		Water Extracted	
Test	30 min.	60 min.	30 min.	60 min.
	(L)	(L)	(L)	(L)
1	4.9	7.9	93.8	130.3
2	4.1	4.3	36.5	57.0
3	0.0	0.3	36.0	54.7
4	1.0	1.0	31.7	51.6
5	4.3	4.9	40.1	58.5
6	3.6	3.8	42.7	64.1
7	2.8	2.8	55.4	76.4
8	0.3	0.8	55.4	78.9
9	0.3	0.3	40.4	57.7
10	1.0	1.0	57.2	79.2
11	0.3	0.3	47.5	67.3
12	0.0	0.0	62.6	80.8

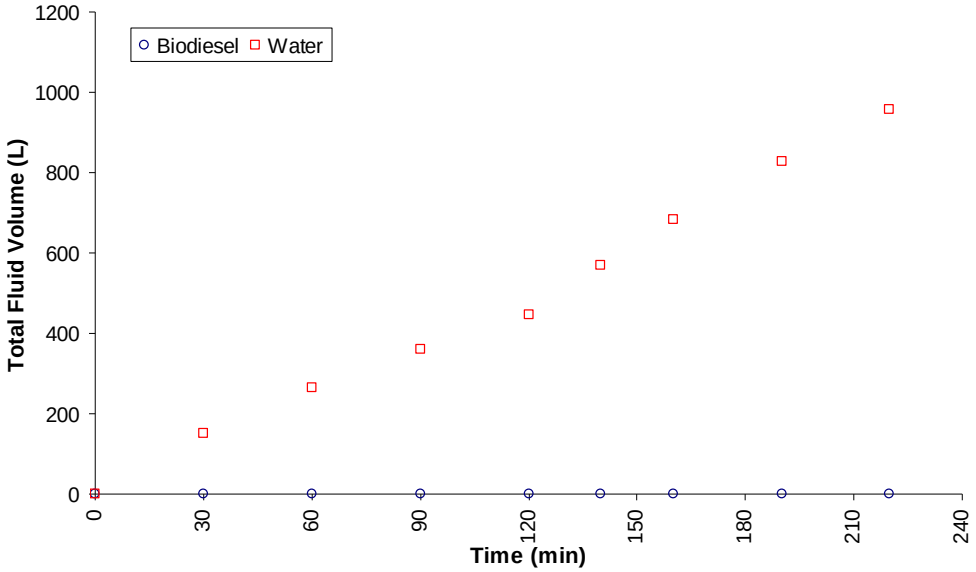

Figure 33. Cumulative Extracted Volume of Water and Biodiesel (Setup 3)

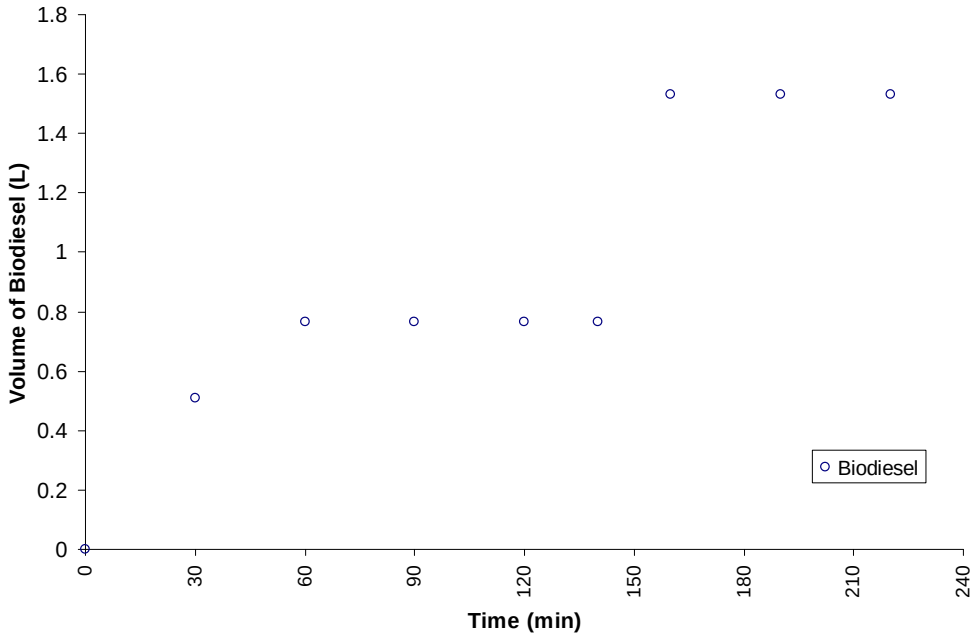

Figure 34. Cumulative Extracted Volume of Biodiesel (Setup 3)

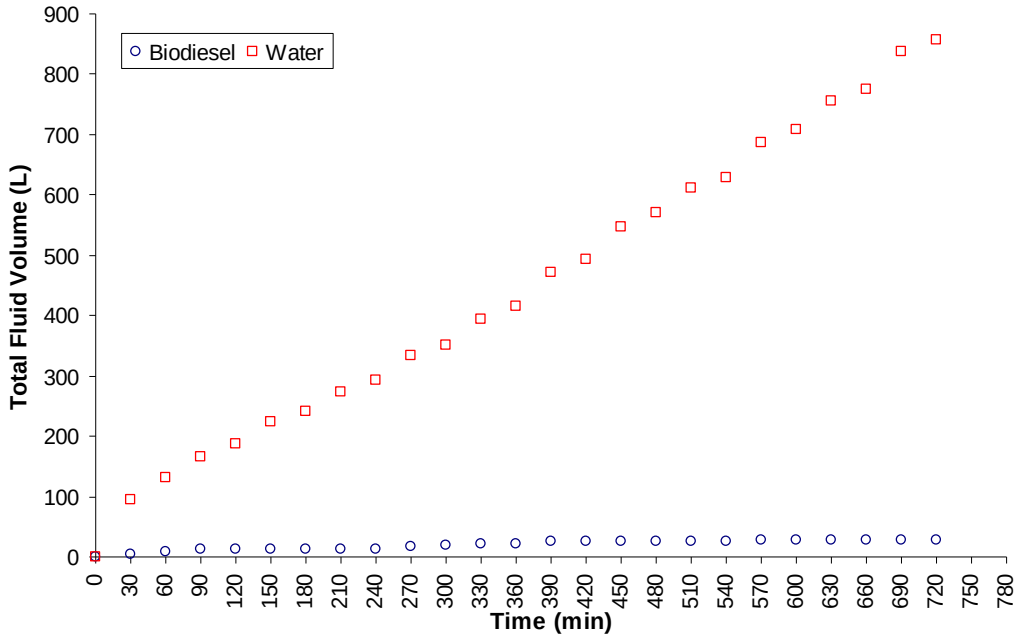

Figure 35. Cumulative Extracted Volume of Water and Biodiesel (Setup 4)

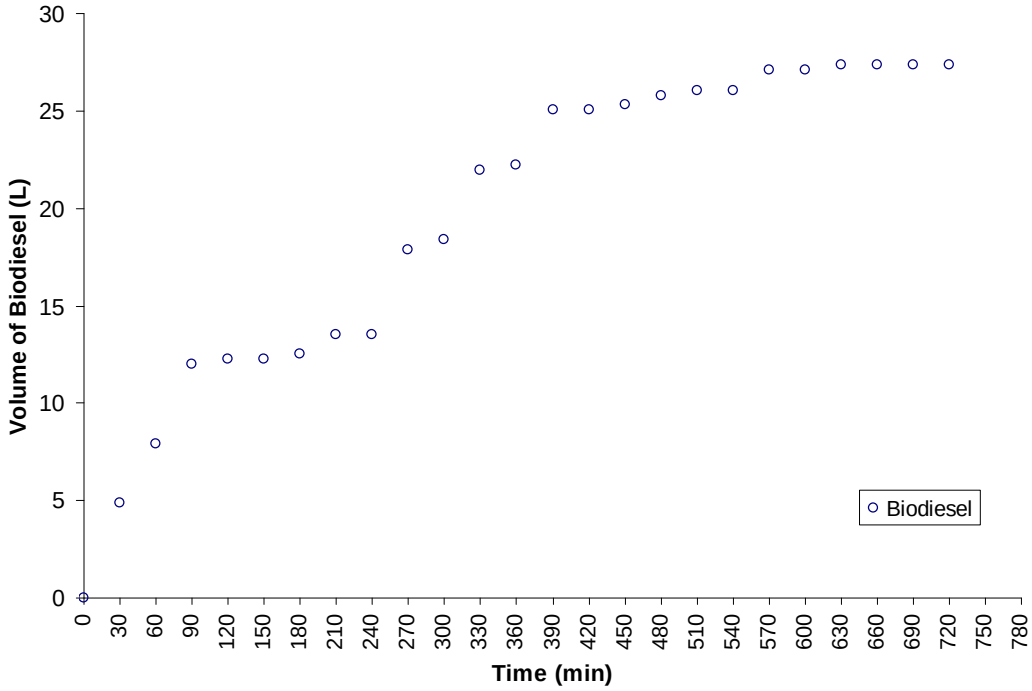

Figure 36. Cumulative Extracted Volume of Biodiesel (Setup 4)

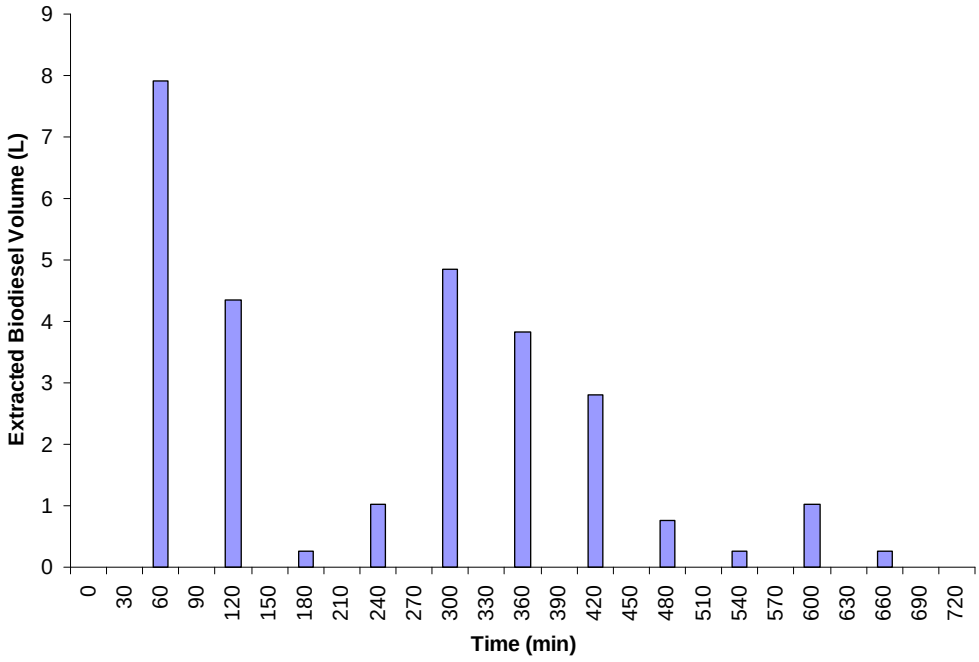

Figure 37. Volume of Biodiesel Extracted Per Test (Setup 4)

Water and LNAPL volumes were measured to compare the extraction efficiency of the PVW at two active lengths. The extraction flow rate data for Setups 3 and 4 are presented in Table 11. Figure 38 displays the flow rate, normalized by dividing it by the active depth of the PVW, as a function of time for the various cases in Setups 3 and 4 as presented in Table 11.

Table 11. Phase II Laboratory Extraction Flow Rate Results (Setup 3 and 4)

Case	Runtime (min)	Outflow rate (L/min)	Inflow Rate (L/min)	Net Outflow (+) or Inflow (-) Rate (L/min)	Active Length (m)	Outflow rate per length of active depth (L/min/m)
Case 5a	30	5.00	2.00	3.00	0.31	16.14
Case 5a	60	3.85	2.00	1.85	0.31	12.42
Case 5a	90	3.22	2.00	1.22	0.31	10.38
Case 5a	120	2.83	2.00	0.83	0.31	9.12
Case 5b	20	6.11	4.20	1.91	0.31	19.69
Case 5b	40	5.77	4.20	1.57	0.31	18.62
Case 5b	70	4.87	4.20	0.67	0.31	15.71
Case 5b	100	4.27	4.20	0.07	0.31	13.76
Case 6a	30	3.29	0.00	3.29	0.15	21.91
Case 6a	60	1.32	0.00	1.32	0.15	8.80
Case 6b	30	1.35	0.00	1.35	0.15	9.03
Case 6b	60	0.69	0.00	0.69	0.15	4.60
Case 6c	30	1.20	0.00	1.20	0.15	8.00
Case 6c	60	0.63	0.00	0.63	0.15	4.20
Case 6d	30	1.09	0.00	1.09	0.15	7.27
Case 6d	60	0.66	0.00	0.66	0.15	4.43
Case 6e	30	1.48	0.00	1.48	0.15	9.88
Case 6e	60	0.63	0.00	0.63	0.15	4.20
Case 6f	30	1.54	0.00	1.54	0.15	10.27
Case 6f	60	0.72	0.00	0.72	0.15	4.83
Case 6g	30	1.94	0.00	1.94	0.15	12.94
Case 6g	60	0.70	0.00	0.70	0.15	4.65
Case 6h	30	1.86	0.00	1.86	0.15	12.38
Case 6h	60	0.80	0.00	0.80	0.15	5.34
Case 6i	30	1.35	0.00	1.35	0.15	9.03
Case 6i	60	0.58	0.00	0.58	0.15	3.86
Case 6j	30	1.94	0.00	1.94	0.15	12.94
Case 6j	60	0.73	0.00	0.73	0.15	4.88
Case 6k	30	1.59	0.00	1.59	0.15	10.62
Case 6k	60	0.66	0.00	0.66	0.15	4.40
Case 6L	30	2.09	0.00	2.09	0.15	13.91
Case 6L	60	0.61	0.00	0.61	0.15	4.05

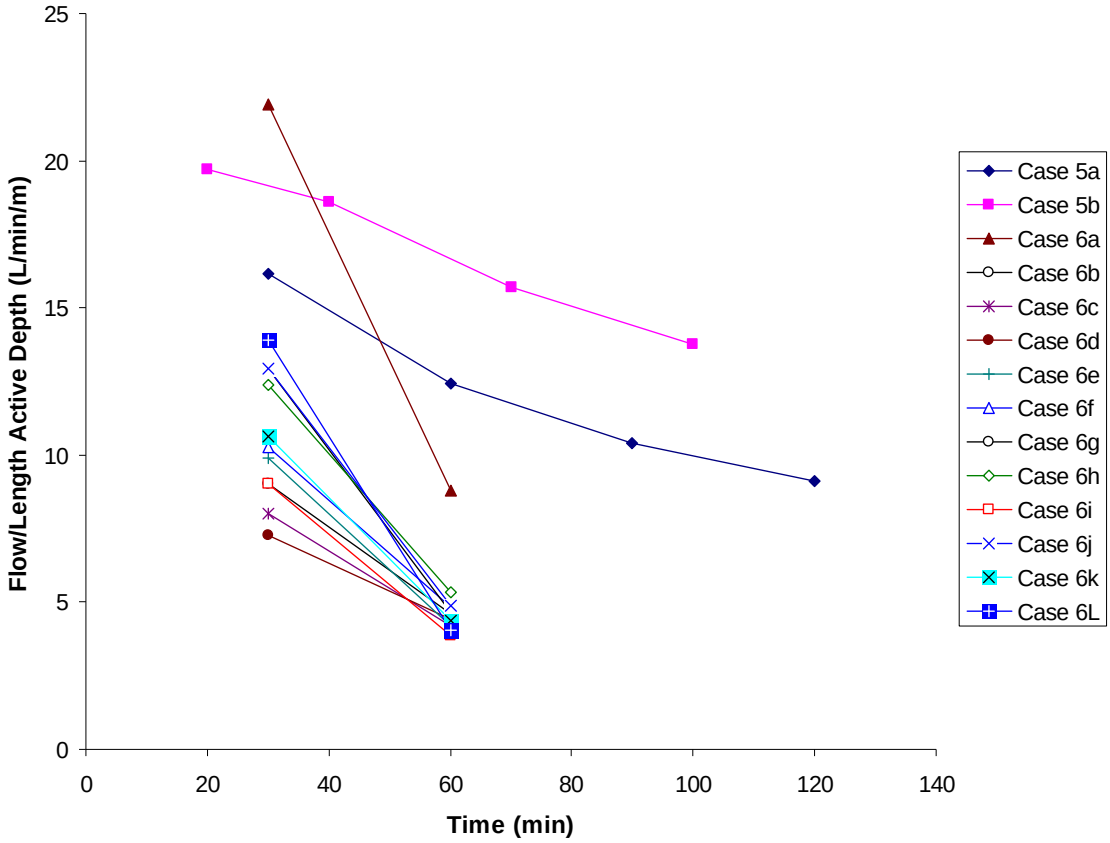

Figure 38. Laboratory Outflow Rate per Length Active Depth vs. Time (Setups 3 and 4)

3.4.3 Residual LNAPL biodiesel

The volume of biodiesel retained as residual in the sand after testing was determined by obtaining samples of the materials and analyzing the fluid contents within the sand. Seventeen samples of the sand were obtained for each lift in a pattern as depicted in Figure 39. The samples were obtained at measured depths from the sand surface in lifts. For Setup 3, samples were obtained at lifts of 0 cm, -15.2 cm, -30.5 cm, -45.7 cm, and -61.0 cm from the sand surface. For Setup 4, samples were obtained at lifts of 0 cm, -15.2 cm, -

25.4 cm, and -33.0 cm from the sand surface. The percent of biodiesel in the samples of the sand was determined gravimetrically by performing a volatile solids (VS) analysis as similarly described in Coulibaly and Borden (2004). The water content was determined by mass loss after drying for 48 hours at 110° C. Directly after water content determination, the biodiesel, or volatile solids, content was determined by mass loss after ignition at 550° C.

Following the determination of the biodiesel and water contents of all the samples, the sample data was developed into several different coordinate systems for mapping and quantity estimation purposes. For each lift, the sample location coordinates (x,y) and biodiesel content (z) was input into a coordinate system, in (x,y,z) format, to create a triangular irregular network (TIN). The TIN was used to analyze and quantify the LNAPL residual. Separate coordinate systems and TINs were developed for each lift and each vertical cross-section, as indicated in Figure 39, for Setups 3 and 4. Aerial plan views of the LNAPL residual distributions are displayed for the lifts in Figure 40 through Figure 47. Vertical cross-sections of the distributions are presented in the Appendix. A table is presented to the right of each distribution map. The table contains the beginning and the end of each range of the percent residual LNAPL biodiesel attributed to each color. Also displayed in each table is the percent of the total area contained within each range and the actual area of each range, in square inches.

For quality control purposes, a VS analysis was performed on five samples of the sand. The analysis of only the sand resulted in a mean VS content of 0.077% with a standard deviation of 0.029%.

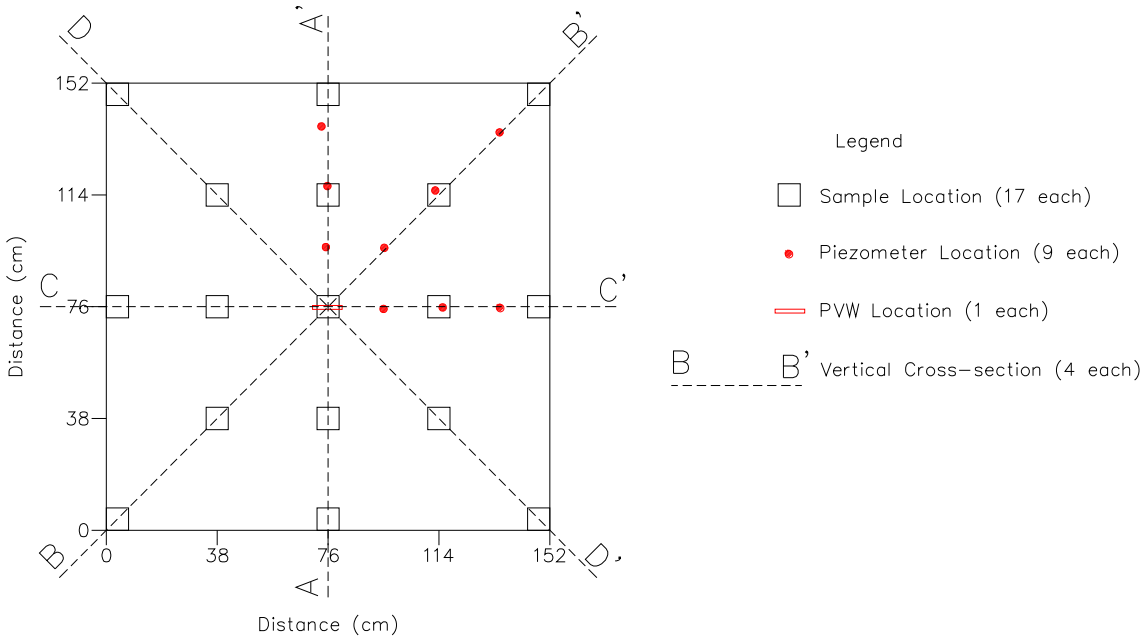

Figure 39. Post-Test Sand Sampling Plan View Layout

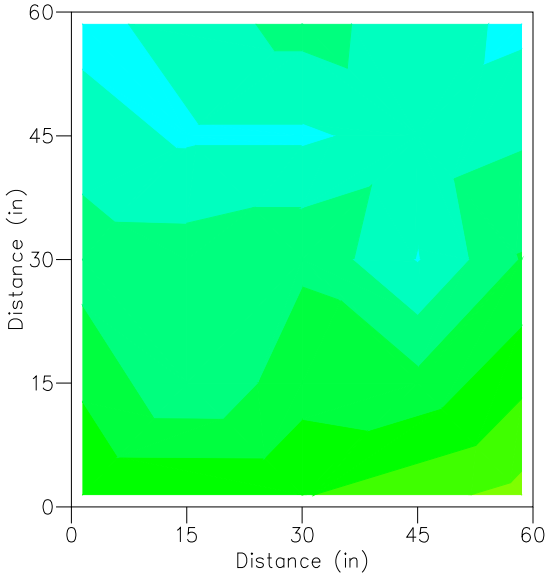

Legend

Color	Range Beg.	Range End	Percent	Area
	0.00	0.25	0.0	0.00
	0.25	1.00	0.0	0.00
	1.00	2.00	0.0	0.00
	2.00	2.25	5.2	170.10
	2.25	2.50	35.6	1156.26
	2.50	2.75	28.0	908.64
	2.75	3.00	16.6	539.28
	3.00	3.25	11.1	360.42
	3.25	3.50	3.3	107.58
	3.50	3.75	0.2	6.72
	3.75	4.00	0.0	0.00
	4.00	4.25	0.0	0.00
	4.25	4.50	0.0	0.00
	4.50	4.75	0.0	0.00
	4.75	5.00	0.0	0.00
	5.00	5.25	0.0	0.00

Figure 40. Plan View of LNAPL Distribution - Lift 1 (-0 cm), Setup 3

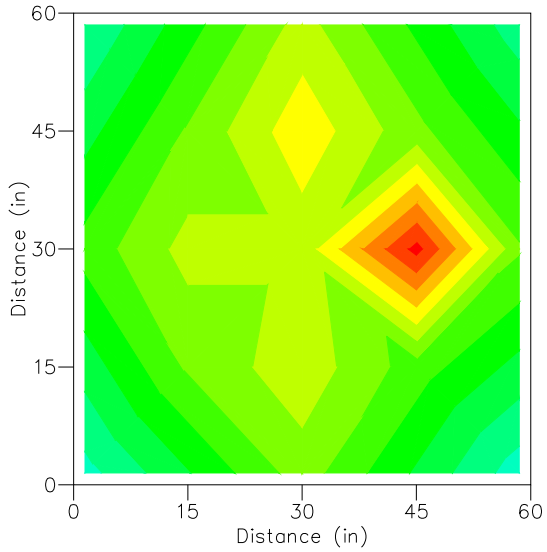

Legend

Color	Range Beg.	Range End	Percent	Area
	0.00	0.25	0.0	0.00
	0.25	1.00	0.0	0.00
	1.00	2.00	0.0	0.00
	2.00	2.25	0.0	0.00
	2.25	2.50	0.3	8.67
	2.50	2.75	3.2	103.91
	2.75	3.00	8.3	270.72
	3.00	3.25	13.6	442.11
	3.25	3.50	18.7	607.36
	3.50	3.75	26.0	843.15
	3.75	4.00	21.0	681.69
	4.00	4.25	4.8	155.08
	4.25	4.50	2.1	69.06
	4.50	4.75	1.4	44.91
	4.75	5.00	0.6	20.77
	5.00	5.25	0.0	1.56

Figure 41. Plan View of LNAPL Distribution - Lift 2 (-15.2 cm), Setup 3

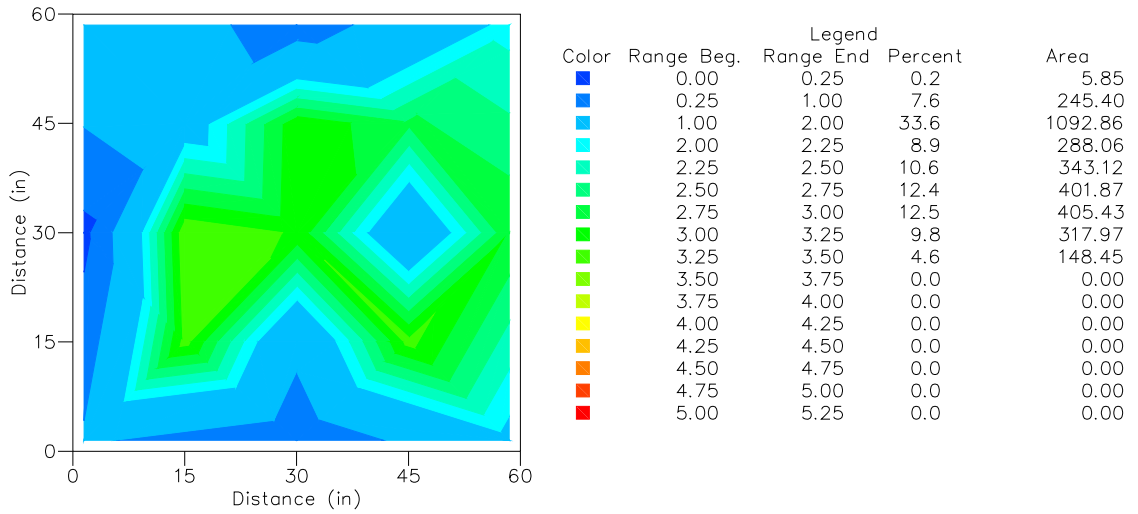

Figure 42. Plan View of LNAPL Distribution - Lift 3 (-30.5 cm), Setup 3

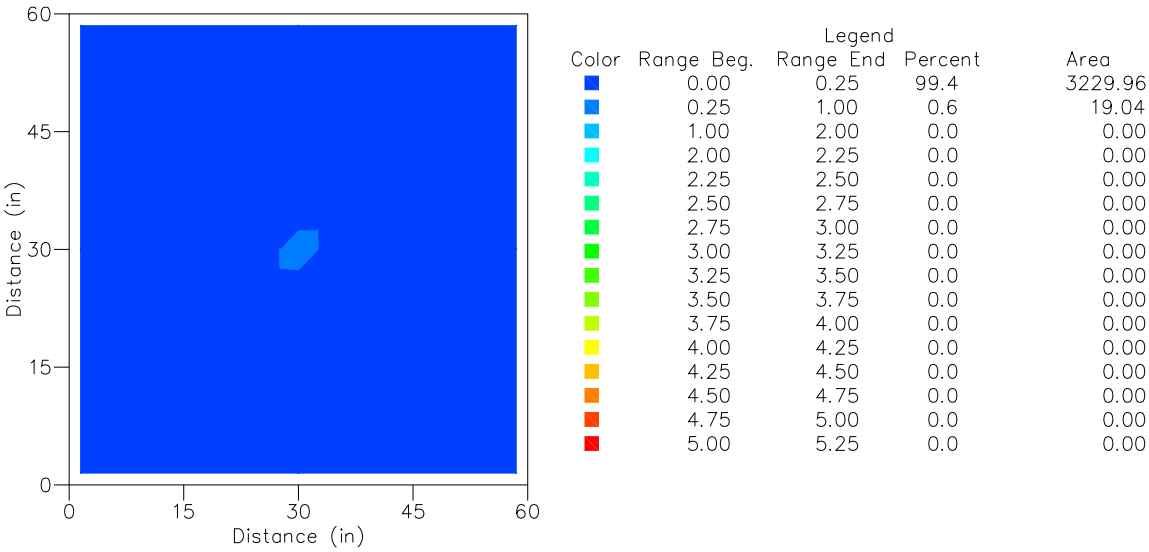

Figure 43. Plan View of LNAPL Distribution - Lift 4 (-45.7 cm), Setup 3

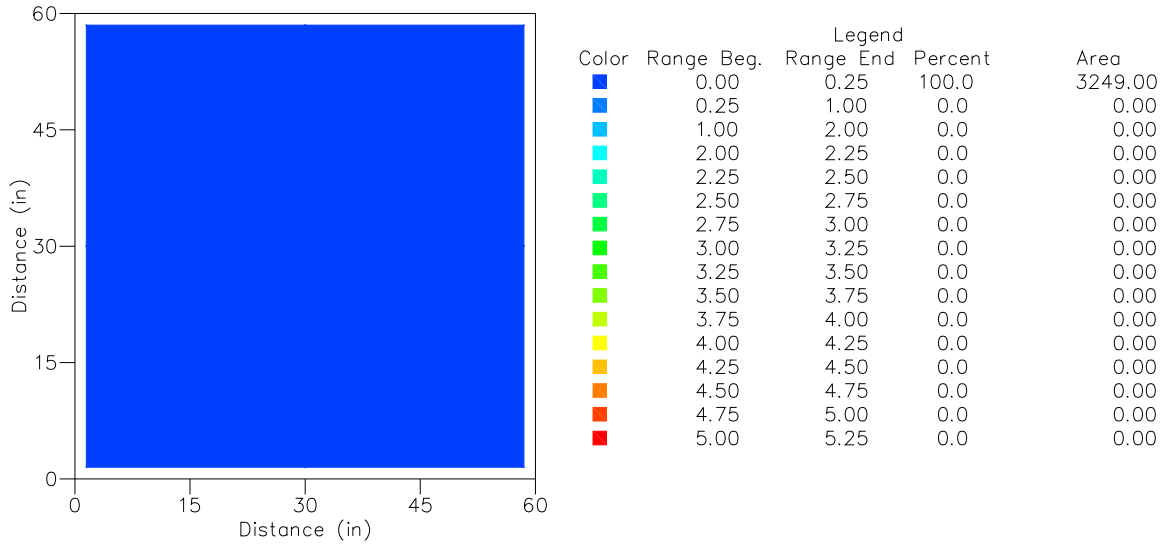

Figure 44. Plan View of LNAPL Distribution - Lift 5 (-61.0 cm), Setup 3

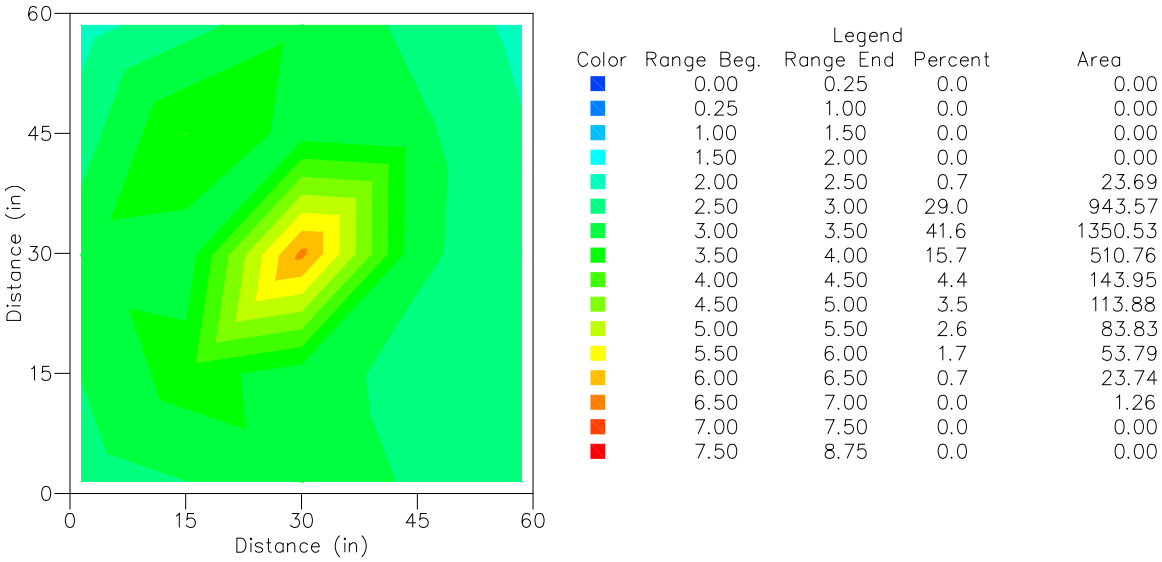

Figure 45. Plan View of LNAPL Distribution - Lift 1 (-0 cm), Setup 4

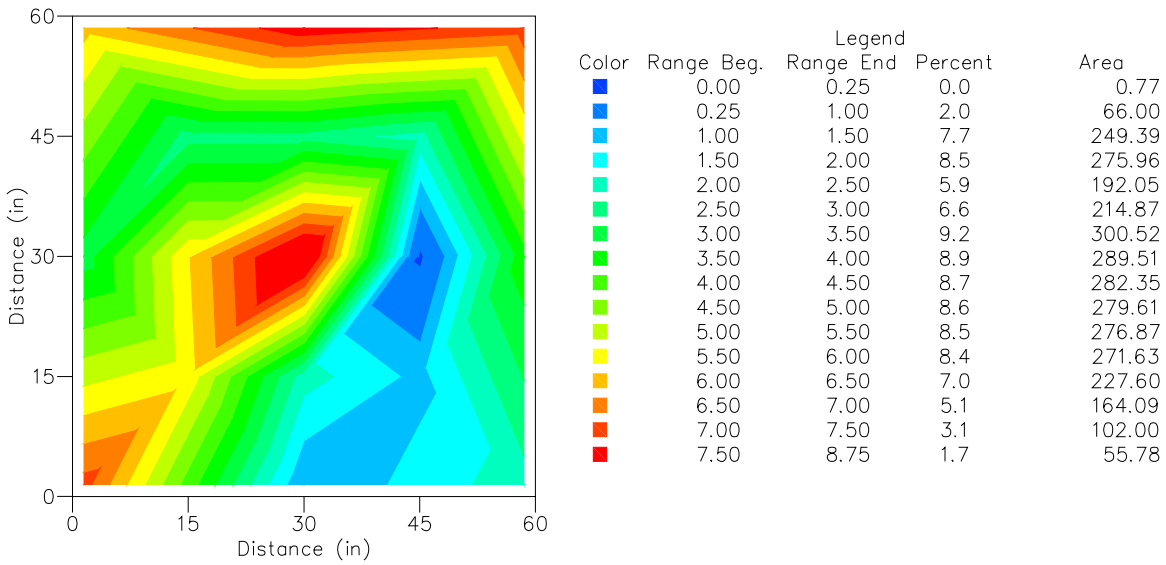

Figure 46. Plan View of LNAPL Distribution - Lift 2 (-15.2 cm), Setup 4

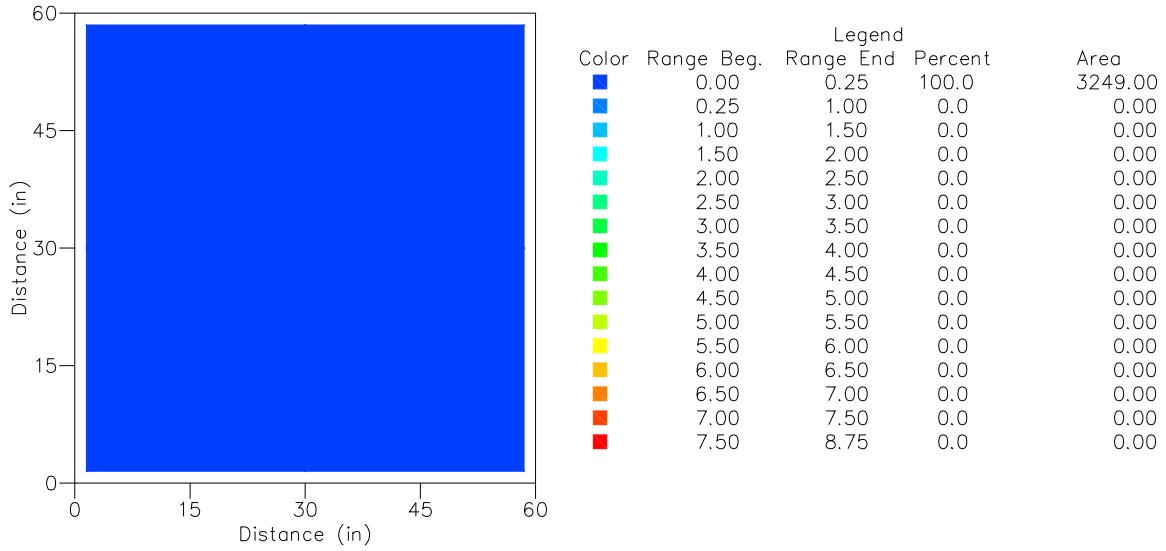

Figure 47. Plan View of LNAPL Distribution - Lift 3 (-25.4 cm), Setup 4

The final lift (-33.0 cm) of Setup 4 is not displayed because no LNAPL was measured, similarly to lift 3 of Setup 4.

The End Area method, a simple volume determination method, was used to determine the actual residual LNAPL volume, using the areas from the biodiesel distribution tables in conjunction with the lifts depths. The End Area method equation is presented as follows:

Equation 3

$$V = d_1 \frac{(A_1 + A_2)}{2} + d_2 \frac{(A_2 + A_3)}{2} + \ldots + d_{n-1} \frac{(A_{n-1} - A_n)}{2}$$

Where:
V = Volume (L^3)
d_n = Lift thickness (L)
A_n = Area (L^2)

In this case, the 'V' is actually the volume of the moist and contaminated soil within the area of the biodiesel content range. To determine the actual volume of residual LNAPL, 'V' is multiplied by the average content over the range. This will result in an average volume determination overall. If the upper portion of the range is used, a higher resulting residual volume would be determined, and visa versa if the lower bound of the range is used. Based on this method, the volume of residual LNAPL biodiesel for Setup 3 ranged from 36.5 L (9.64 gal) to 43.8 L (11.57 gal) with a median of 40.2 L (10.62 gal). In percentages of the total LNAPL, the residual LNAPL in the sand accounted for 48.0 % to 57.6 % with a median of 52.8 %. For Setup 4, the volume of residual LNAPL biodiesel for Setup 3 ranged from 26.5 L (7.00 gal) to 30.8 L (8.14 gal) with a median of 28.7 L (7.58 gal). In percentages of the total LNAPL, the residual LNAPL in the sand accounted for 34.9 % to 40.5 % with a median of 37.8%.

From the LNAPL distribution maps for Setup 3, with an active length of 31 cm and a placement depth of 65 cm, in Figure 40 through Figure 44, the distribution was spread in the sand down to approximately 46 cm (18") below the sand surface. For Setup 4, with an active length of 15 cm and a placement depth of 19 cm, with distribution maps shown from Figure 45 through Figure 47, the distribution was spread in the sand down less than 25 cm (10") below the sand surface. The quantity of residual LNAPL in Setup 3 (40.2 L) was significantly greater than that of Setup 4 (28.7 L), demonstrating a decrease in residual LNAPL of 28.6 % from Setup 3 to Setup 4. Based on the distribution of the residual LNAPL, Setup 3 produced the more desirable results by minimizing the LNAPL distribution in the subsurface domain and by extracting the greater volume of LNAPL.

3.4.4 Mass Balance of LNAPL

The recovered volume of LNAPL biodiesel was determined in both Setups 3 and 4 to evaluate the active length and placement depth effects on LNAPL extraction efficiency and to ensure mass balance. The mass of the LNAPL into the system in each case was 67.26 kg (76 L multiplied by the specific gravity of 0.885). The mass of LNAPL removed from the system was a combination of the total mass of free LNAPL extracted in each test and the mass of LNAPL dissolved in the extracted water. The mass of the gas phase of biodiesel was assumed to be negligible. The mass balance equation is as follows:

Equation 4

$$M_{in} = M_{free} + M_{dis} + M_{res} + M_{bio}$$

Where:
M_{in} = Mass of LNAPL placed in the system
M_{free} = Mass of free/mobile LNAPL
M_{dis} = Mass of dissolved LNAPL
M_{res} = Mass of residual LNAPL remaining in system
M_{bio} = Mass of LNAPL that biodegraded during testing process

Laboratory temperatures were maintained approximately between 20° C and 25° C. To simplify the mass balance equation further, the temperature of the water is assumed equal to the temperature of the biodiesel, and each mass term in Equation 4 can be replaced with volume. The total volume placed in each system during Phase II of testing was 76.0 L (20.08 gal).

For Setup 3, the total extracted volume was 1.5 L (0.40 gal). Testing was halted for Setup 3 after 220 minutes. The water table was gradually raised above the sand surface and allowed to equilibrate for 24 hours. An additional 8.7 L (2.30 gal) of free product was removed from the water table surface by skimming using vacuum and a tube. The low, median, and high residual volumes for Setup 3 were 36.5 L (9.65 gal), 40.2 L (10.61 gal), 43.8 L (11.57 gal), respectively. Therefore, the unaccounted LNAPL for Setup 3 is approximately between 22.0 L (5.8 gal) to 29.3 L (7.7 gal), with a median of 25.6 L (6.8 gal).

The total extracted volume for Setup 4 was 27.3 L (7.22 gal). The low, median, and high residual volumes for Setup 4 were 26.5 L (7.01 gal), 28.7 L (7.58 gal), and 30.8 L (8.14 gal), respectively. Hence, the unaccounted LNAPL for Setup 4 is approximately between 17.8 L (4.72 gal) to 22.1 L (5.85 gal), with a median of 20.0 L (5.28 gal). Dissolution and biodegradation accounts for these volumes, though the exact percentages of the two categories were not determined.

The large quantity of unaccounted LNAPL biodiesel as determined from the mass balance of the LNAPL was unforeseen in the early design of the laboratory experimentation. The review of literature pertaining to biodiesel suggested the LNAPL was immiscible with water and that dissolution would be minimal throughout the testing. The previously described tests performed on the LNAPL regarding volatility and solubility were performed after the large scale laboratory testing was complete. However, considering future research regarding biodiesel and considering the present information, the effluent water should be tested to determine dissolution of the LNAPL in the water extracted.

3.4.5 Vacuum Measurement

Vacuum pressures were measured along the PVW system during the testing for Setups 1, 2 and 3. Vacuum gauges were located (1) at the vacuum pump (2) at the tee leading to the PVW connection, and (3) at various locations along the PVW depending upon the active length. For Setup 1, three vacuum gauges were located along the PVW as depicted in

Figure 27. For Setups 2 and 3, two vacuum gauges were placed along the length of the PVW as depicted in Figure 28. Measurements of the vacuum pressures were obtained throughout the test duration. The vacuum pressures measured during testing for Setup 1, Setup 2, and Setup 3 are illustrated in Figure 48, Figure 49, and Figure 50, respectively. In Figure 49, though vacuum pressure was observed at the tee connection to the PVW, no vacuum pressure was observed within the PVW. For Setups 1 and 3, vacuum pressure was observed in the gauges placed in the upper portion of the PVWs. The vacuum pressure in the upper PVW gauge increased from 0 kPa to 3.4 kPa as the water table dropped in Setup 1. With Setup 4, the vacuum pressure in the upper gauge increased from 0 kPa to 6.8 kPa, also as the water table dropped.

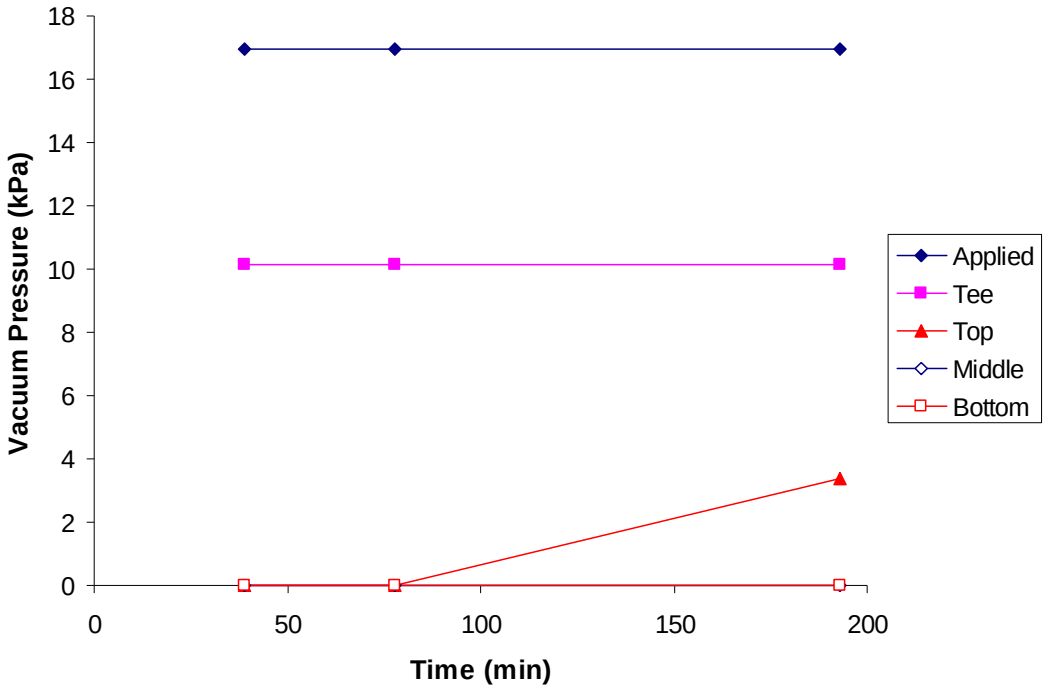

Figure 48. Vacuum Pressure vs. Time (Setup 1)

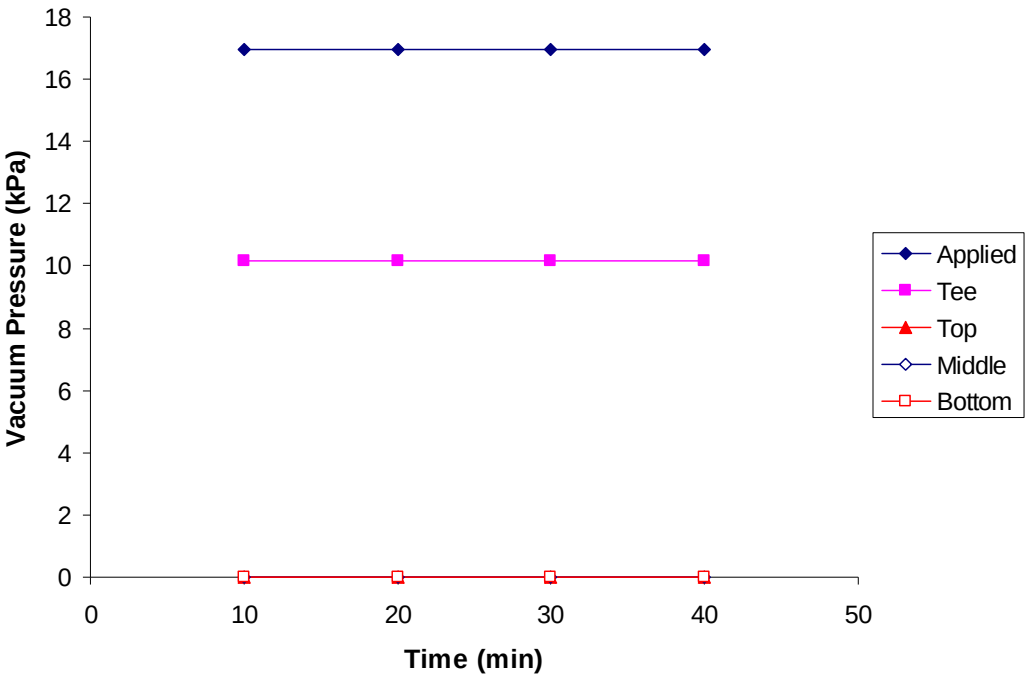

Figure 49. Vacuum Pressure vs. Time (Setup 2)

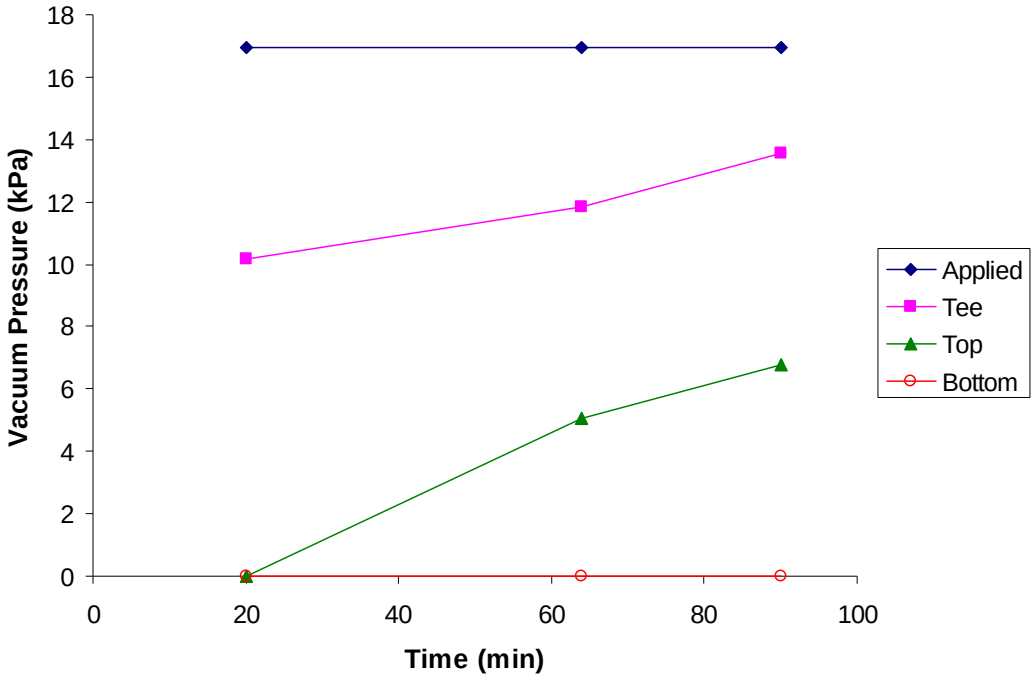

Figure 50. Vacuum Pressure vs. Time (Setup 3, test 2)

3.4.6 Hydraulic Head

The total head distribution was determined by measuring the water surface elevation in each piezometer during testing for transient water table conditions. Contour maps of the total hydraulic head are displayed in Figure 51 through Figure 53, for Setups 1 and 2. The contour maps display the hydraulic head in the instrumented quadrant for each test at the end of each test period. The (x,y) coordinate axis indicate the location, in inches, inside the test box, with dimensions 152 cm (60") by 152 cm (60"). The center of the PVW was located approximately at x = 76 cm (30") and y = 76 cm for all cases. Each contour indicates an elevation, in inches, above the datum (bottom of the test box).

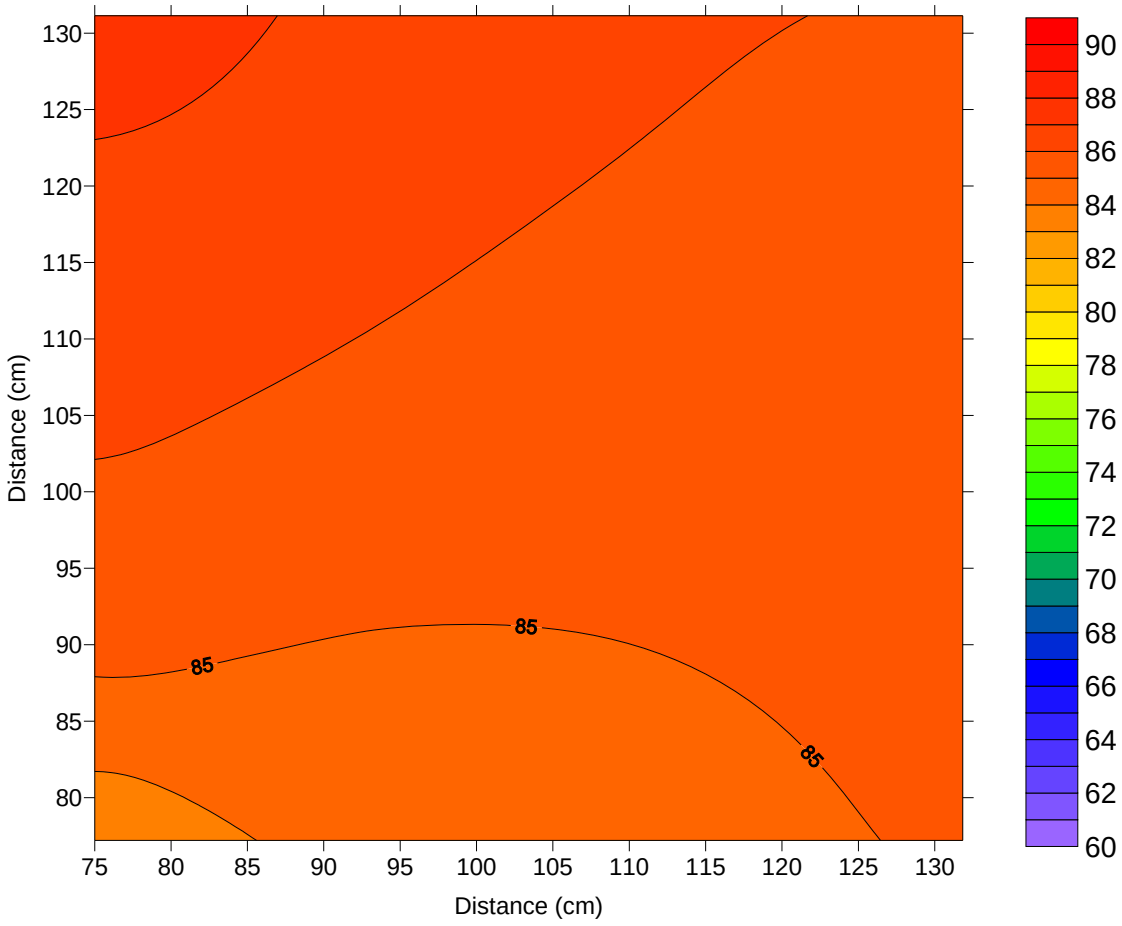

Figure 51. Total Hydraulic Head (inches) Contour Map for Setup 1, Case 1 Final, Inflow = 0.95 L/min (Datum = Bottom of Test Box)

As shown in Figure 51, the contours appear more irregular and the heads are higher compared to those in Figure 52 and Figure 53, indicating the effect of inflow. The outflow was consistently greater than 0.96 L/min (0.25 gpm) (water vapor was not included in this case.) The total head difference between the highest and the lowest elevation in the contours displayed in Figure 53 is greater than the total head difference in the contours shown in Figure 52. In summary, Setup 2, with an active depth of 31 cm (12.2”), exhibited higher outflow rates than Setup 1, with an active depth of 61 cm (24.0”). Based on the

contour maps of the hydraulic head, there is a difference in the total drawdown between the two Setups with the different PVWs' active length.

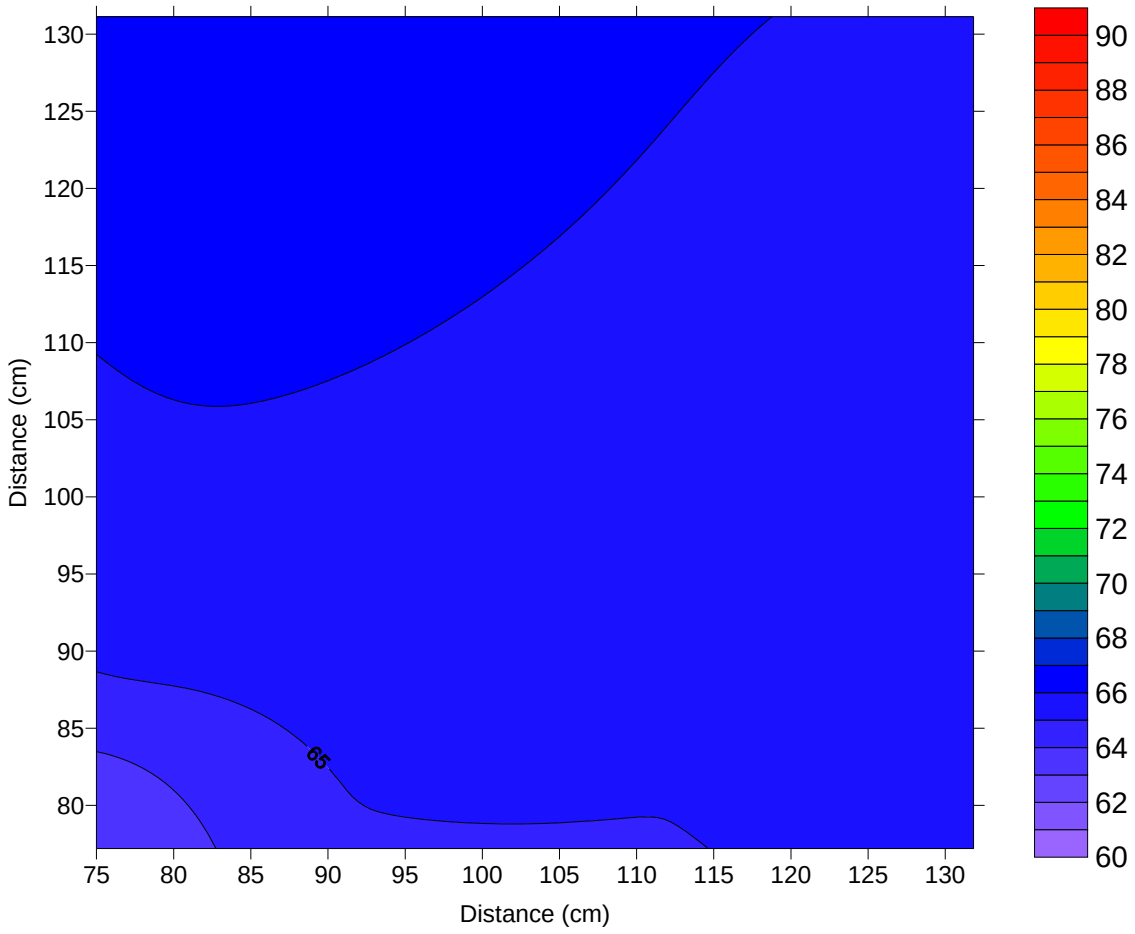

Figure 52. Total Hydraulic Head (inches) Contour Map for Setup 1, Case 3, Inflow = 0.0 L/min (Datum = Bottom of Test Box)

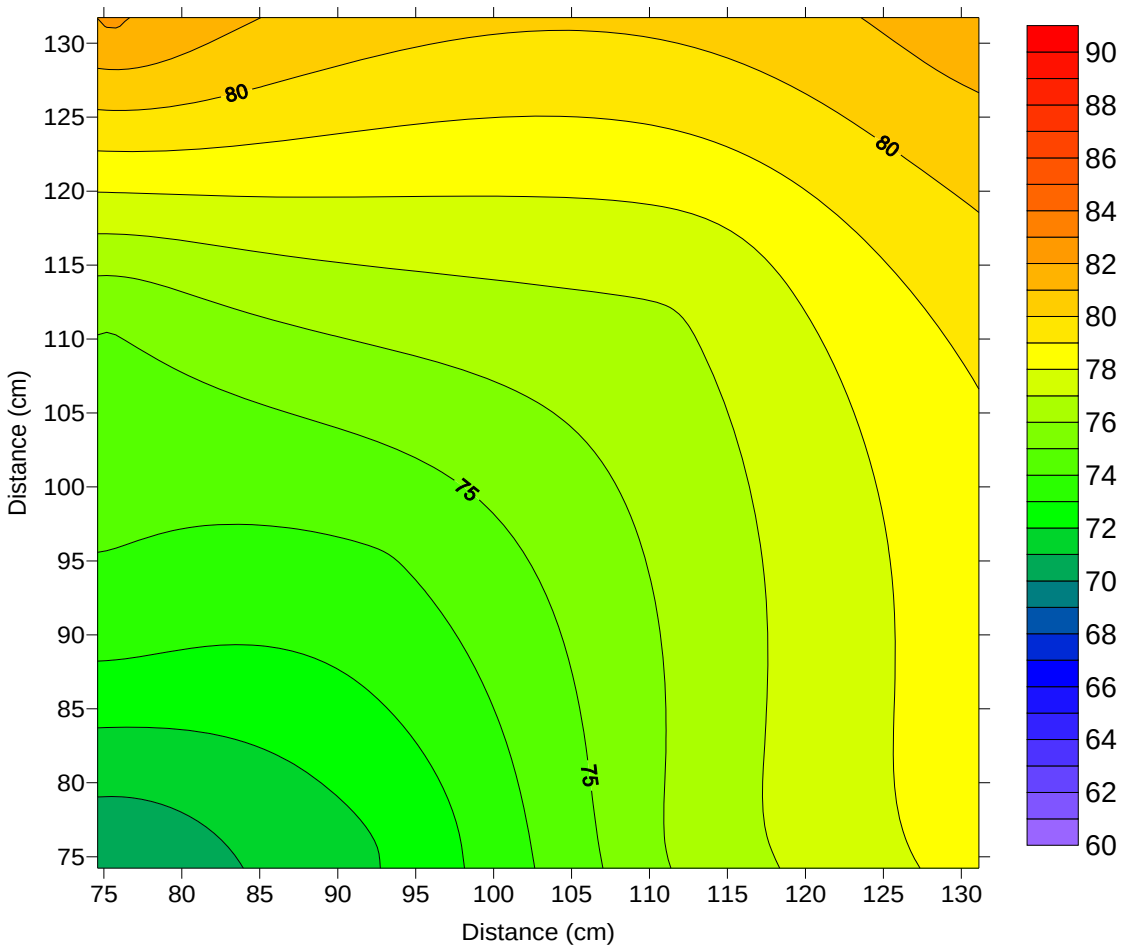

Figure 53. Total Hydraulic Head (inches) Contour Map for Setup 2, Case 4 Final, Inflow = 0 L/min (Datum = Bottom of Test Box)

To better understand the difference in the outflow rates for each Setup, Darcy's law as presented in Equation 1 is used to further evaluate the results. The equation is simplified as presented below in Equation 5:

Equation 5

$$q = kiA$$

Where:
q = Fluid flow (m^3/s)
k = Permeability (m/s)
I = Hydraulic gradient (m/m)
A = Cross sectional area of flow(m^2)

Equation 5 can also be rewritten in terms of the hydraulic gradient as shown in Equation 6.

Equation 6

$$i = \frac{q}{kA}$$

The cross sectional area is assumed equivalent to the area per unit length of the PVW (and can be defined in term of gross area or area of voids.) The same PVW section was used for all setups. Therefore, to account for the area and simplify Equation 6, the flow rate is normalized by dividing it by the active length of the PVW for each respective Setup. This procedure results in normalized flow rate, q^*, and is incorporated in Equation 7.

Equation 7

$$i = \frac{q^*}{k}$$

The permeability of the samples in each setup is assumed to be 6.9×10^{-5} m/s, an average of the permeabilities measured. With the aforementioned equations, the hydraulic gradient induced by each respective setup is presented in Table 12 for Phase I testing and Table 13 for Phase II testing. Figure 54 illustrates a portion of the test box and the total hydraulic head produced, for both Setups 1 and 2, along piezometers P7 through P9.

Table 12. Hydraulic Gradients (Setups 1 and 2)

Case	Time (min)	Outflow rate (m^3/min)	Inflow Rate (m^3/min)	Net Flow Rate (m^3/min)	Active Length (m)	q* (m^3/min/m)	k (m/s)	i (m/m)
Case 1a, 1b	39	1.4E-03	9.6E-04	4.3E-04	0.61	2.3E-03	6.9E-05	0.55
Case 2a, 2b	39	2.0E-03	2.3E-03	-3.7E-04	0.61	3.2E-03	6.9E-05	0.78
Case 3	116	9.7E-04	0.0E+00	9.7E-04	0.61	1.6E-03	6.9E-05	0.38
Case 4	10	5.4E-03	0.0E+00	5.4E-03	0.31	1.7E-02	6.9E-05	4.18
Case 4	20	4.9E-03	0.0E+00	4.9E-03	0.31	1.6E-02	6.9E-05	3.78
Case 4	30	4.6E-03	0.0E+00	4.6E-03	0.31	1.5E-02	6.9E-05	3.58
Case 4	40	4.2E-03	0.0E+00	4.2E-03	0.31	1.4E-02	6.9E-05	3.30

Table 13. Hydraulic Gradients (Setups 3 and 4)

Case	Time (min)	Outflow rate (m^3/min)	Inflow Rate (m^3/min)	Net Flow Rate (m^3/min)	Active Length (m)	q* (m^3/min/m)	k (m/s)	i (m/m)
Case 5a	30	5.0E-03	2.0E-03	3.0E-03	0.31	1.6E-02	6.9E-05	3.90
Case 5a	60	3.8E-03	2.0E-03	1.8E-03	0.31	1.2E-02	6.9E-05	3.00
Case 5a	90	3.2E-03	2.0E-03	1.2E-03	0.31	1.0E-02	6.9E-05	2.51
Case 5a	120	2.8E-03	2.0E-03	8.3E-04	0.31	9.1E-03	6.9E-05	2.20
Case 5b	20	6.1E-03	4.2E-03	1.9E-03	0.31	2.0E-02	6.9E-05	4.76
Case 5b	40	5.8E-03	4.2E-03	1.6E-03	0.31	1.9E-02	6.9E-05	4.50
Case 5b	70	4.9E-03	4.2E-03	6.7E-04	0.31	1.6E-02	6.9E-05	3.80
Case 5b	100	4.3E-03	4.2E-03	6.6E-05	0.31	1.4E-02	6.9E-05	3.32
Case 6a	30	3.3E-03	0.0E+00	3.3E-03	0.15	2.2E-02	6.9E-05	5.29
Case 6a	60	1.3E-03	0.0E+00	1.3E-03	0.15	8.8E-03	6.9E-05	2.13
Case 6b	30	1.4E-03	0.0E+00	1.4E-03	0.15	9.0E-03	6.9E-05	2.18
Case 6b	60	6.9E-04	0.0E+00	6.9E-04	0.15	4.6E-03	6.9E-05	1.11
Case 6c	30	1.2E-03	0.0E+00	1.2E-03	0.15	8.0E-03	6.9E-05	1.93
Case 6c	60	6.3E-04	0.0E+00	6.3E-04	0.15	4.2E-03	6.9E-05	1.01
Case 6d	30	1.1E-03	0.0E+00	1.1E-03	0.15	7.3E-03	6.9E-05	1.76
Case 6d	60	6.6E-04	0.0E+00	6.6E-04	0.15	4.4E-03	6.9E-05	1.07
Case 6e	30	1.5E-03	0.0E+00	1.5E-03	0.15	9.9E-03	6.9E-05	2.39
Case 6e	60	6.3E-04	0.0E+00	6.3E-04	0.15	4.2E-03	6.9E-05	1.01
Case 6f	30	1.5E-03	0.0E+00	1.5E-03	0.15	1.0E-02	6.9E-05	2.48
Case 6f	60	7.2E-04	0.0E+00	7.2E-04	0.15	4.8E-03	6.9E-05	1.17
Case 6g	30	1.9E-03	0.0E+00	1.9E-03	0.15	1.3E-02	6.9E-05	3.13
Case 6g	60	7.0E-04	0.0E+00	7.0E-04	0.15	4.7E-03	6.9E-05	1.12
Case 6h	30	1.9E-03	0.0E+00	1.9E-03	0.15	1.2E-02	6.9E-05	2.99
Case 6h	60	8.0E-04	0.0E+00	8.0E-04	0.15	5.3E-03	6.9E-05	1.29
Case 6i	30	1.4E-03	0.0E+00	1.4E-03	0.15	9.0E-03	6.9E-05	2.18
Case 6i	60	5.8E-04	0.0E+00	5.8E-04	0.15	3.9E-03	6.9E-05	0.93
Case 6j	30	1.9E-03	0.0E+00	1.9E-03	0.15	1.3E-02	6.9E-05	3.13
Case 6j	60	7.3E-04	0.0E+00	7.3E-04	0.15	4.9E-03	6.9E-05	1.18
Case 6k	30	1.6E-03	0.0E+00	1.6E-03	0.15	1.1E-02	6.9E-05	2.56
Case 6k	60	6.6E-04	0.0E+00	6.6E-04	0.15	4.4E-03	6.9E-05	1.06
Case 6L	30	2.1E-03	0.0E+00	2.1E-03	0.15	1.4E-02	6.9E-05	3.36
Case 6L	60	6.1E-04	0.0E+00	6.1E-04	0.15	4.1E-03	6.9E-05	0.98

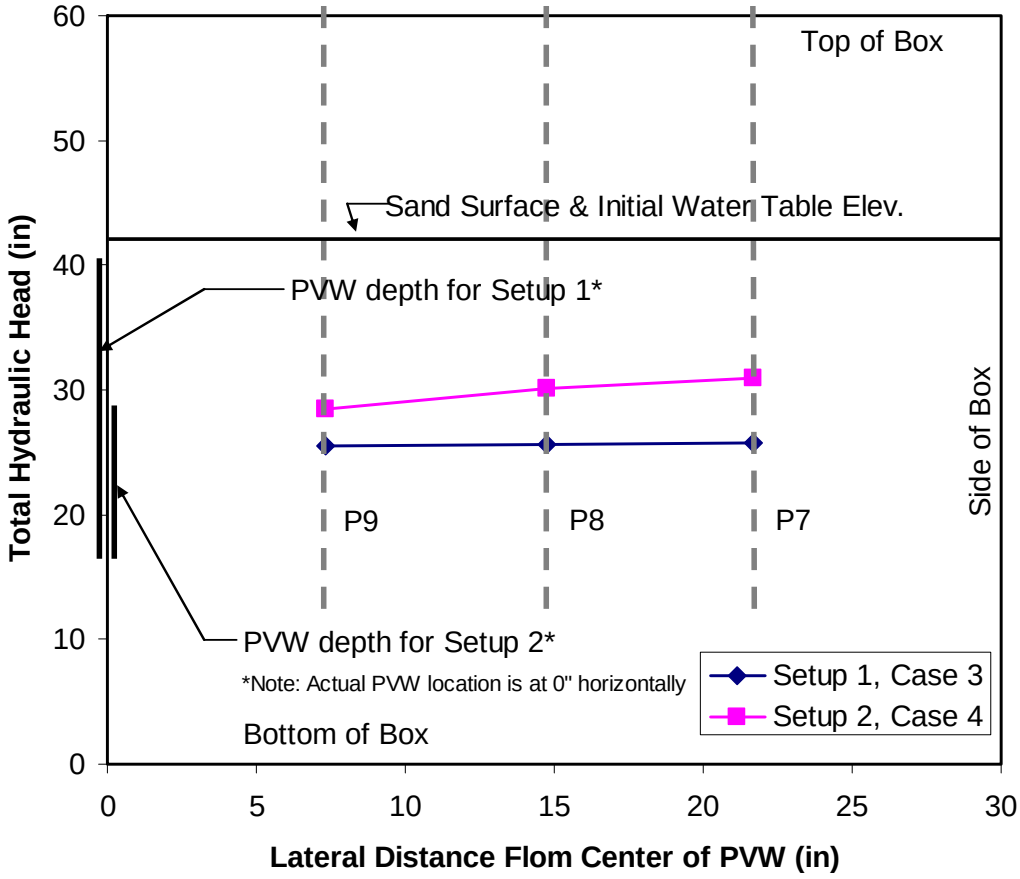

Figure 54. Total Hydraulic Head as a Function of Lateral Distance From the Center of PVW (Piezometers P7-P9) (Setup 1 and 2)

The mean extraction outflow rates were $1.4x10^{-3}$ m/s, $4.8x10^{-3}$ m/s, $4.5x10^{-3}$ m/s, and $1.2x10^{-3}$ m/s with standard deviations of $4.99x10^{-4}$ m/s, $4.73x10^{-4}$ m/s, $1.2x10^{-3}$ m/s, and $6.6x10^{-4}$ m/s for Setups 1, 2, 3, and 4 respectively. The mean hydraulic gradients were 0.57, 3.71, 3.50, and 1.98 with standard deviations of 0.197, 0.368, 0.908, and 1.070 for Setups 1, 2, 3 and 4, respectively.

Data in Table 12 and Figure 54 indicate that hydraulic gradients achieved by the smaller active length are higher than those from the PVW with longer active length at the same placement depth. Even though the active length for Setup 2 and 3 is roughly half the active length for Setup 1, the nearly one order of magnitude higher flow rate observed from Setup 2 and 3 can be explained by the higher value of hydraulic gradient. As such, it may be advantageous in the field to reduce the size of the active length while ensuring that the limits of the capture zone cover the extraction domain. The shorter length process is advantageous for liquid removal. Since vapor removal is performed under vacuum, a capture zone with a gradient is created at the location of the PVWs. Accordingly the shorter length should still be effective in vapor removal, although this specific aspect has not been evaluated in the lab.

Assuming that the permeability is constant throughout the sample and that Darcy's Law is valid, Figure 55 illustrates the relationship between the active length and depth of placement for all setups. Both Setups 1 and 4 placed the upper portion of the PVW within 4 cm (1.6") of the sand surface, and Setup 1 produced extraction flow rates approximately in the same range as Setup 4. However, the hydraulic gradients observed for Setup 4 were approximately 4 to 5 times greater than those for Setup 1, at the same flow rate. With Setups 2 and 3 having the same geometric PVW configuration, the same linear trend is observed for both. The slope of the results is directly proportional to the active length of the PVW; however, the ranges of the outflow and hydraulic gradient along this linear trend are a function of the depth of placement within the subsurface. With the top of the PVW

being 4 cm (1.6”) from the sand surface, the ranges of outflows and hydraulic gradients for Setups 1 and 4 are closer to the origin than that of Setups 2 and 3, where the top of the PVW was 34 cm (13.4”) below the sand surface.

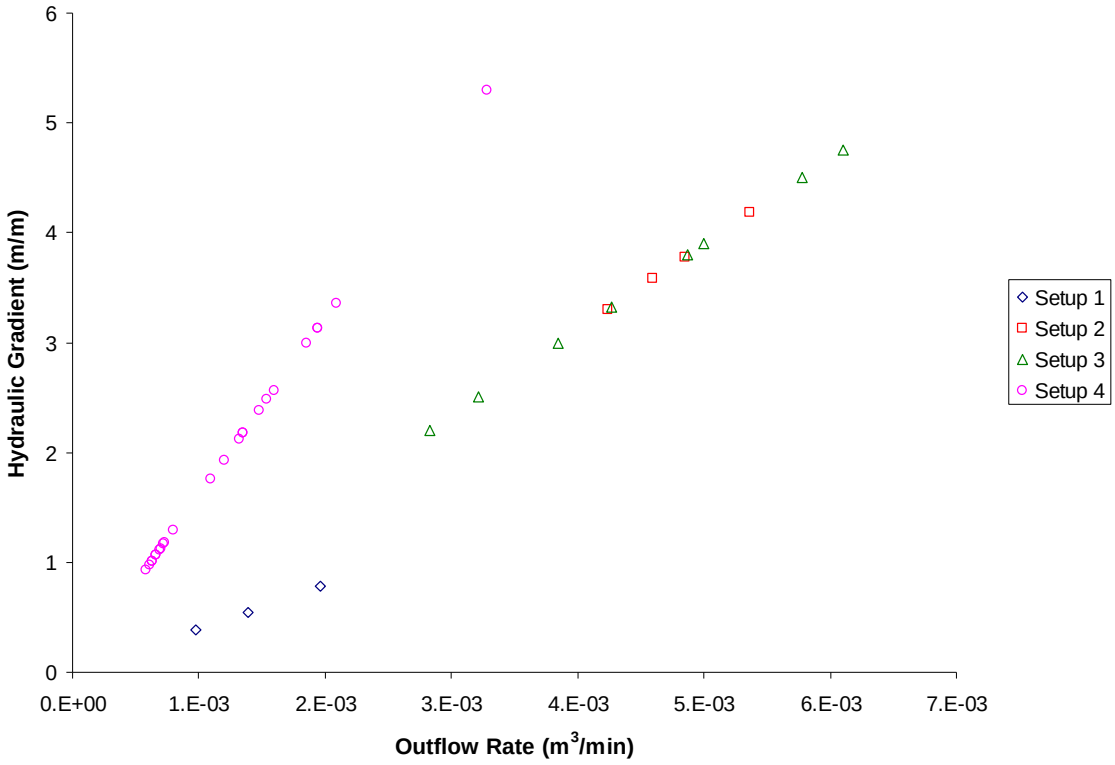

Figure 55. Hydraulic Gradient vs. Outflow Rate

Figure 56 presents the relationship of the hydraulic gradient to time over the testing periods. Setup 1 exhibited the lower hydraulic gradients and the least change in gradient over the testing period. Setups 2 and 3 exhibited the highest gradients with similar trends in the rate of change of the gradient. Setup 4 produced the steepest decline in hydraulic gradient, which can be attributed to the shortest active length of all the setups.

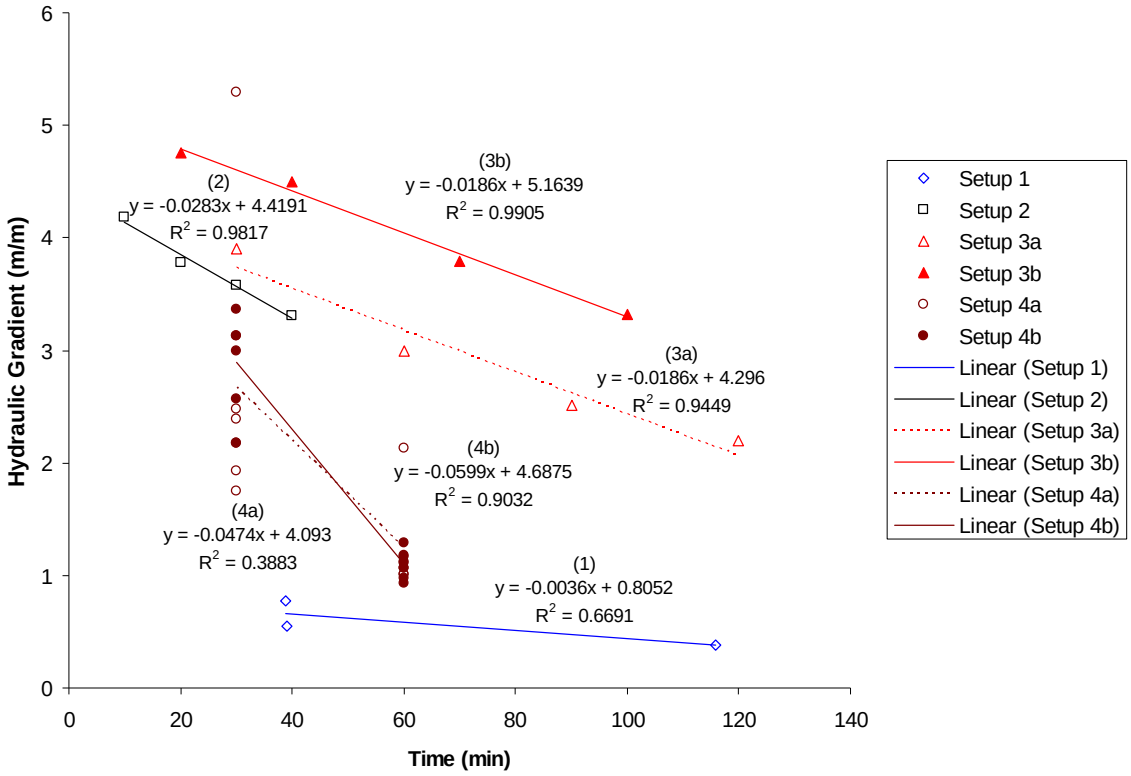

Figure 56. Hydraulic Gradient vs. Time

3.4 Laboratory Experimentation Summary

Laboratory experimentation was conducted to investigate the Cofra PVW system performance, while varying the active depth of the PVW and PVW depth of placement. The first phase of experimentation was to evaluate the system with the extraction of water only, and the second phase was to evaluate the system performance for LNAPL biodiesel extraction.

The laboratory test soil was a fine homogeneous sand. Tests were performed on the sand that was methodically placed in a waterproofed steel test box. Two methods were used in

placing the sand for testing, which resulted in and average unit weight of 16.23 kN/m^3 (103.3 pcf) for the first method used on Setup 1 and an average unit weight of 15.21 kN/m^3 (96.8 pcf) for the second method used on Setups 2, 3, and 4. All tests were comprised of applying 16.9 kPa (5 ”Hg) vacuum pressure to the PVW system while monitoring flow rates and head distribution. The prototype PVW system, as developed by Cofra, consisted of a single geocomposite PVW, quick connect pipe components, and HDPE piping. A vacuum was applied to the PVW system using a barrel-mounted venturi vacuum to extract air, water, and biodiesel. Vacuum gauges were installed throughout the system to monitor the vacuum pressures over time. The test sand was instrumented with piezometers to measure the hydraulic head distribution.

Using the configurations as presented in Setups 1 through 4, a total of 21 tests were conducted. The PVW active lengths studied in the laboratory testing included 0.61 m (2.0 ft), 0.31 m (1.0 ft), 0.31 m (1.0 ft), and 0.15 m (0.5 ft) for Setups 1, 2, 3, and 4, respectively. Vacuum pressures were measured in the PVW for Setups 1 through 3 and at the quick connect tee for all setups. A loss of pressure of approximately 6 kPa was observed from the venturi vacuum to the vacuum gauge at the tee. Vacuum pressures were not observed in the PVW generally until the water table dropped below the point of measurement in the PVW.

The mean extraction outflow rates were 1.4×10^{-3} m/s, 4.8×10^{-3} m/s, 4.5×10^{-3} m/s, and 1.2×10^{-3} m/s and the mean hydraulic gradients were 0.57, 3.71, 3.50, and 1.98 for Setups 1,

2, 3 and 4, respectively. Phase II of testing, comprised of Setups 3 and 4, included the placement of 76.0 L (20.08 gal) of LNAPL biodiesel into the system on the water table. For Setups 3 and 4, the volume of free product extracted was 1.5 L (0.40 gal) and 36.0 L (9.51 gal) respectively. The median residual LNAPL remaining in the system was determined as 40.2 L (10.62 gal) and 28.7 L (7.58 gal). The remaining biodiesel unaccounted for can be attributed to dissolution and biodegradation.

4. MODEL DEVELOPMENT

Groundwater and contaminant transport modeling was utilized for the analysis of the system performance. The modeling was intended to aid in studying effectiveness and time dependence of the remediation approach within the test sample and to develop an optimized scheme of operation addressing a given contaminant phase extraction mode. In this case, several issues were investigated, including variation of groundwater and contaminant profile with varying extraction times, and the possibility of lowering the groundwater in the test area such that circulation of air can be implemented to assist in the extraction of LNAPL residual saturation. The modeling study consists of two parts: i) groundwater modeling using SEEP/W, ii) contaminant transport modeling using Bioslurp. Both of these codes are based on continuum analyses of the flow domain using the finite element approach.

4.1 Groundwater Modeling

The groundwater flow was modeled using SEEP/W version 5, by Geo-Slope International. The advantage of this program is the ability to perform the analysis under coupled saturated and unsaturated conditions. The SEEP/W code is used to determine hydraulic heads distribution due to the extracted flow rate as well as permeability variations with induced vacuum within the subsurface environment.

4.1.1 Model Description

Modeling using SEEP/W considers the subsurface profile as an axi-symmetric media for evaluation of hydraulic head distributions and changes in saturation fronts. Material properties required for analysis for the soil type include grain size distribution, volumetric water content (volume of water/total volume) function, and hydraulic conductivity function. A permeability ratio is required if anisotropic conditions are to be modeled, which was not the case for this experiment.

Volumetric water content functions are used for modeling unsaturated conditions, since water content variations (or the amount of saturation) affect hydraulic conductivity values. SEEP/w provides the capability of defining volumetric water content and hydraulic conductivity functions based on methods developed by Arya and Paris (1981) and Fredlund and Xing (1994), among others. The hydraulic conductivity variation with suction head is then developed from the corresponding volumetric water content function. SEEP/W uses the relationships developed by Green and Corey (1971), among others, to estimate the hydraulic conductivity distribution with matric suction based on the soil-water characteristics relationship.

4.1.2 Model Parameters

Finite element analyses was performed on the two scenarios tested in Phase II, with generally the same conditions except for the PVW active depth and depth of placement as

described: (i) Setup 3 with a PVW active length = 30 cm, where the bottom of the PVW is located 65 cm from the surface of the sand (ii) Setup 4 with a PVW active length = 15 cm, where the bottom of the PVW is located 19 cm from the surface of the sand.

Model parameters such as the extraction rates, recharge rates, hydraulic conductivity, and well diameter were obtained from actual measurements and laboratory testing results. The PVW used in this research has dimensions of 4.34 mm by 100 mm, with a circumference of 208 mm. According to Kjellman (1948), the circumference of the PVW is more significant than the cross sectional area, and an equivalent diameter d_e, of 66 mm was used to model the PVW.

The mesh used in the finite element analyses was comprised of 3146 nodes and 3030 elements (quadrilaterals) for Setup 3 and 3584 nodes and 3458 elements (quadrilaterals) for Setup 4. The meshes for Setup 3 and Setup 4 are shown in Figure 57 and Figure 58, respectively. The figures illustrate the water table locations, the PVW locations, and the boundary conditions imposed on the models. The solid (blue) triangles at the bottom and the right side of the mesh represent a "no flow" boundary. The solid (green) triangles applied across the length of the PVWs located on the left represent unit fluxes to account for the extraction flow rates. Unit fluxes are also applied on the top of the mesh for scenario (i) to represent inflow. Table 14 presents the input and layout parameters for SEEP/w.

The model idealization considers a PVW at the center of the idealized domain. Because the program was operated in axi-symmetric mode, the model considers a "1 radian" thick slice of a circular domain. Therefore, Figure 57 and Figure 58 represent a 1 radian thick slice with a domain radius of 0.76 m (2.5 ft) and a well radius of 33 mm (1.3"). For this type of analysis, the program considers the y-axis (or the left side of the graph) as the rotation point, and the x-axis as the radius of the domain. Because of the axial symmetry requirement for the input, certain adaptations to the actual laboratory parameters were necessary. These adaptations were mainly associated with the well spacing, and subsequent flow rates.

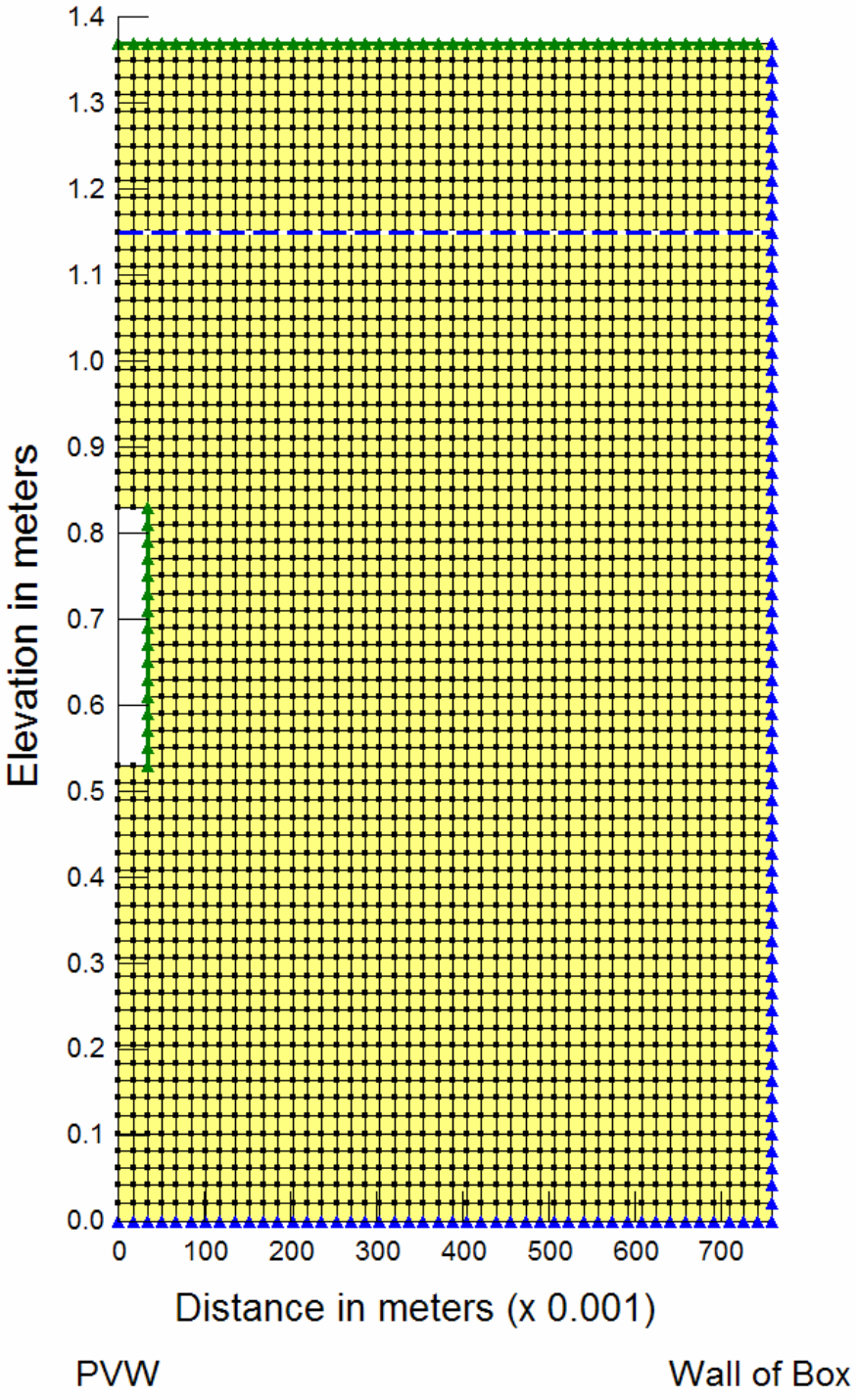

Figure 57. Discretized Mesh Generated in SEEP/W for Setup 3

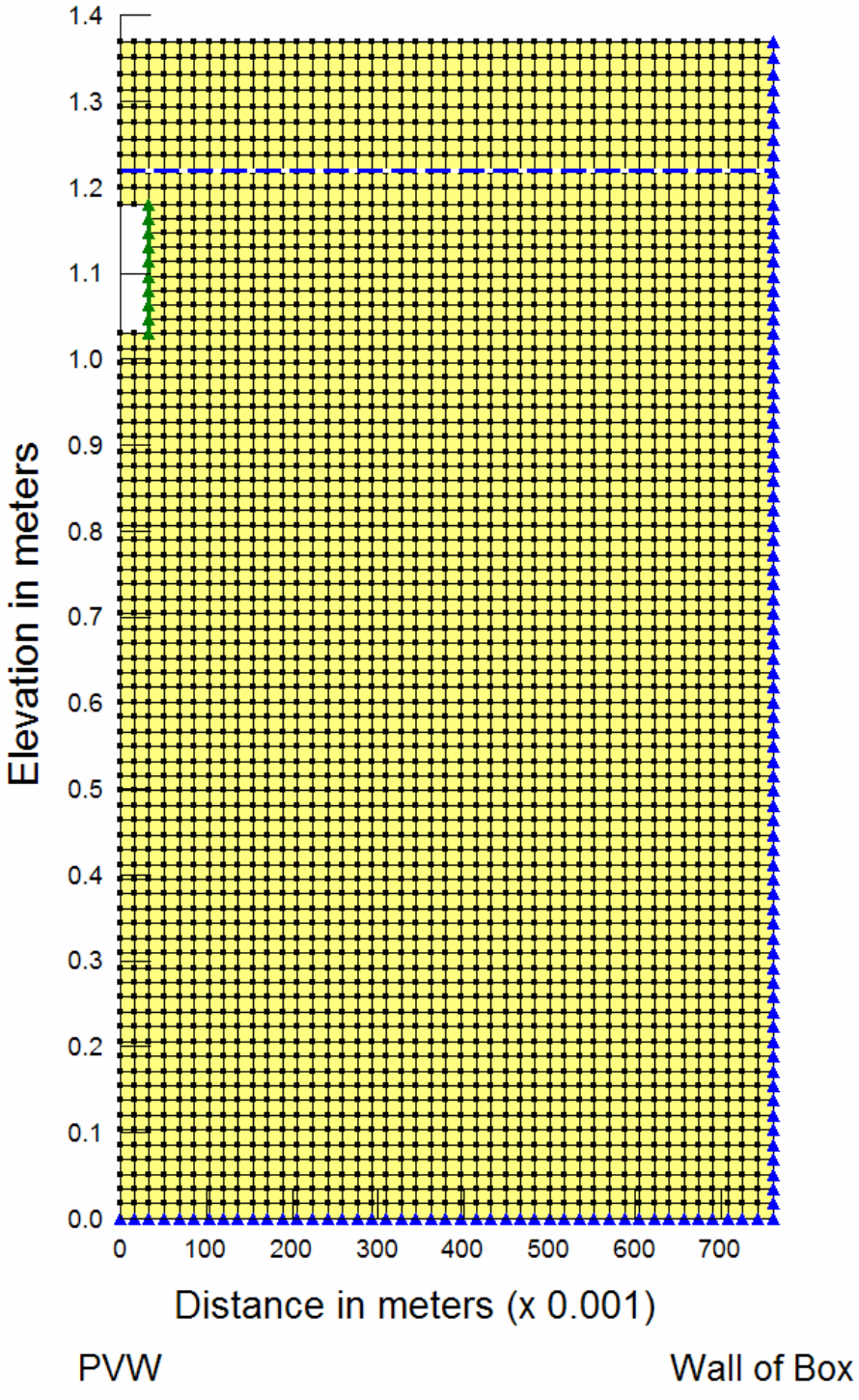

Figure 58. Discretized Mesh Generated in SEEP/W for Setup 4

Table 14. SEEP/W Input and Layout Parameters

Test Setup Description		Setup 3	Setup 4
Parameter Description	**Units**	**Parameter Values**	
Horizontal Elements (Nodes)		45(46)	44 (45)
Vertical Elements (Nodes)		68(69)	79(80)
Total Elements (Nodes)*		3030 (3146)	3458 (3584)
PVW Active Length	m	0.30	0.15
Unit Weight of Water	kN/m^3	9.807	9.807
Simulation Time	min	60	60
Porosity**		0.4	0.4
Gravimetric Water Content @ Saturation	%	25	25
Volumetric Water Content @ Saturation	%	40	40
Hydraulic Conductivity**	m/s	6.9E-05	6.9E-05
Recharge Flux (q)	m/s	6.7E-07	0.0E+00
PVW Extraction Flux (q)	m/s	-1.7E-03	-1.3E-03

* Does not exclude elements removed from PVW location

** Measured in Laboratory

4.1.3 Model Calibration and Results

After refining the sample domain and modeling parameters, transient (or time dependent) analysis was conducted based on a recharge and extraction mode for Setup 3 and an extraction-only mode for Setup 4 to verify and calibrate the model. The model was simulated according to the schedule performed in the lab. The laboratory experimentation and model were operated for 120 and 100 minutes for Setup 3 and for 60 minutes for Setup 4.

The SEEP/w model was validated by comparing the groundwater depth obtained from the model to the actual depths measured in the piezometers during laboratory experimentation.

Head measurements in the laboratory experimentation obtained at various time increments were compared to the model output at the same time increments. Figure 59 presents the calibrated model solution for Setup 4, test 2. In Figure 59, the water table is depicted as a solid blue curvilinear line through the model, representing the water table at 0, 30 and 60 minutes. Figure 60 shows the total head profile obtained from the model for the aforementioned times during system operation, taken at the location of the end of the piezometers in the model (approximately 0.4 m from the bottom of the box) and is presented with lab results for Setup 4 test 2. Figure 60 presents the actual lab data in an axi-symmetric format similar to the model presentation, displaying an equivalent diameter well representing the PVW to the left and radial distances to the measured head data from the piezometers.

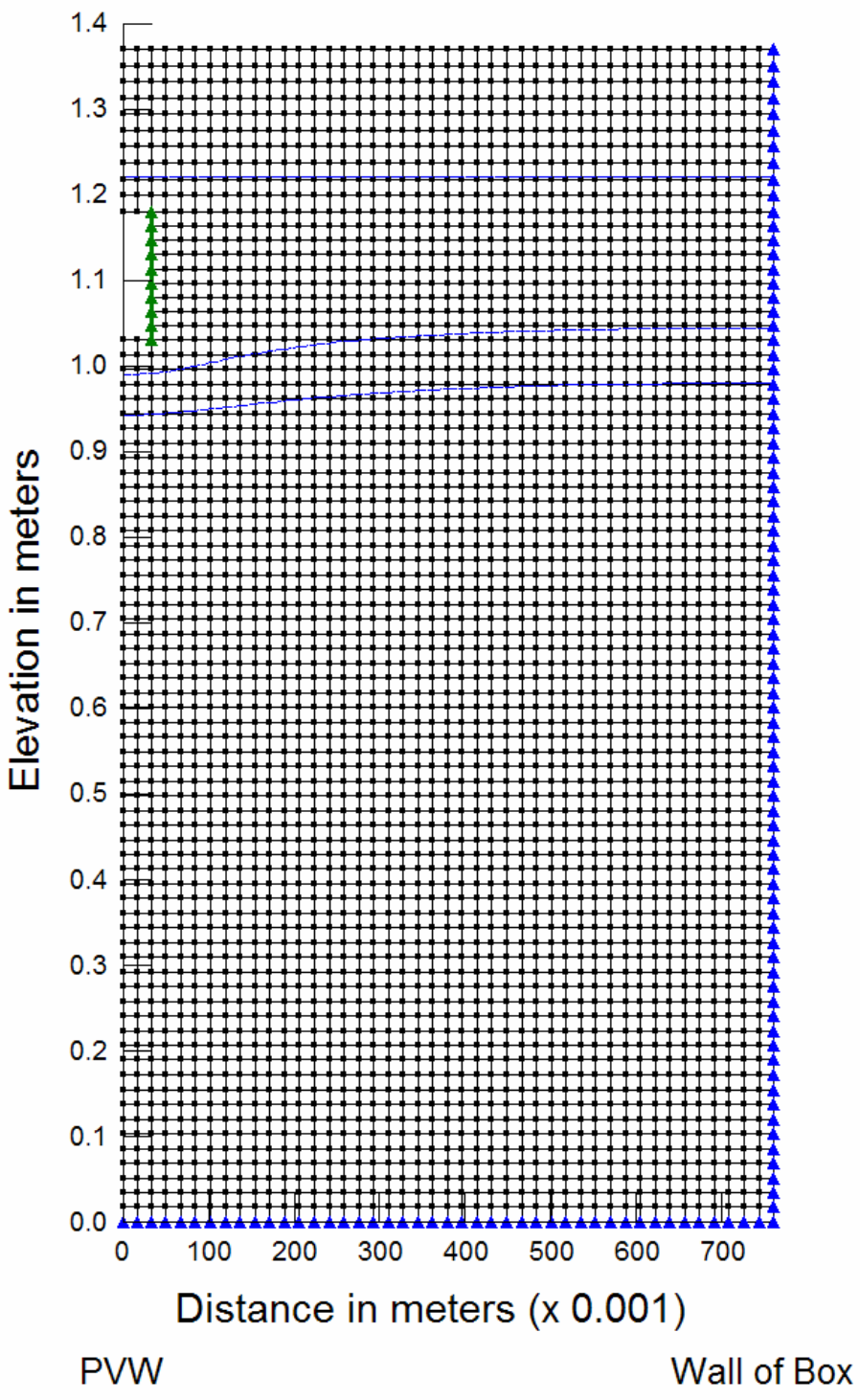

Figure 59. Idealized Model Output for Setup 4, Test 2

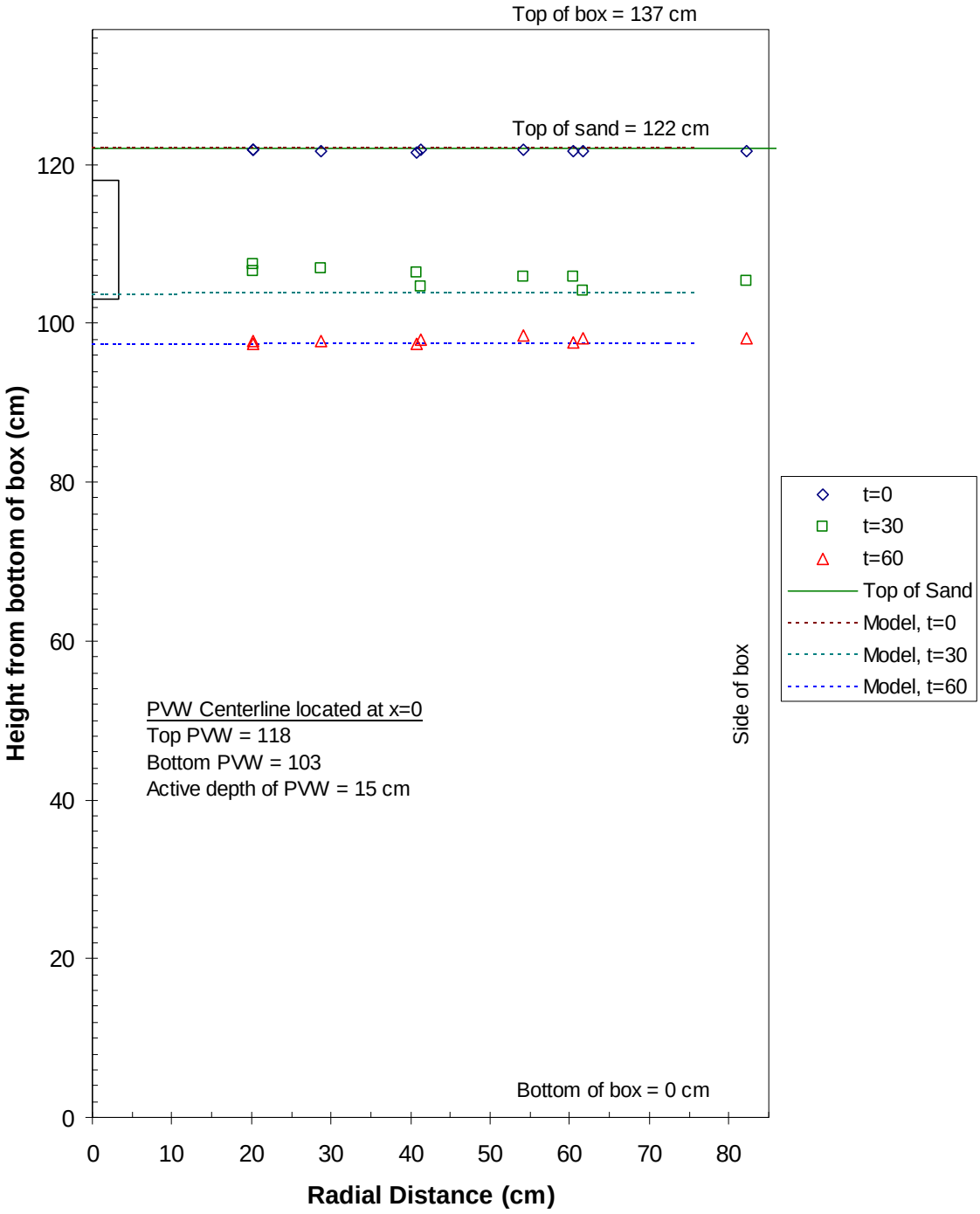

Figure 60. Model Verification Plot (Setup 4, Test 2)

The SEEP/w computer model was used to predict the water surface for all fourteen tests conducted during Phase II of the laboratory experimentation. In several cases the model produced slightly varied drawdowns for many of the time increments. Figure 60 shows that the initial water table is lowered down at the rate of approximately 0.365 m (1.2 ft) per hour in the first 30 minutes and 0.127 m (0.4 ft) per hour in the last 30 minutes of testing, using an extraction rate of 2.5 L/min.

4.2 Multiphase Flow and Transport Modeling

A vadose-saturated model (VSM) is used to study the mobilization of the two phases of the biodiesel, soluble and free product, with the application of vacuum head and extraction flow rate. The multiphase flow model was developed with the objective of investigating the extracted mass and remediation time within the subsurface environment considering the trapped free phase in soil pores. The multiphase modeling was only conducted on Setup 4.

4.2.1 Model Description

The computer software used for the multiphase flow and transport is a commercially available program called Bioslurp. The advantage of this program is the ability to simulate the vacuum enhanced recovery of multiphase fluids. The BIOSLURP flow module invokes an assumption of near equilibrium conditions in the vertical direction. This assumption reduces the nonlinearity in the constitutive model and transforms a 3D problem into a 2D

aerial problem. BIOSLURP uses three phases' constitutive relations to update phase saturations (water, free product, and gas) with depth. In addition, water, free product, and gas transmissivities are continuously updated during the simulation depending on the hydraulic head and matric suction conditions. During each time step, a steady state gas phase solution is obtained for the corresponding boundary conditions. The Van Genuchten constitutive model, along with fluid scaling parameters, is used to compute water and free product phase volumes.

The BIOSLURP flow module continuously updates the distribution of LNAPL specific volume in the characterized domain and defines its temporal and spatial variation for the transport module. The transport module simulates the aqueous and gas phases transport, and computes and updates the temporal and spatial variation of the contaminant concentration for the interphase mass transfer (extraction mode) each time step during the simulation.

4.2.2 Model Parameters

The subsurface profile was idealized to include groundwater table and a representation of the installed PVW. The conceptual model for multiphase transport was based on a single layer of soil with 6.9×10^{-5} m/s of hydraulic conductivity. This hydraulic conductivity is the value determined for the test sand as reported earlier in the laboratory experimentation section. Required input for flow analyses consists of initial air-free product level and air-

water table level distribution. The liquid (free product on top of groundwater) elevation was set at the surface, as approximately conducted in the lab. The water table depth was measured from piezometers and free product was initially measured as 76.0 L.

Figure 61 represents the idealized test pad. A total aerial domain of 1.52 m by 1.52 m was discretized using 2401 nodes. An approximate nodal spacing of 0.031 m was used in both the x and y directions. Measured lab data is used to estimate product thickness. The thick solid yellow line along the boundary of the test pad represents a no flow boundary. All boundaries were treated as no flow for the free product phase. Along the four boundaries, gas pressure was assumed atmospheric.

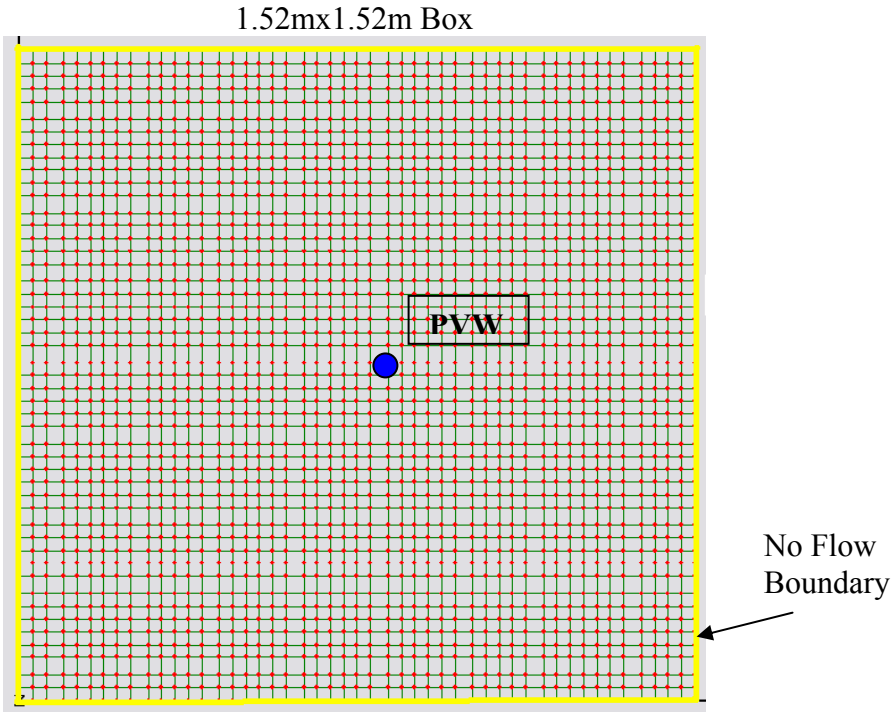

Figure 61. Mesh Generated by Bioslurp

Figure 62 illustrates the piezometer and monitoring well placement in the modeled domain. The piezometers are labeled with red numbers 1 through 21. Though only 9 piezometers were placed in the lab sample, for modeling purposes, the instrumented quadrant is mirrored in the other three quadrants. Thirteen dummy monitoring wells were placed throughout the domain and labeled A through M as illustrated in Figure 62.

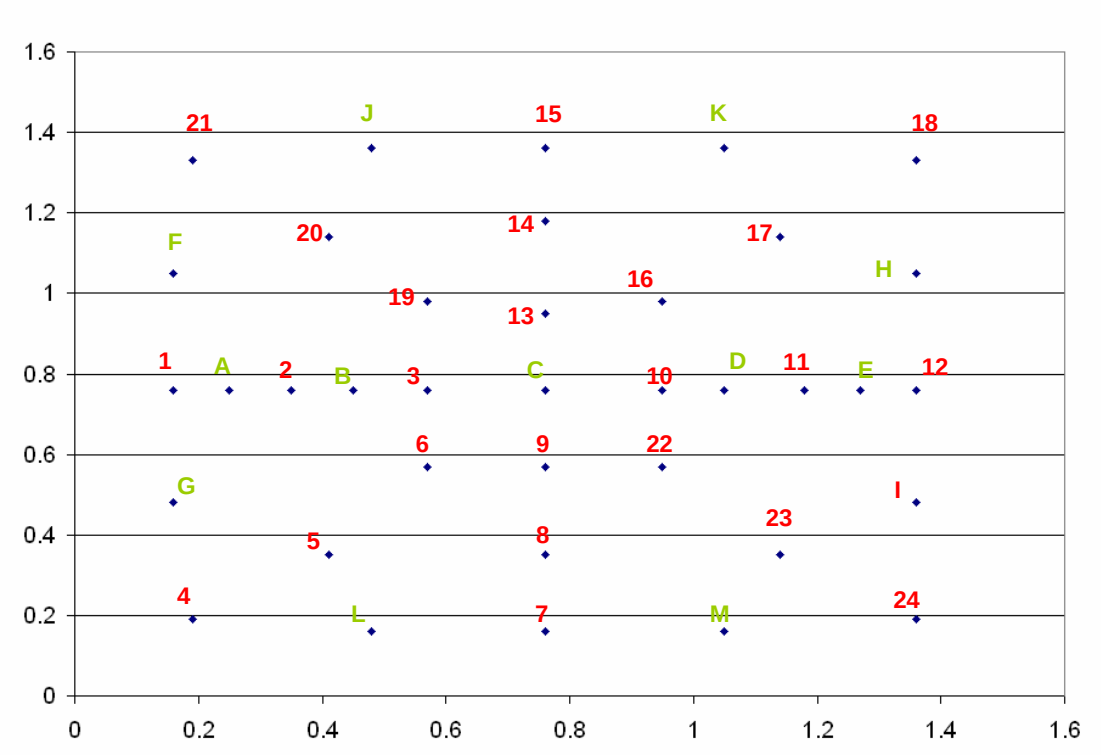

Figure 62. Monitoring Well/Piezometer Location in Bioslurp Model

Soil properties needed for flow simulation are saturated hydraulic conductivity in principal flow directions, soil porosity, irreducible water content and Van Genuchten retention parameters α and n. The porosity of the soil was 0.40. The maximum residual free

product saturation was considered as 10% in the saturated zone and 2% in the unsaturated zone. The Van Genuchten retention parameters α and n are obtained from the technical documentation of BIOSLURP. Soil retention parameters (residual water saturation, maximum residual free product saturation, and unsaturated zone maximum residual saturation) are according to Carsel and Parish (1988). The soil characterization data for the modeled soil are presented in Table 15. The bottom boundary of the model (aquifer bottom) is assumed level and sealed. The thickness of the capillary zone is assumed to be 0.3m (1 ft).

Table 15. Bioslurp Subsurface Characteristics Input

Groundwater Table Depth (from Ground Surface)	0 m
Soil Type	fine sand (SP)
Water Content %	25
Permeability m/s	$6.9x10^{-5}$
Specific Gravity, Gs	2.65
Residual water Saturation	0.05
Maximum residual free product Saturation	0.1
Unsaturated zone maximum residual saturation	0.02
Van Genuchten, α, /ft	2.7
Van Genuchten, n	2

4.2.3 Fluid Properties

Fluid properties required by Bioslurp are specific gravity, ρ_{ro} , of free product to water, dynamic viscosity ratio, η_{ro}, and fluid scaling parameter. (The fluid scaling parameter

includes both air-free product and free product-water scaling parameters). The air-free product and free product-water scaling parameters, βao and βow respectively, are related to the surface tension and interfacial surface tension as follows:

Equation 8

$$\beta ao = \frac{\sigma_w}{\sigma_o}$$

Equation 9

$$\beta ow = \frac{\sigma_w}{\sigma_{ow}}$$

Where σ_w is the surface tension of water, σ_o is the surface tension of free product, and σ_{ow} is the free product-water interfacial surface tension. The fluid properties were obtained from the technical documentation and user guide of Bioslurp and are presented in Table 16.

Table 16. Input Fluid Parameters

Name of Fluid Properties	Numerical Value
Density of Biodiesel	885 kg/m^3
Density of air	1.20 kg/m^3
Air-free product scaling parameters, βao	2.2
Free product-water scaling parameters, βow	1.9
Air to water dynamic viscosity ratio	0.018

4.2.4 Physiochemical Properties of Contaminant

Contaminant transport is assumed to be governed by both advection and dispersion with possible retardation due to adsorption. The seepage velocity calculated from the Bioslurp model governs soluble phase movement by advection. For dispersion, longitudinal and transverse dispersivities are assumed. The free product/water nonequilibrium mass transfer coefficient was 1.25 m^{-1}, and the air/free product nonequilibrium mass transfer coefficient was 1.25 m^{-1}.

4.2.5 Model Calibration and Results

The first objective of the modeling is to develop a vadose-saturated model (VSM) which can replicate the laboratory extraction results. To this end, initial hydraulic head distribution is established. The average free product thickness measured as 0.033 m on the water surface in the laboratory, was used in the model as shown in Figure 63. The LNAPL was assumed to be evenly distributed across the area of the test box. In addition, the dummy monitoring wells were assigned with 0.577 m to 0.5812m of free product throughout the domain to represent an average plume thickness.

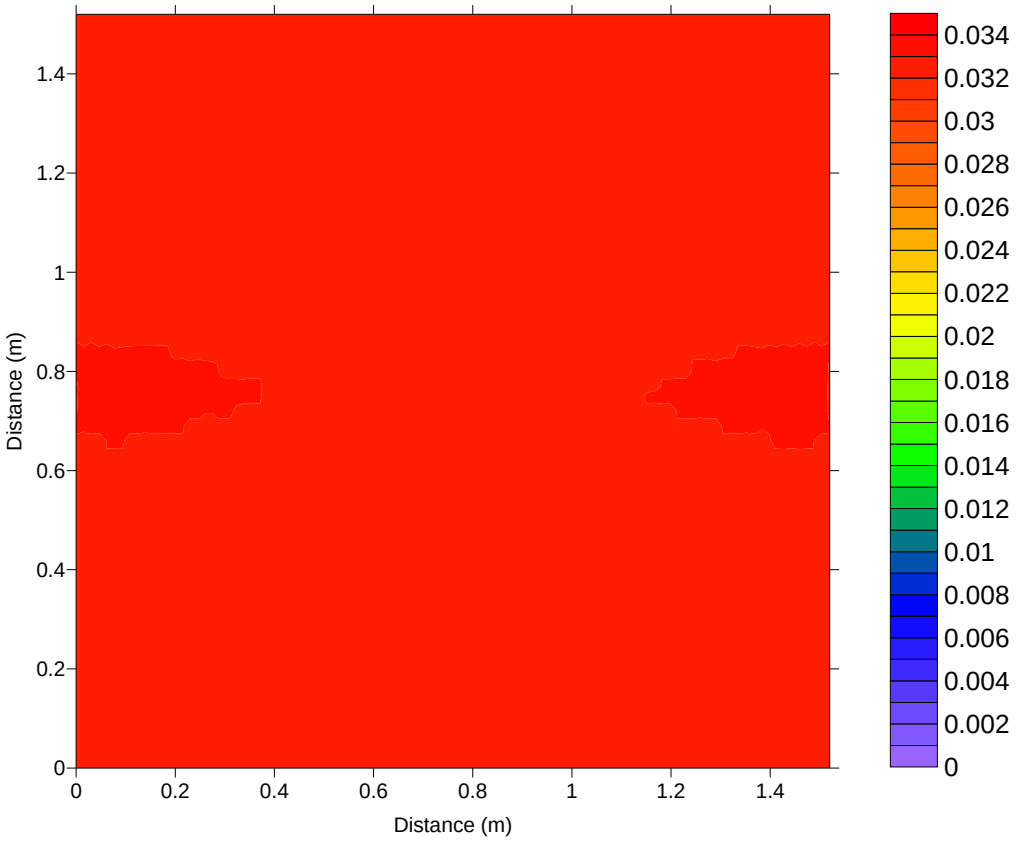

Figure 63. Contour Diagram of Initial BD Distribution (Specific Volume (m)) (0.033m*1.52m*1.52m=76 liter of BD) (Map Indicates a Uniform Distribution of 0.033 m of LNAPL)

Laboratory testing using Setup 4 resulted in an extraction of a total of 27.3 L of LNAPL and 856.5 L of water after 720 minutes of testing. Figure 64 and Figure 65 show the comparison between field and model results obtained for groundwater and free product volume recovery after a period of 600 minutes of testing, respectively. The operation time simulated one hour of system operation per day for ten days. The resulting biodiesel distribution after ten days of operation is presented in Figure 66. The experimental results

obtained from the VS analysis, in percent of biodiesel by mass, were modified to compare to the Bioslurp model output, which was in specific volume (m). To accomplish this, the experimentally measured volumes of biodiesel determined in each lift for Setup 4 were combined at each horizontal (x,y) coordinate to present an aerial distribution of the biodiesel over the contaminated zone. The sampled area at each coordinate location was estimated to be 4.5 cm (1.75") by 4.5 cm (1.75"), or 20 cm^2 (3.1 in^2). The specific volume was determined at each location by totaling the volumes over the sampled area and is presented in Figure 67. The model results presented in Figure 66 shows a greater specific volume of the LNAPL throughout the entire aerial domain and shows a more symmetrical distribution of the LNAPL than the experimental illustration in Figure 67. The model generated specific volumes that ranged from 0.0184 m (0.72") to 0.0349 m (1.37"), while the experimental results yielded specific volumes ranging from 0.0043 m (0.17") to 0.0263 m (1.04"). The greater specific volumes obtained from the model can partly be explained by the conversion process of the experimental data. The specific volume determined experimentally was obtained at specific depths from the surface, and the Bioslurp model determines the specific volume continuously throughout the vertical profile. In determining the specific volumes for the experiment, the sum of the experimental volumes would be greater if the LNAPL volume was measured continuously throughout the vertical profile at each horizontal coordinate. The Bioslurp model output for the biodiesel distribution in the unsaturated and saturated zones after ten days of operation are presented in Figure 68 and Figure 69, respectively.

After the model was calibrated, it was used to predict the remediation time for 0.033 m of free product thickness, assuming the system was operated one hour per day. The objectives of this analysis are to predict the extraction time to remove free product. The blue dashed lines shown in Figure 64 and Figure 65 are the projected extraction volumes produced by the model. Based on the model output for Setup 4, a total of approximately 1800 L of water and 39 L of biodiesel would be extracted over a period of 22 days of operation.

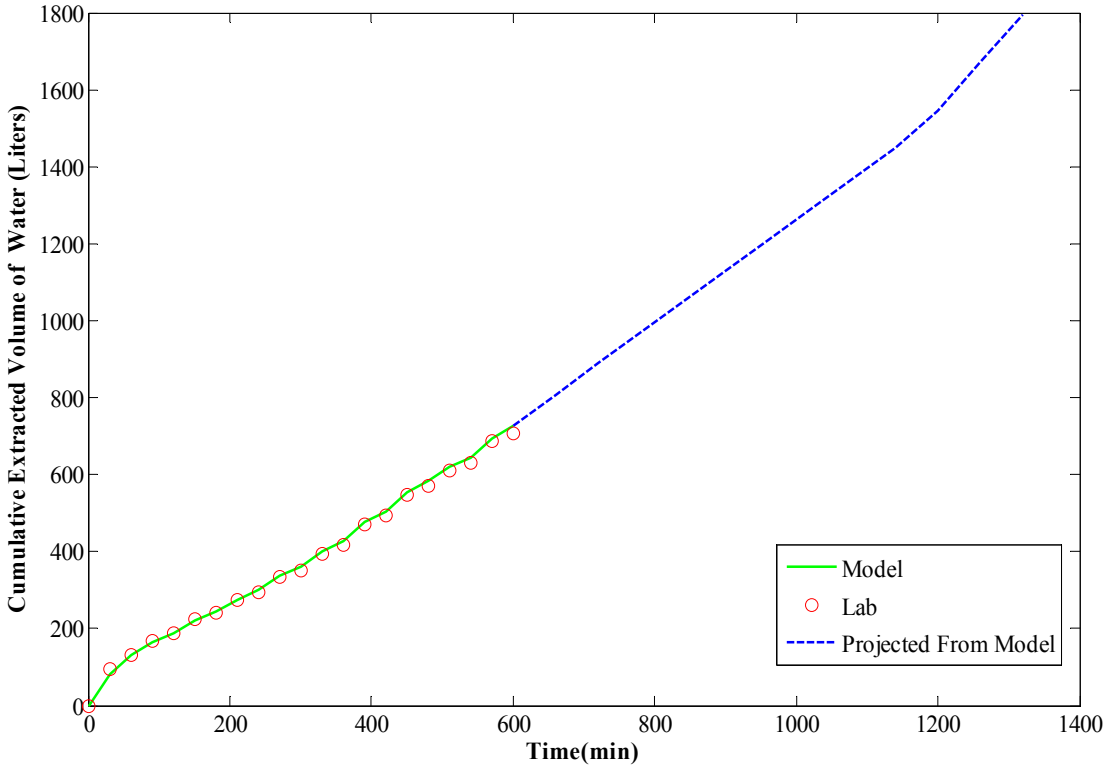

Figure 64. Cumulative Water Extracted Over Time

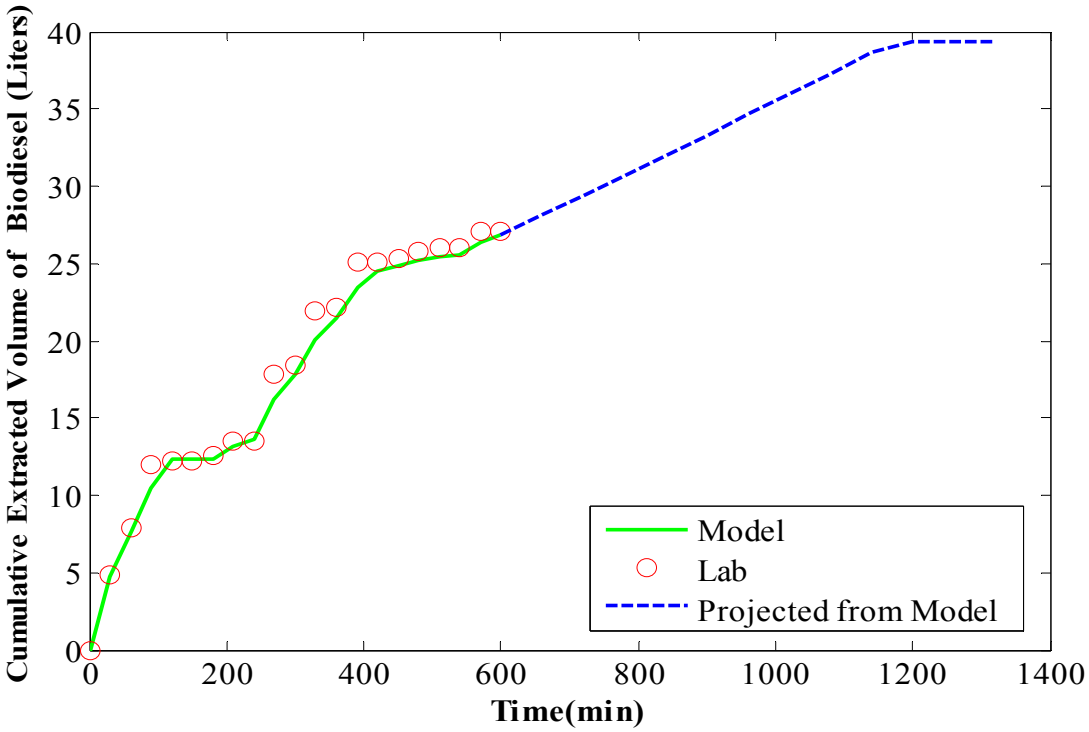

Figure 65. Cumulative Biodiesel Extracted Over Time

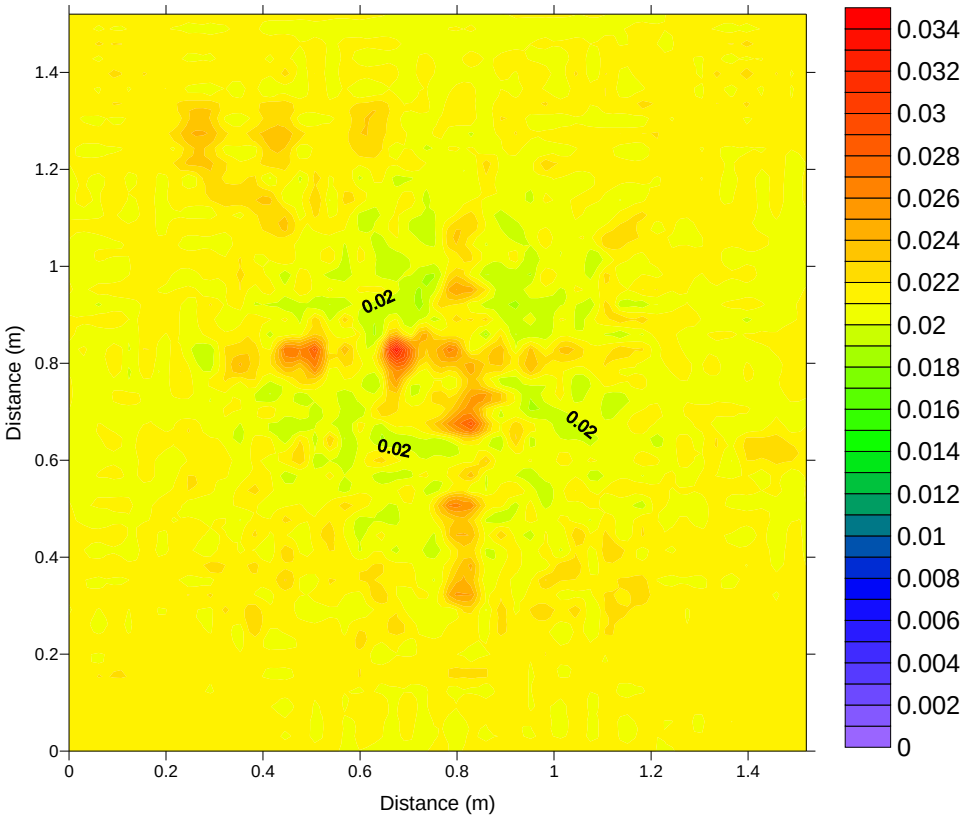

Figure 66. Contour Diagram of Total BD Distribution After 10 Days (1hr System Run Time Per Day for a Total of 600 min) of Operation (Specific Volume (m))

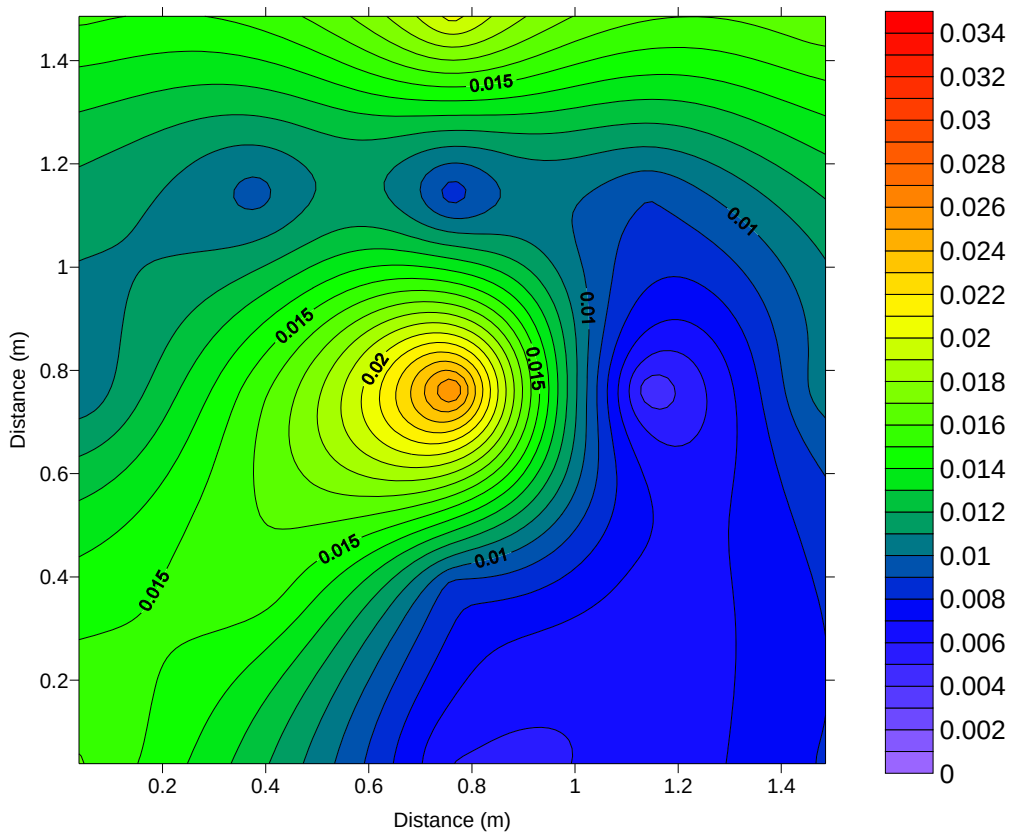

Figure 67. Contour Diagram of Total Residual BD Distribution After 12 days (1 hr System Run Time per Day for a Total of 720 min) of Operation (Specific Volume (m))

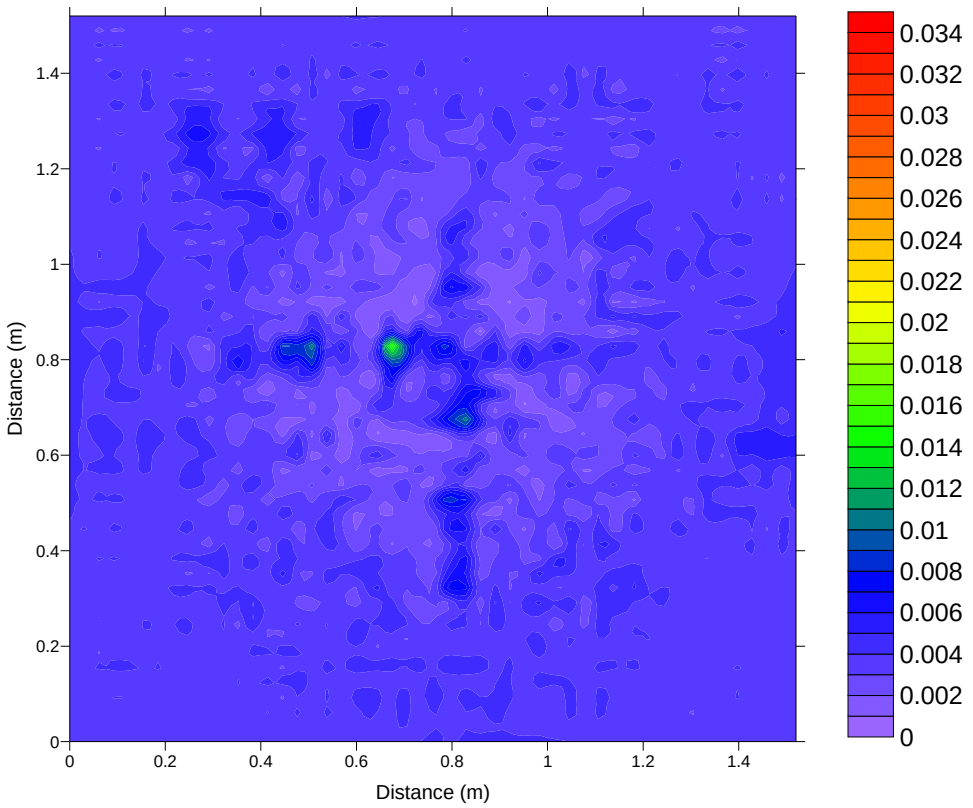

Figure 68. Contour Diagram of Trapped BD Distribution in the Saturated Zone After 10 Days (1hr System Run Time Per Day for a Total of 600 min) of Operation (Specific Volume (m))

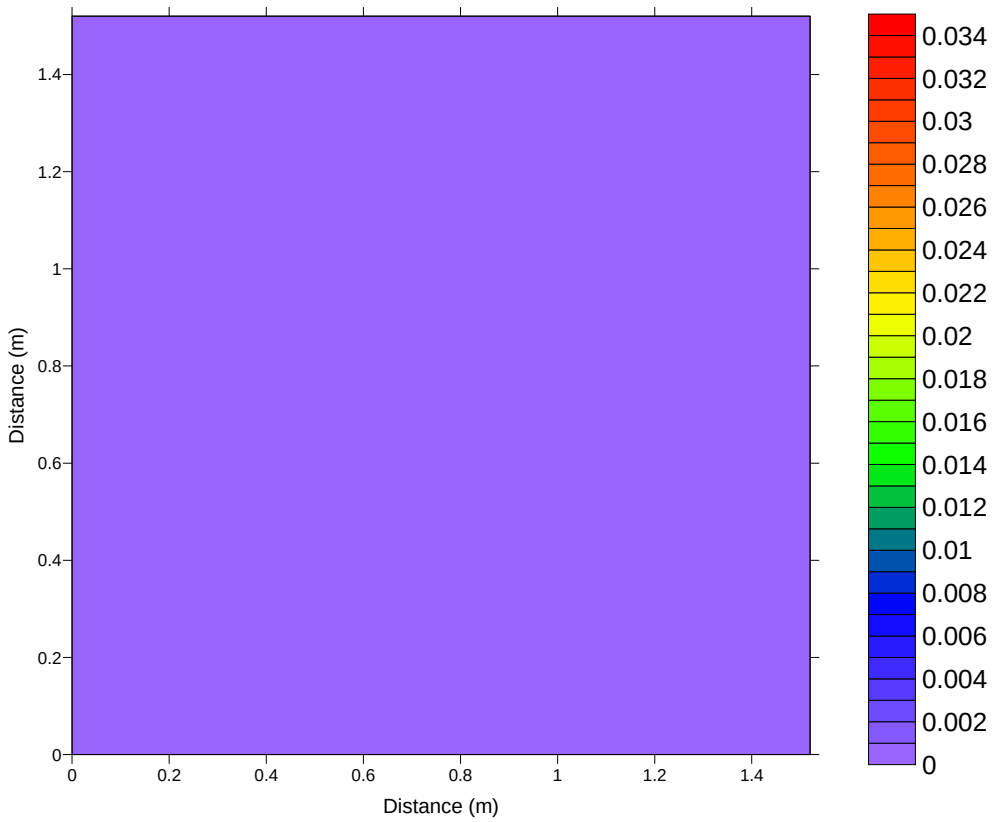

Figure 69. Contour Diagram of Trapped BD Distribution in the Unsaturated Zone After 10 Days (1hr System Run Time Per Day for a Total of 600 min) of Operation (Specific Volume (m)) (Map Indicates Insignificant Volume of LNAPL)

From the model, the resulting biodiesel distribution after 22 days of operation is presented in Figure 70. The biodiesel distributions in the unsaturated and saturated zones after 22 days of operation are presented in Figure 71 and Figure 72, respectively.

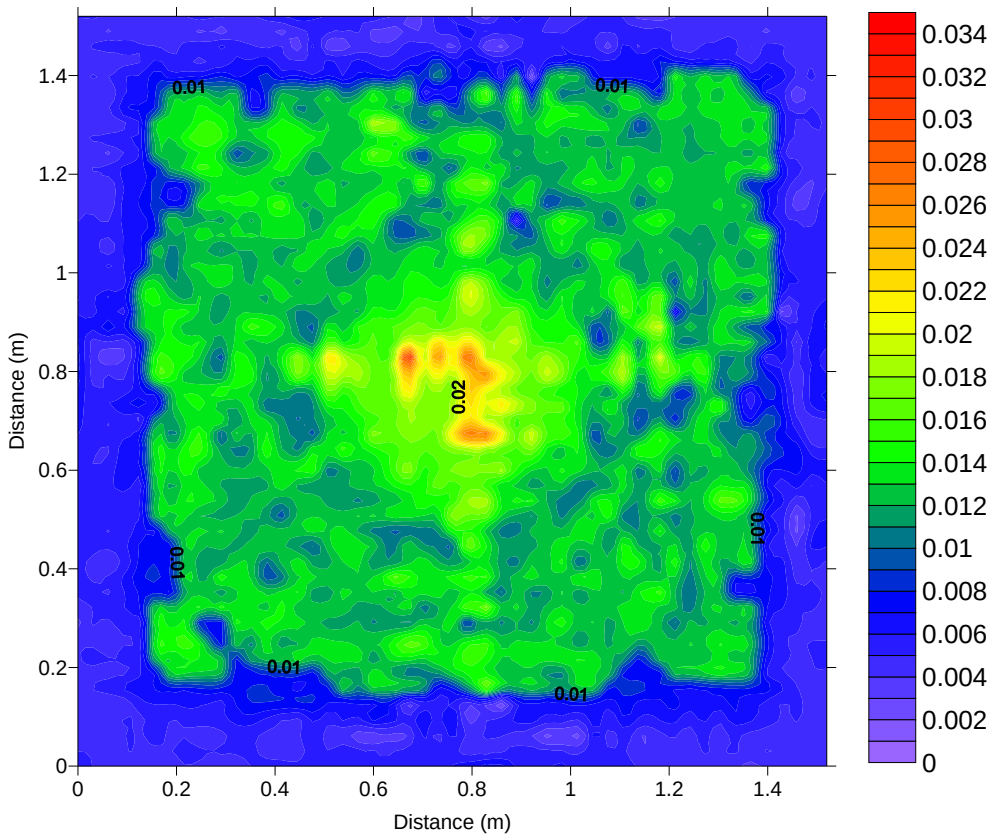

Figure 70. Contour Diagram of Total BD Distribution After 22 days (1hr System Run Time per Day for a Total of 1320 min) of Operation (Specific Volume (m))

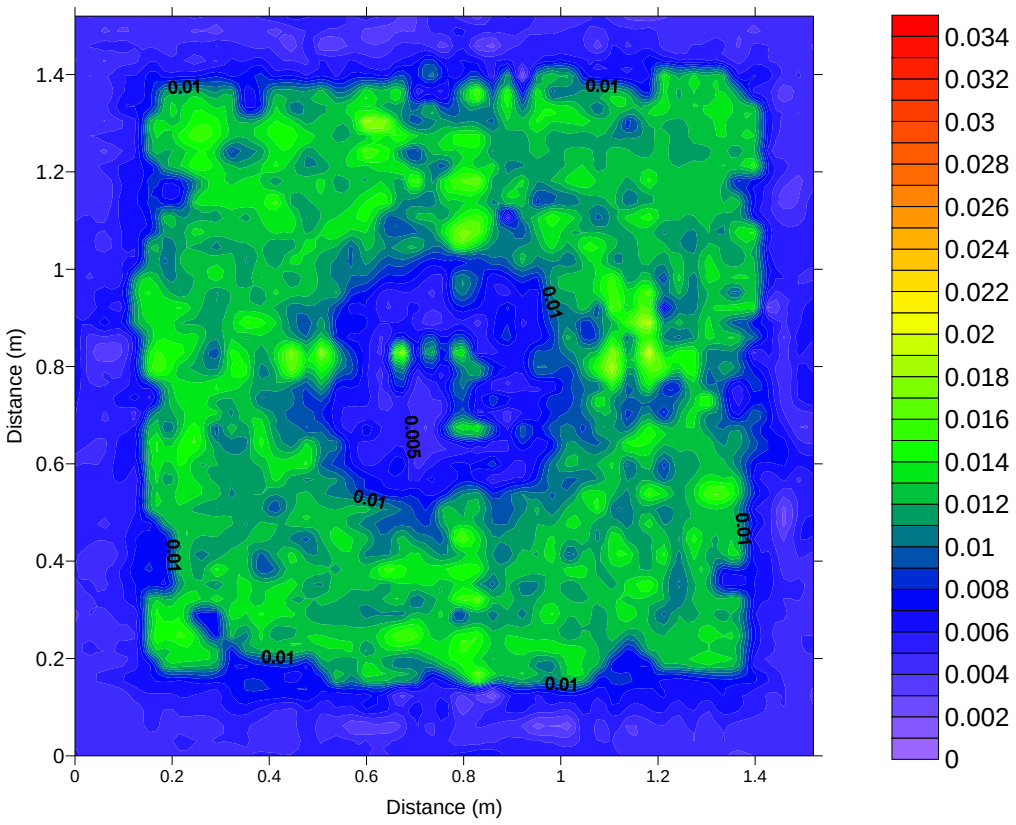

Figure 71. Contour Diagram of Trapped BD Distribution in the Saturated Zone After 22 days (1hr System Run Time per Day for a Total of 1320 min) (Specific Volume (m))

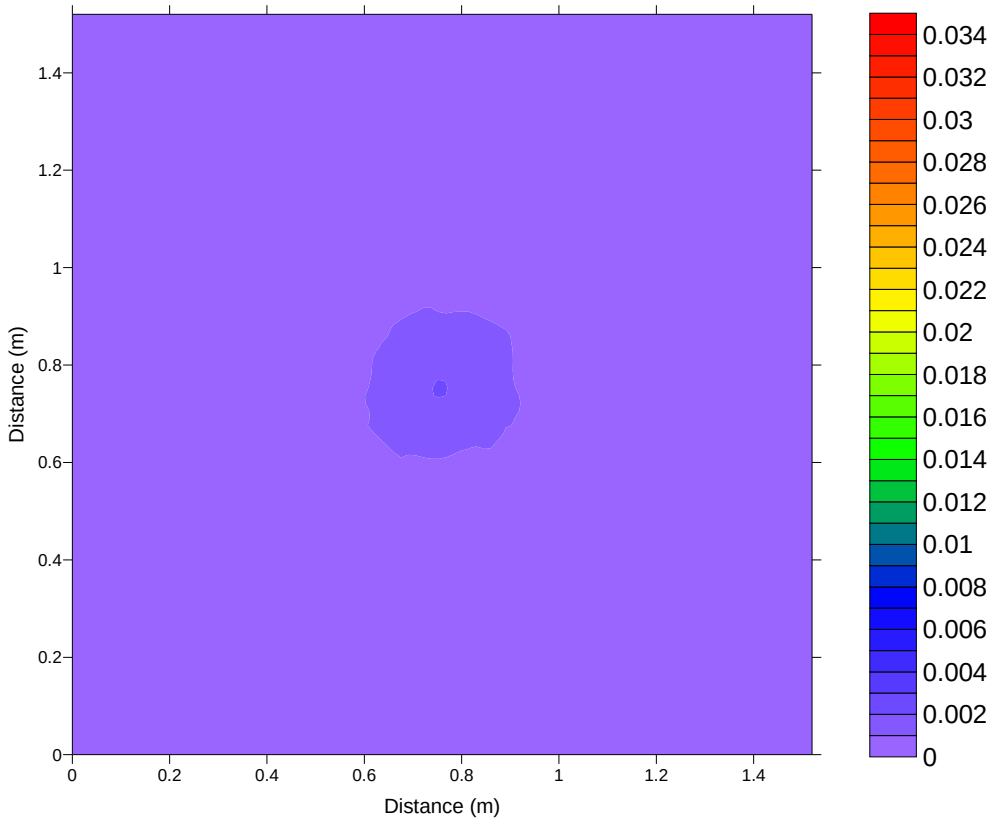

Figure 72. Contour Diagram of Trapped BD Distribution in the Unsaturated Zone After 22 days (1hr System Run Time per Day for a Total of 1320 min) (Specific Volume (m))

5. RESEARCH SUMMARY AND CONCLUSIONS

The research and results presented herein document the performance of a single Prefabricated Vertical Well (PVW), as developed by Cofra, in extracting subsurface water and Light Nonaqueous Phase Liquids (LNAPL), to further develop the in-situ technology known as Well Injection Depth Extraction (WIDE). The research consisted of two main components: a laboratory experimentation and numerical modeling.

The laboratory experimentation consisted of two phases aimed at evaluating the performance of the Cofra PVW system. Phase I testing was performed to compare the active length and placement depth for two scenarios referred to as Setup 1 and 2. Phase II went further by introducing 76.0 L of LNAPL biodiesel, and compared the performance in terms of extracted liquid from the two scenarios, Setup 3 and 4. Based on the results from this research, the following can be concluded:

1) The mean extraction rates were $1.4x10^{-3}$ m/s, $4.8x10^{-3}$ m/s, $4.5x10^{-3}$ m/s, and $1.2x10^{-3}$ m/s and the mean hydraulic gradients were 0.57, 3.71, 3.50, and 1.98 for Setups 1, 2, 3 and 4, respectively. Higher extraction flow rates and hydraulic gradients are the result of the lower placement depths used in Setups 2 and 3 with a shorter active length than that of Setup 1. As the water table dropped, the loss of vacuum pressure through the upper portions of the PVWs, as observed in the vacuum gauge data, resulted in less liquid extraction for Setups 1 and 4. The PVWs in Setups 2 and 3 remained below the water table longer than the PVWs in

Setups 1 and 4. In general higher water removal rates were achieved when the water table was elevated significantly above the PVW and the soil remained saturated.

2) According to Darcy's Law, the flow velocity is directly proportional to the hydraulic gradient. However, the flow rate is not directly proportional to the active length. Setup 2 and 3 exhibited higher flow rates than both Setups 1 and 4, due to the higher hydraulic gradients. The slope of the relationship between outflow and hydraulic gradient is a function of the active length of the PVW; however, data indicated that the ranges of the outflow and hydraulic gradient along this linear trend are a function of the depth of placement within the subsurface. For example, in Setup 1 the active length was nearly ¼ the active length of the PVW in Setup 4 and the top of the PVW in both setups was placed within 4 cm (1.6") from the sand surface; yet the range of flow rates was approximately the same. Also, the hydraulic gradients estimated for Setup 4 were four to five times higher than those estimated for Setup 1.

3) The change in hydraulic gradient over time for all the setups was analyzed. The results indicate the longer active lengths produced the least amount of change in the hydraulic gradient. Setup 1, with an active length of 0.61 m (2.0 ft), exhibited the lowest hydraulic gradients and the least change in gradient over the testing period. Setups 2 and 3, both having an active length of 0.31 m (1.0 ft), exhibited the highest gradients and an increased rate of change of the gradient. Setup 4, with an active length of 0.15 m (0.5 ft), produced the steepest decline in hydraulic gradient.

4) Phase II of the laboratory experimentation, consisting of Setups 3 and 4, evaluated the performance of the PVW system for the extraction of 76.0 L (20.08 gal) of LNAPL biodiesel. Setup 3 and Setup 4 removed 1.5 L (0.40 gal) and 27.3 L (7.22 gal) of biodiesel, respectively. A volatile solids (VS) analysis of the sand was conducted to quantify the amount of residual LNAPL trapped in the sand after experimental testing was completed. The results of the analysis indicated median residual LNAPL volumes of 40.2 L (10.61 gal) and 28.7 L (7.58 gal) for Setups 3 and 4, respectively. Aerial mapping of the (VS) results showed the largest percentage of residual concentrations is around the PVW. Cross-sections of the (VS) results showed the residual concentrations are the highest near and above the water table surface, as expected.
5) It seems that the shorter active length PVW at the shallow placement depth exhibited greater recovery of free product with a lesser volume of smeared residual LNAPL in a lesser volume of contaminated soil. Hence, Setup 4 produced the more desirable results, for free product removal, of the two setups during Phase II testing.
6) Mass balance of the LNAPL biodiesel placed in the system indicated the dissolved and biodegraded portions of LNAPL account for approximately 25.6 L (6.77 gal) and 20.0 L (5.28 gal) of LNAPL biodiesel for Setups 3 and 4, respectively. The higher volume of unaccounted LNAPL using Setup 3, as compared with Setup 4, can partially be explained by the significantly higher flow rate through the system in Setup 3. The water flow rate through the system using Setup 3 was 4.35 L/min

over a period of 220 minutes, where the flow rate through the system using Setup 4 was 1.19 L/min over a period of 720 minutes. The system in Setup 3 was exposed to more fresh water (957 L of water) (and more air as result of having a longer active length and lower placement depth) than the system in Setup 4 (856.5 L of water) at a faster rate of flow. Essentially, Setup 3, with greater water and air flow rates through the system, provided improved conditions for biodegradation and dissolution of the LNAPL biodiesel. This agrees with the work by Leung et al. (2006) regarding the influence of water and air on the degradation of biodiesel; however, under stored conditions.

7) A comparison between Setups 1 and 2 and the respective liquid extraction results indicate that the shorter active length placed at a greater depth below the water table, as utilized in Setup 2, will extract greater volumes of fluids. This knowledge is advantageous if groundwater extraction is the key goal. However, a comparison of Setups 3 and 4, with Setup 3 having the same active length and placement depth used in Setup 2, indicates that an even shorter active length placed with a shallow placement depth is more efficient for the removal of free LNAPL with less smearing of residual LNAPL.

Hydraulic and contaminant transport analyses were also performed utilizing finite element analysis software programs to model the subsurface domain and gain insight into system performance. The modeling results were used to study the impact of the extraction process on LNAPL mobilization. The SEEP/w computer model was used to predict the water

surface for the tests conducted during Phase II of the laboratory experimentation. The model produced slightly varied drawdowns for many of the time increments. The initial water table was lowered down at the rates ranging from 0.1 m (0.33 ft) per hour to 0.4 m (1.3 ft) per hour using extraction rates that varied from 1.5 L/min to 3.0 L/min. The Bioslurp model was calibrated successfully to match the 27.0 L of LNAPL extracted in the first ten days of testing, under a transient water table with a no flow boundary. The Bioslurp model predicted the LNAPL distribution within the subsurface domain and was compared to actual experimental results. The comparison indicated that the model should reasonably predict the residual LNAPL volumes within the contaminated zone, though the actual distribution varies. The model also indicated a more symmetrical and uniform distribution of the residual LNAPL whereas the actual results showed a greater degree of variation. The bioslurp model was then used to predict the removal of a total of approximately 39 L of free product and to predict the distribution of the residual LNAPL in the sand specimen after 22 days of operation.

6. FUTURE RESEARCH

Recommendations for future research include the following:

i. The vacuum pressure applied to the system remained constant at 16.9 kPa as measured at the venturi vacuum pump. Vacuum pressures within the PVW were not observed until the water level dropped below the vacuum gauge location. The vacuum head could be varied to observe the effects of vacuum head on the gradient and LNAPL extraction.

ii. The LNAPL biodiesel extraction rates varied significantly between tests 3 and 4 of Setup 4, and were affected by the water table elevations, the availability of free product for gradient flow, and possibly by the hysteretical effects resulting from the sample saturation and equilibration. Additional research should evaluate the hysteretical and time dependent effects of LNAPL extraction.

iii. WIDE utilizes injection and extraction whereas this research focuses on extraction only. Further work should attempt to address scenarios including injection and extraction while varying the active length and placement depths of PVWs in both modes of operation.

iv. As previously concluded, a shallow depth of placement with a short active length performs better at free product removal with less smear, while a longer active length at a greater placement depth removes more fluids. Additional research should evaluate the use of both of these strategies in conjunction.

v. A substantial volume of LNAPL biodiesel was unaccounted for in both Setups 3 and 4 as determined from the mass balance of the LNAPL within the system. Additional research can be performed to determine the solubility and biodegradation rate of biodiesel under similar conditions as described herein.

REFERENCES

Anonymous "Electrical Conductivity of Biodiesel." National Biodiesel Board, Washington, DC 20004.

Arya, L. M., and Paris, J. F. (1981). "Physicoemperical Model to Predict the Soil Moisture Characteristic From Particle-Size Distribution and Bulk Density Data." *Soil Sci.Soc.Am.J.,* 45(6), 1023-1030.

ASTM D 4253-00, Standard Test Methods for Maximum Index Density and Unit Weight of Soils Using a Vibratory Table.

ASTM D 4254-00, Standard Test Methods for Minimum Index Density and Unit Weight of Soils and Calculation of Relative Density.

ASTM D 5084-03, Standard Test Methods for Measurement of Hydraulic Conductivity of Saturated Porous Materials Using a Flexible Wall Permeameter.

Barron, R. A. (1948). "Consolidation of Fine-Grained Soils by Drain Wells." *Transactions of the American Society of Civil Engineers,* 113 718-742.

BIOSLURP, Technical Documentation and User Guide, Resources and System International, Inc. Suite 2415, 1700 Kraft Drive, Blacksburg, VA 24060.

Borden, R. C., and Kao, C. (1992). "Evaluation of Groundwater Extraction for Remediation of Petroleum-Contaminated Aquifers." *Res.J.Water Pollut.Control Fed.,* 64(1), 28-36.

Bowders, J. J., Gabr, M. A., Collazos, O. M., and Quaranta, J. D. (2005). "Prefabricated Vertical Drains for Enhanced In Situ Remediation." *Geo-Frontiers 2005,* ASCE, Austin, TX, 4141-4153.

Bowders, J. J., and Gabr, M. A. (1995). "Strip-drains for In Situ Clean Up of Contaminated Fine-Grained Soils." *Geotech News,* 13(3), 21-25.

Charbeneau, R. J. (2000). *Groundwater Hydraulics and Pollutant Transport.* Prentice Hall, Upper Saddle River, NJ.

Cohen, R. M., Mercer, J. M., Greenwald, R. M., and and Beljin, M. S. (1997). "Design Guidelines for Conventional Pump and Treat Systems." U.S. Environmental Protection Agency, EPA/540/S-97/50.

Coulibaly, K. M., and Borden, R. C. (2004). "Impact of Edible Oil Injection on the Permeability of Aquifer Sands." *J.Contam.Hydrol.,* 71(1-4), 219-237.

Fortin, J., Jury, W. A., and Anderson, M. A. (1997). "Enhanced Removal of Trapped Non-Aqueous Phase Liquids from Saturated Soil Using Surfactant Solutions." *Journal of Contaminant Hydrology,* 24(3-4), 247-267.

Fredlund, D. G., and Xing, A. (1994). "Equations for the Soil-Water Characteristic Curve." *Canadian Geotechnical Journal,* 31(4), 521-532.

Gabr, M. A., Bowders, J. J., Wang, J., and Quaranta, J. (1996). "In Situ Soil Flushing Using Prefabricated Vertical Drains." *Canadian Geotechnical Journal,* 33(1), 97-105.

Gabr, M. A., Bowders, J. J., and Wokasien, S. (1995). "Prefabricated Vertical Drains (PVD) for Enhanced Soil Flushing." *Proceedings of the Specialty Conference on Geotechnical Practice in Waste Disposal,* ASCE, New Orleans, LA, 1250-1264.

Gabr, M. A., Quaranta, J. D., Cook, E. E., and Mooney, D. T. (1997). "Prefabricated Vertical Drains in Geotechnical Engineering: State of the Art Review." *Proceedings of the 1997 7th International Offshore and Polar Engineering Conference,* Int Soc of Offshore and Polar Engineerns (ISOPE), Honolulu, HI, 714-718.

Gabr, M. A., Sabodish, M., Williamson, A., and Bowders, J. J. (1999). "BTEX Extraction from Clay Soil Using Prefabricated Vertical Drains." *J.Geotech.Geoenviron.Eng.,* 125(7), 615-618.

Gabr, M. A., Sharmin, N., Godwin, J., and Quaranta, J. "WIDE Implementation for LNAPL Extraction Rickenbacker International Airport Area of Concern 3 (AOC – 3)" Phase III – Final Report submitted to the Army Corps of Engineers, Louisville, December 2007, 157pp.

Green, R. E., and Corey, J. C. (1971). "Calculation of Hydraulic Conductivity: A Further Evaluation of Some Predictive Methods." *Soil Science Society of America Proceedings,* 35 3-8.

Hansbo, S. (1979). "Consolidation of Clay by Band-Shaped Prefabricated Drains." *Ground Engineering,* 12(5), 16-18.

Hunt, J. R., Sitar, N., and Udell, K. S. (1988a). "Nonaqueous Phase Liquid Transport and Cleanup 1. Analysis of Mechanisms." *Water Resour. Res.,* 24(8), 1247-1258.

Hunt, J. R., Sitar, N., and Udell, K. S. (1988b). "Nonaqueous Phase Liquid Transport and Cleanup 2. Experimental Studies." *Water Resour. Res.,* 24(8), 1259-1269.

Kjellman, W. (1948). "Accelerating Consolidation of Fine-Grained Soils by Means of Card-Board Wicks." *Proc. 2nd Int. Conf. Soil Mech. and Found. Eng., Volume* 2, 302-305.

Leung, D. Y. C., Koo, B. C. P., and Guo, Y. (2006). "Degradation of Biodiesel Under Different Storage Conditions." *Bioresour.Technol.,* 97(2), 250-256.

Mualem, Y. (1986). "Hydraulic Conductivity of Unsaturated Soils: Prediction and Formulas." *Methods of Soil Analysis, Part 1. Physical and Mineralogical Methods,* Soil Science Society of America, 799-823.

Newell, C. J., Acree, S. D., Ross, R. R., and Huling, S. G. (1995). *Groundwater Issue: Light Nonaqueous Phase Liquids.* U.S. Environmental Protection Agency, Office of Research and Development, Office of Solid Waste and Emergency Response, Washington, DC, EPA/540/S-95/500.

Norris, R. D., Hinchee, R. E., Brown, R., McCarty, P. L., Semprini, L., Wilson, J. T., Kampbell, D. H., Reinhard, M., Bouwer, E. J., Borden, R. C., Vogel, T. M., Thomas, J. M., Ward, C. H., and Matthews, J. E. (1994). *Handbook of Bioremediation.* Lewis Publishers, Boca Raton, FL.

Quaranta, J. D., and Gabr, M. A. (2000). "Prefabricated Vertical Drains Flow Resistance Under Vacuum Conditions." *J.Geotech.Geoenviron.Eng.,* 126(1), 81-84.

Quaranta, J. D., Kunberger, T., and Gabr, M. A. (2005). "WIDE Application for Subsurface Hydraulic Head Control." *Geo-Frontiers 2005,* ASCE, Reston, VA, 3725-3736.

Quaranta, J. D., Sabodish, M. S.,Jr, Gates, K. A., and Gabr, M. A. (2000). "Enhanced Subsurface Flushing of Mixed Waste: A Field Study." *GeoDenver 2000 Conference 'Environmetal Geotechnics',* ASCE, Denver, CO, 132-141.

Schwartz, F. W., and Zhang, H. (2003). *Fundamentals of Ground Water.* Wiley, New York.

SEEP/W,Verson 5.18 GEO-SLOPE International, Calgary, Alberta, Canada. http:/www.geo-slope.com/.

Topp, G. C., and Miller, E. E. (1966). "Hysteretic Moisture Characteristics and Hydraulic Conductivities for Glass-Bead Media." *Soil Science Society of America -- Proceedings,* 30(2), 156-162.

U.S. EPA (1996). “A Citizen’s Guide to In Situ Soil Flushing.” EPA/542/F-96/006.

U.S. EPA (2004). “How to Evaluate Alternative Cleanup Technologies for Underground Storage Tank Sites: A Guide for Corrective Action Plan Reviewers.” EPA/510/R-04/002.

van Genuchten, M. Th. (1980). "A Closed-form Equation for Predicting the Hydraulic Conductivity of Unsaturated Soils." *Soil Sci.Soc.Am.J.,* 44(5), 892-898.

Warren, K. A. (2002). "A Fundamental Investigation of Well Injection Depth Extraction (WIDE) System Performance Aspects in Fine-Grained Soil Contaminated with Trichloroethylene." PhD dissertation, North Carolina State University.

Warren, K. A., and Gabr, M. A. (2005). "Liquid Extraction Using Prefabricated Vertical Wells (PVWs) Under Vacuum in Clay." *Geotech Test J,* 28(4), 328-335.

Zhang, X., Peterson, C., Reece, D., Haws, R., and Moller, G. (1998). "Biodegradability of Biodiesel in the Aquatic Environment." *Trans.ASAE,* 41(5), 1423-1430.

APPENDICES

APPENDIX A: Fluid Extraction Data (Setups 3 and 4)

Setup 3

Time (min)	Biodiesel (L)	Water (L)	Percent of Biodiesel Extracted (%)
0	0	0	0.0
30	0.51	149.57	0.7
60	0.77	264.78	1.0
90	0.77	361.34	1.0
120	0.77	446.15	1.0
140	0.77	568.26	1.0
160	1.53	683.72	2.0
190	1.53	829.07	2.0
220	1.53	957.05	2.0

Setup 4

Time (min)	Biodiesel (L)	Water (L)	Percent of Biodiesel Extracted (%)
0	0	0	0.0
30	4.85	93.75	6.4
60	7.92	130.28	10.4
90	12.01	166.81	15.8
120	12.26	187.25	16.1
150	12.26	223.27	16.1
180	12.52	241.91	16.5
210	13.54	273.59	17.8
240	13.54	293.52	17.8
270	17.88	333.62	23.5
300	18.39	352.01	24.2
330	21.97	394.67	28.9
360	22.22	416.13	29.2
390	25.03	471.57	32.9
420	25.03	492.51	32.9
450	25.29	547.95	33.3
480	25.80	571.45	33.9
510	26.06	611.81	34.3
540	26.06	629.18	34.3
570	27.08	686.40	35.6
600	27.08	708.37	35.6
630	27.33	755.89	36.0
660	27.33	775.66	36.0
690	27.33	838.25	36.0
720	27.33	856.50	36.0

APPENDIX B: Water and LNAPL Contents for Setup 3

X	Y	Z	Gravimetric Water Content	Gravimetric Biodiesel Content	Total Fluid Content
(cm)	(cm)	(cm)	(%)	(%)	(%)
3.81	148.59	117.44	0.76	2.16	2.93
76.20	148.59	117.44	0.98	2.59	3.57
148.59	148.59	117.44	0.82	2.19	3.00
38.10	114.30	117.44	0.98	2.21	3.19
76.20	114.30	117.44	0.91	2.21	3.12
114.30	114.30	117.44	0.86	2.36	3.22
3.81	76.20	117.44	1.00	2.63	3.63
38.10	76.20	117.44	1.02	2.62	3.65
76.20	76.20	117.44	1.00	2.71	3.71
114.30	76.20	117.44	0.87	2.24	3.11
148.59	76.20	117.44	0.95	2.77	3.72
38.10	38.10	117.44	0.91	2.53	3.44
76.20	38.10	117.44	0.98	2.89	3.87
114.30	38.10	117.44	1.05	2.83	3.87
3.81	3.81	117.44	0.89	3.24	4.12
76.20	3.81	117.44	0.90	3.23	4.12
148.59	3.81	117.44	1.22	3.58	4.80
3.81	148.59	103.56	5.93	2.51	8.44
76.20	148.59	103.56	11.27	3.85	15.12
148.59	148.59	103.56	6.22	2.61	8.83
38.10	114.30	103.56	11.86	3.53	15.40
76.20	114.30	103.56	9.37	4.17	13.54
114.30	114.30	103.56	8.76	3.58	12.34
3.81	76.20	103.56	9.85	3.35	13.20
38.10	76.20	103.56	11.20	3.84	15.03
76.20	76.20	103.56	10.20	3.84	14.04
114.30	76.20	103.56	11.35	5.09	16.44
148.59	76.20	103.56	10.02	3.53	13.55
38.10	38.10	103.56	8.17	3.54	11.71
76.20	38.10	103.56	11.02	3.91	14.92
114.30	38.10	103.56	8.72	3.38	12.10
3.81	3.81	103.56	5.75	2.41	8.15
76.20	3.81	103.56	10.54	3.63	14.17
148.59	3.81	103.56	6.48	2.36	8.84
3.81	148.59	89.50	22.98	1.92	24.90
76.20	148.59	89.50	22.18	0.59	22.77
148.59	148.59	89.50	24.20	2.15	26.35
38.10	114.30	89.50	21.41	1.67	23.08

76.20	114.30	89.50	20.98	3.18	24.16
114.30	114.30	89.50	19.96	2.81	22.77
3.81	76.20	89.50	25.23	0.05	25.28
38.10	76.20	89.50	22.01	3.47	25.49
76.20	76.20	89.50	21.78	3.22	25.00
114.30	76.20	89.50	23.20	1.30	24.50
148.59	76.20	89.50	24.75	2.98	27.73
38.10	38.10	89.50	22.07	3.35	25.42
76.20	38.10	89.50	24.83	1.26	26.09
114.30	38.10	89.50	23.19	3.34	26.53
3.81	3.81	89.50	22.94	1.10	24.05
76.20	3.81	89.50	25.09	0.40	25.49
148.59	3.81	89.50	23.06	1.87	24.93
3.81	148.59	71.84	28.00	0.06	28.06
76.20	148.59	71.84	25.71	0.04	25.76
148.59	148.59	71.84	28.16	0.05	28.21
38.10	114.30	71.84	26.24	0.08	26.33
76.20	114.30	71.84	25.55	0.05	25.59
114.30	114.30	71.84	25.25	0.05	25.29
3.81	76.20	71.84	26.27	0.16	26.43
38.10	76.20	71.84	25.14	0.05	25.19
76.20	76.20	71.84	24.91	0.29	25.21
114.30	76.20	71.84	26.99	0.06	27.04
148.59	76.20	71.84	26.12	0.05	26.17
38.10	38.10	71.84	25.97	0.04	26.01
76.20	38.10	71.84	25.37	0.06	25.43
114.30	38.10	71.84	26.23	0.06	26.29
3.81	3.81	71.84	26.38	0.05	26.43
76.20	3.81	71.84	25.88	0.05	25.94
148.59	3.81	71.84	26.16	0.03	26.19
3.81	148.59	54.19	23.50	0.04	23.53
76.20	148.59	54.19	23.88	0.04	23.92
148.59	148.59	54.19	24.22	0.04	24.26
38.10	114.30	54.19	24.53	0.03	24.56
76.20	114.30	54.19	26.17	0.09	26.25
114.30	114.30	54.19	25.47	0.04	25.51
3.81	76.20	54.19	24.97	0.09	25.05
38.10	76.20	54.19	23.70	0.14	23.84
76.20	76.20	54.19	25.18	0.02	25.20
114.30	76.20	54.19	23.82	0.08	23.90
148.59	76.20	54.19	25.47	0.00	25.47
38.10	38.10	54.19	24.83	0.04	24.87
76.20	38.10	54.19	25.84	0.03	25.87

114.30	38.10	54.19	27.77	0.05	27.82
3.81	3.81	54.19	26.47	0.02	26.48
76.20	3.81	54.19	26.36	0.04	26.41
148.59	3.81	54.19	26.76	0.07	26.82

APPENDIX C: Water and LNAPL Contents for Setup 4

X	Y	Z	Gravimetric Water Content	Gravimetric Biodiesel Content	Total Fluid Content
(cm)	(cm)	(cm)	(%)	(%)	(%)
3.81	148.59	122.00	1.34	2.30	3.64
76.20	148.59	122.00	3.39	3.40	6.79
148.59	148.59	122.00	1.34	2.38	3.72
38.10	114.30	122.00	3.48	4.00	7.48
76.20	114.30	122.00	2.52	3.31	5.83
114.30	114.30	122.00	1.89	3.11	5.00
3.81	76.20	122.00	1.86	3.30	5.16
38.10	76.20	122.00	1.85	3.20	5.05
76.20	76.20	122.00	4.06	6.65	10.71
114.30	76.20	122.00	3.67	3.09	6.75
148.59	76.20	122.00	1.37	2.74	4.11
38.10	38.10	122.00	1.81	3.74	5.55
76.20	38.10	122.00	2.30	3.23	5.52
114.30	38.10	122.00	1.42	2.82	4.23
3.81	3.81	122.00	1.19	2.76	3.94
76.20	3.81	122.00	1.87	3.27	5.14
148.59	3.81	122.00	1.08	2.64	3.72
3.81	148.59	106.76	22.76	6.17	28.93
76.20	148.59	106.76	15.88	7.84	23.71
148.59	148.59	106.76	14.10	7.28	21.38
38.10	114.30	106.76	23.11	2.81	25.92
76.20	114.30	106.76	22.95	2.82	25.78
114.30	114.30	106.76	23.40	2.30	25.70
3.81	76.20	106.76	20.78	3.25	24.03
38.10	76.20	106.76	21.56	5.95	27.52
76.20	76.20	106.76	16.90	8.62	25.52
114.30	76.20	106.76	25.35	0.16	25.51
148.59	76.20	106.76	20.77	3.81	24.58
38.10	38.10	106.76	19.58	5.83	25.41
76.20	38.10	106.76	21.57	2.22	23.78
114.30	38.10	106.76	20.94	1.35	22.30
3.81	3.81	106.76	14.21	7.22	21.43
76.20	3.81	106.76	23.04	1.01	24.05
148.59	3.81	106.76	21.09	2.31	23.39
3.81	148.59	96.60	26.13	0.09	26.23
76.20	148.59	96.60	27.37	0.12	27.49
148.59	148.59	96.60	23.67	0.06	23.73

38.10	114.30	96.60	24.98	0.06	25.03
76.20	114.30	96.60	22.72	0.05	22.77
114.30	114.30	96.60	24.26	0.06	24.32
3.81	76.20	96.60	24.64	0.05	24.69
38.10	76.20	96.60	22.95	0.04	22.99
76.20	76.20	96.60	22.73	0.05	22.78
114.30	76.20	96.60	24.15	0.05	24.20
148.59	76.20	96.60	24.15	0.05	24.20
38.10	38.10	96.60	24.14	0.05	24.18
76.20	38.10	96.60	23.46	0.02	23.49
114.30	38.10	96.60	22.72	0.02	22.73
3.81	3.81	96.60	24.32	0.04	24.37
76.20	3.81	96.60	24.47	0.04	24.51
148.59	3.81	96.60	23.64	0.04	23.68
3.81	148.59	88.98	30.35	0.06	30.42
76.20	148.59	88.98	23.05	0.04	23.09
148.59	148.59	88.98	25.66	0.04	25.70
38.10	114.30	88.98	26.12	0.03	26.15
76.20	114.30	88.98	22.98	0.03	23.01
114.30	114.30	88.98	24.47	0.03	24.51
3.81	76.20	88.98	31.66	0.03	31.68
38.10	76.20	88.98	24.42	0.03	24.44
76.20	76.20	88.98	23.52	0.03	23.55
114.30	76.20	88.98	24.28	0.02	24.30
148.59	76.20	88.98	24.24	0.04	24.28
38.10	38.10	88.98	22.25	0.04	22.28
76.20	38.10	88.98	21.73	0.05	21.78
114.30	38.10	88.98	23.76	0.03	23.79
3.81	3.81	88.98	25.16	0.04	25.20
76.20	3.81	88.98	24.68	0.05	24.73
148.59	3.81	88.98	25.13	0.05	25.18

APPENDIX D: Cross-sections of Residual LNAPL Distribution for Setup 3

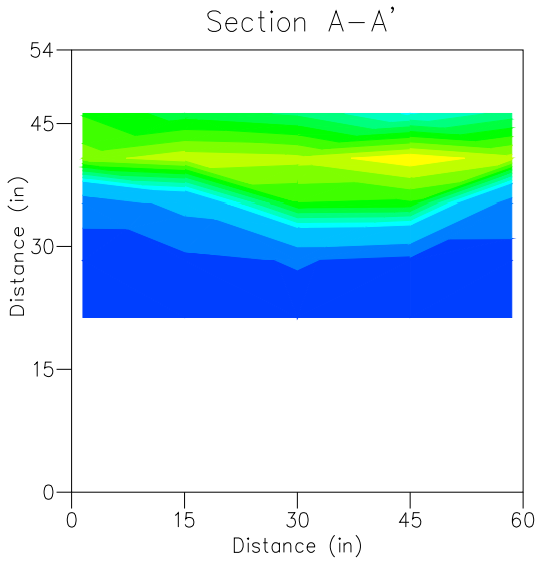

Legend

Color	Range Beg.	Range End	Percent	Area
	0.00	0.25	33.5	475.11
	0.25	1.00	12.0	170.18
	1.00	2.00	8.8	124.52
	2.00	2.25	2.1	30.06
	2.25	2.50	2.9	40.74
	2.50	2.75	3.9	55.47
	2.75	3.00	5.2	73.79
	3.00	3.25	7.1	101.42
	3.25	3.50	9.1	129.85
	3.50	3.75	9.0	127.39
	3.75	4.00	5.7	80.55
	4.00	4.25	0.8	10.78
	4.25	4.50	0.0	0.00
	4.50	4.75	0.0	0.00
	4.75	5.00	0.0	0.00
	5.00	5.25	0.0	0.00

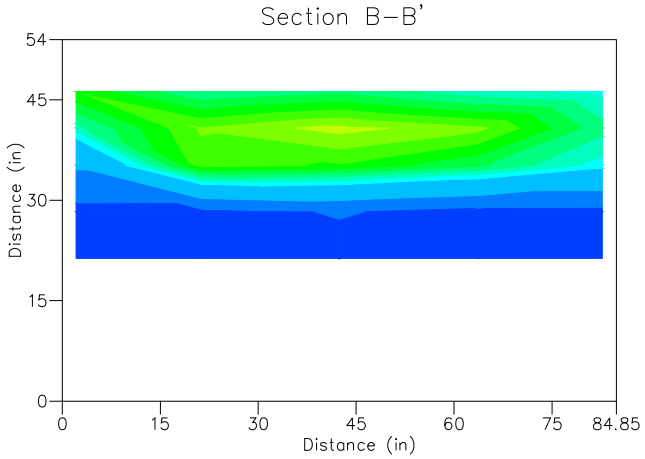

Legend

Color	Range Beg.	Range End	Percent	Area
	0.00	0.25	30.0	601.35
	0.25	1.00	9.0	180.76
	1.00	2.00	9.9	199.61
	2.00	2.25	2.7	54.27
	2.25	2.50	4.8	95.40
	2.50	2.75	7.7	154.89
	2.75	3.00	8.8	176.13
	3.00	3.25	9.6	192.71
	3.25	3.50	11.6	232.65
	3.50	3.75	5.5	110.77
	3.75	4.00	0.5	9.20
	4.00	4.25	0.0	0.00
	4.25	4.50	0.0	0.00
	4.50	4.75	0.0	0.00
	4.75	5.00	0.0	0.00
	5.00	5.25	0.0	0.00

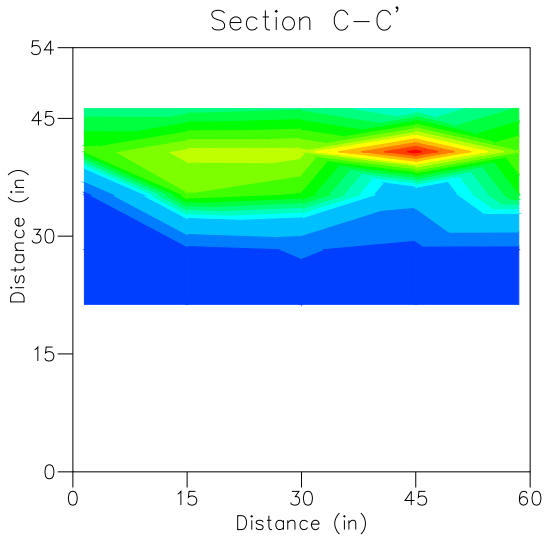

Legend

Color	Range Beg.	Range End	Percent	Area
	0.00	0.25	32.5	461.12
	0.25	1.00	9.0	127.22
	1.00	2.00	10.3	146.95
	2.00	2.25	2.6	37.24
	2.25	2.50	3.2	46.08
	2.50	2.75	5.7	80.56
	2.75	3.00	7.6	107.51
	3.00	3.25	6.8	97.23
	3.25	3.50	7.6	108.55
	3.50	3.75	8.2	116.58
	3.75	4.00	3.5	49.15
	4.00	4.25	1.2	16.87
	4.25	4.50	0.9	12.52
	4.50	4.75	0.6	8.16
	4.75	5.00	0.3	3.81
	5.00	5.25	0.0	0.31

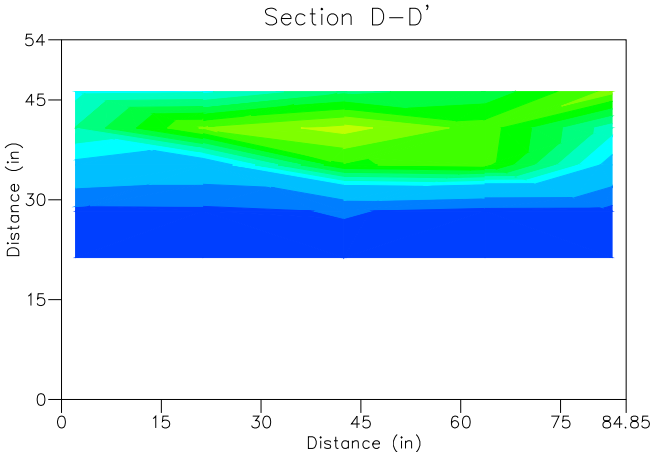

Legend

Color	Range Beg.	Range End	Percent	Area
	0.00	0.25	29.3	588.38
	0.25	1.00	9.7	194.67
	1.00	2.00	12.4	248.01
	2.00	2.25	4.0	80.83
	2.25	2.50	5.4	108.50
	2.50	2.75	6.0	121.23
	2.75	3.00	8.1	162.36
	3.00	3.25	8.5	170.60
	3.25	3.50	11.8	237.70
	3.50	3.75	4.4	88.68
	3.75	4.00	0.4	7.05
	4.00	4.25	0.0	0.00
	4.25	4.50	0.0	0.00
	4.50	4.75	0.0	0.00
	4.75	5.00	0.0	0.00
	5.00	5.25	0.0	0.00

APPENDIX E: Cross-sections of Residual LNAPL Distribution for Setup 4

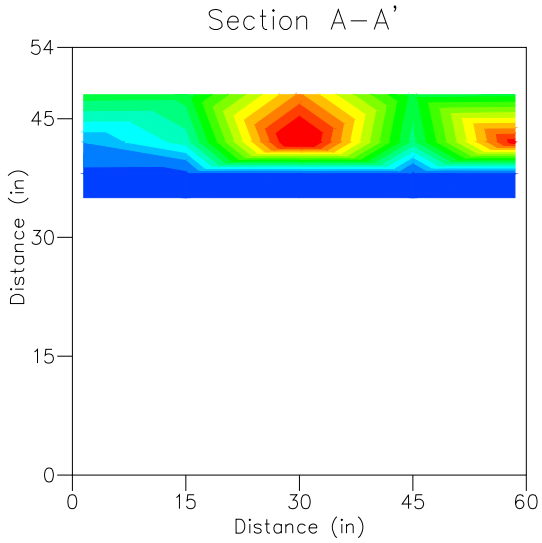

Legend

Color	Range Beg.	Range End	Percent	Area
	0.00	0.25	25.2	186.49
	0.25	1.00	6.2	45.79
	1.00	1.50	4.0	29.36
	1.50	2.00	5.0	37.29
	2.00	2.50	5.9	43.77
	2.50	3.00	6.0	44.38
	3.00	3.50	6.4	47.26
	3.50	4.00	6.2	45.62
	4.00	4.50	5.8	43.27
	4.50	5.00	5.5	40.93
	5.00	5.50	5.2	38.59
	5.50	6.00	4.9	36.24
	6.00	6.50	4.6	33.90
	6.50	7.00	4.0	29.86
	7.00	7.50	2.8	21.05
	7.50	8.75	2.3	17.22

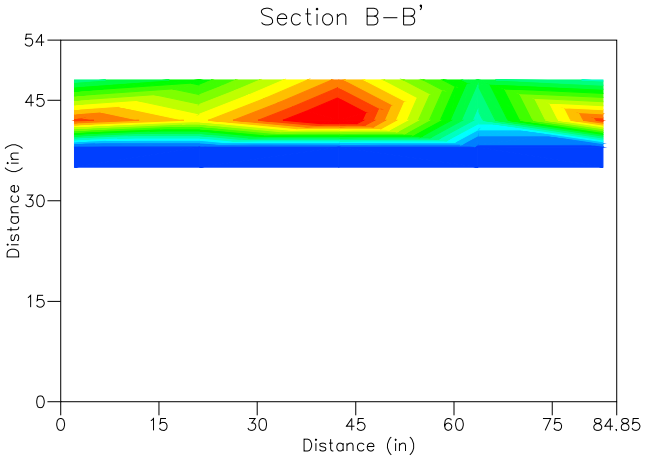

Legend

Color	Range Beg.	Range End	Percent	Area
	0.00	0.25	24.3	254.83
	0.25	1.00	4.5	47.31
	1.00	1.50	2.8	29.32
	1.50	2.00	2.6	27.54
	2.00	2.50	2.6	27.13
	2.50	3.00	4.1	43.31
	3.00	3.50	5.9	61.89
	3.50	4.00	6.3	65.84
	4.00	4.50	6.7	69.96
	4.50	5.00	7.1	74.19
	5.00	5.50	7.5	78.42
	5.50	6.00	7.8	81.53
	6.00	6.50	6.8	71.23
	6.50	7.00	5.2	54.48
	7.00	7.50	3.1	32.48
	7.50	8.75	2.7	28.48

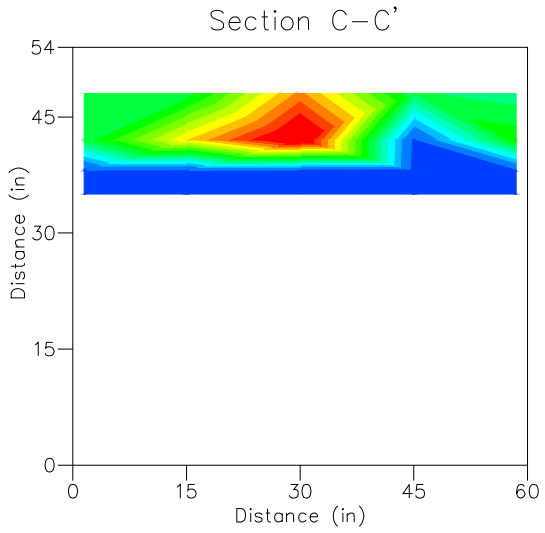

Legend

Color	Range Beg.	Range End	Percent	Area
	0.00	0.25	27.8	205.86
	0.25	1.00	4.9	35.98
	1.00	1.50	3.5	26.27
	1.50	2.00	3.8	28.10
	2.00	2.50	4.0	29.93
	2.50	3.00	5.3	39.17
	3.00	3.50	14.4	106.72
	3.50	4.00	5.6	41.58
	4.00	4.50	4.6	33.89
	4.50	5.00	4.5	32.99
	5.00	5.50	4.3	32.10
	5.50	6.00	4.2	31.20
	6.00	6.50	4.1	30.26
	6.50	7.00	3.7	27.67
	7.00	7.50	2.8	20.48
	7.50	8.75	2.5	18.79

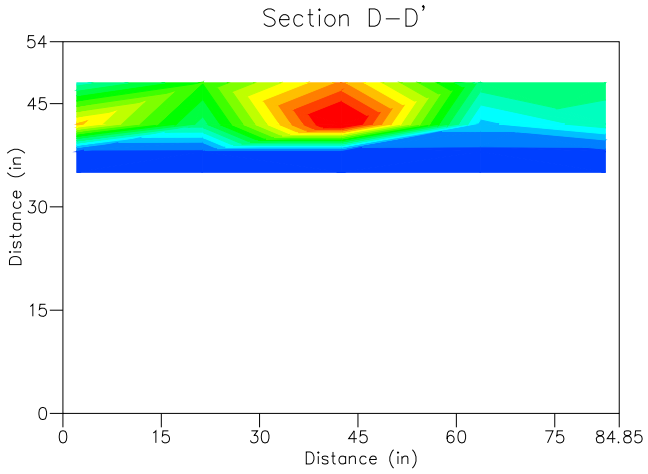

Legend

Color	Range Beg.	Range End	Percent	Area
	0.00	0.25	26.1	273.72
	0.25	1.00	8.8	91.97
	1.00	1.50	4.1	43.16
	1.50	2.00	4.7	49.39
	2.00	2.50	6.9	72.09
	2.50	3.00	8.0	84.16
	3.00	3.50	4.3	44.75
	3.50	4.00	5.7	59.45
	4.00	4.50	6.0	63.36
	4.50	5.00	5.4	56.14
	5.00	5.50	4.7	48.91
	5.50	6.00	4.0	41.69
	6.00	6.50	3.5	36.25
	6.50	7.00	3.3	34.21
	7.00	7.50	2.4	25.39
	7.50	8.75	2.2	23.29

APPENDIX F: Residual LNAPL Volume Calculations

The following are calculations performed to determine the volume of LNAPL biodiesel retained as residual in the sand after testing was completed for setups 3 and 4. The biodiesel contents were determined gravimetrically, and the sampling and distributions were previously presented. The areas within the different biodiesel content ranges were obtained from the analysis presented in the laboratory experimentation chapter of this work. LNAPL volumes were determined using the End Area method. These calculations were made using MathCAD v13 by Mathsoft. Units were input as measured during testing and the results are displayed in English and Metric units.

1. Input biodiesel content ranges to be used in conjunction with areas determined from sampling layout plans. Two arrays are used to input the beginning and end of the ranges:

Setup 3

$$Range3_{beg} := \begin{pmatrix} 0\% \\ 0.25\% \\ 1\% \\ 2\% \\ 2.25\% \\ 2.5\% \\ 2.75\% \\ 3\% \\ 3.25\% \\ 3.5\% \\ 3.75\% \\ 4\% \\ 4.25\% \\ 4.5\% \\ 4.75\% \\ 5\% \end{pmatrix} \quad Range3_{end} := \begin{pmatrix} 0.25\% \\ 1\% \\ 2\% \\ 2.25\% \\ 2.5\% \\ 2.75\% \\ 3\% \\ 3.25\% \\ 3.5\% \\ 3.75\% \\ 4\% \\ 4.25\% \\ 4.5\% \\ 4.75\% \\ 5\% \\ 5.25\% \end{pmatrix}$$

Setup 4

$$Range4_{beg} := \begin{pmatrix} 0\% \\ 0.25\% \\ 1\% \\ 1.5\% \\ 2\% \\ 2.5\% \\ 3\% \\ 3.5\% \\ 4\% \\ 4.5\% \\ 5\% \\ 5.5\% \\ 6\% \\ 6.5\% \\ 7\% \\ 7.5\% \end{pmatrix} \quad Range4_{end} := \begin{pmatrix} 0.25\% \\ 1\% \\ 1.5\% \\ 2\% \\ 2.5\% \\ 3\% \\ 3.5\% \\ 4\% \\ 4.5\% \\ 5\% \\ 5.5\% \\ 6\% \\ 6.5\% \\ 7\% \\ 7.5\% \\ 8.75\% \end{pmatrix}$$

2. Using the defined ranges, the average biodiesel content is determined within each range:

Setup 3

$$BdContent3_{ave} := \frac{Range3_{beg} + Range3_{end}}{2}$$

$BdContent3_{ave} =$

	1
1	0.125
2	0.625
3	1.5
4	2.125
5	2.375
6	2.625
7	2.875
8	3.125
9	3.375
10	3.625
11	3.875
12	4.125
13	4.375
14	4.625
15	4.875
16	5.125

%

Setup 4

$$BdContent4_{ave} := \frac{Range4_{beg} + Range4_{end}}{2}$$

$BdContent4_{ave} =$

	1
1	0.125
2	0.625
3	1.25
4	1.75
5	2.25
6	2.75
7	3.25
8	3.75
9	4.25
10	4.75
11	5.25
12	5.75
13	6.25
14	6.75
15	7.25
16	8.125

%

3. With a void ratio and porosity as shown the biodiesel content as a *percent of the pore volume* is determined:

$$e := 0.71 \qquad n := \frac{e}{1+e} \qquad n = 0.415$$

Setup 3

$$\frac{BdContent3_{ave}}{n} =$$

	1
1	0.301
2	1.505
3	3.613
4	5.118
5	5.72
6	6.322
7	6.924
8	7.526
9	8.129
10	8.731
11	9.333
12	9.935
13	10.537
14	11.139
15	11.741
16	12.343

%

Setup 4

$$\frac{BdContent4_{ave}}{n} =$$

	1
1	0.301
2	1.505
3	3.011
4	4.215
5	5.419
6	6.623
7	7.827
8	9.032
9	10.236
10	11.44
11	12.644
12	13.849
13	15.053
14	16.257
15	17.461
16	19.569

%

4. The area within each biodiesel content range is input for each lift, and units are assigned to the areas:

Setup 3

$$L1_3 := \begin{pmatrix} 0 \\ 0 \\ 0 \\ 170.1 \\ 1156.26 \\ 908.64 \\ 539.28 \\ 360.42 \\ 107.58 \\ 6.72 \\ 0 \\ 0 \\ 0 \\ 0 \\ 0 \\ 0 \end{pmatrix} \quad L2_3 := \begin{pmatrix} 0 \\ 0 \\ 0 \\ 0 \\ 8.67 \\ 103.91 \\ 270.72 \\ 442.11 \\ 607.36 \\ 843.15 \\ 681.69 \\ 155.08 \\ 69.06 \\ 44.91 \\ 20.77 \\ 1.56 \end{pmatrix} \quad L3_3 := \begin{pmatrix} 5.85 \\ 245.4 \\ 1092.86 \\ 288.06 \\ 343.12 \\ 401.87 \\ 405.43 \\ 317.97 \\ 148.45 \\ 0 \\ 0 \\ 0 \\ 0 \\ 0 \\ 0 \\ 0 \end{pmatrix} \quad L4_3 := \begin{pmatrix} 3229.96 \\ 19.04 \\ 0 \\ 0 \\ 0 \\ 0 \\ 0 \\ 0 \\ 0 \\ 0 \\ 0 \\ 0 \\ 0 \\ 0 \\ 0 \\ 0 \end{pmatrix} \quad L5_3 := \begin{pmatrix} 3249 \\ 0 \\ 0 \\ 0 \\ 0 \\ 0 \\ 0 \\ 0 \\ 0 \\ 0 \\ 0 \\ 0 \\ 0 \\ 0 \\ 0 \\ 0 \end{pmatrix}$$

$$L1_3 := L1_3 \cdot in^2 \quad L2_3 := L2_3 \cdot in^2 \quad L3_3 := L3_3 \cdot in^2 \quad L4_3 := L4_3 \cdot in^2 \quad L5_3 := L5_3 \cdot in^2$$

4. (continued):

Setup 4

$$L1_4 := \begin{pmatrix} 0 \\ 0 \\ 0 \\ 0 \\ 23.69 \\ 943.57 \\ 1350.53 \\ 510.76 \\ 143.95 \\ 113.88 \\ 83.83 \\ 53.79 \\ 23.74 \\ 1.26 \\ 0 \\ 0 \end{pmatrix} \qquad L2_4 := \begin{pmatrix} 0.77 \\ 66 \\ 249.39 \\ 275.96 \\ 192.05 \\ 214.87 \\ 300.52 \\ 289.51 \\ 282.35 \\ 279.61 \\ 276.87 \\ 271.63 \\ 227.6 \\ 164.09 \\ 102 \\ 55.78 \end{pmatrix} \qquad L3_4 := \begin{pmatrix} 3249 \\ 0 \\ 0 \\ 0 \\ 0 \\ 0 \\ 0 \\ 0 \\ 0 \\ 0 \\ 0 \\ 0 \\ 0 \\ 0 \\ 0 \\ 0 \end{pmatrix}$$

$$L1_4 := L1_4 \cdot in^2 \qquad L2_4 := L2_4 \cdot in^2 \qquad L3_4 := L3_4 \cdot in^2$$

5. The incremental lift thicknesses are input as (dN_n), where n denotes the Setup and N denotes the lift (lifts were consistently 6 inches in Setup 3):

Setup 3

$$d_3 := 6in$$

Setup 4

$$d1_4 := 6in$$

$$d2_4 := 4in$$

$$d3_4 := 3in$$

6. The specific gravity of the biodiesel, the approximate unit weight of the sand, and the unit weight of water is input for volume calculations:

$$SG_{bd} := 0.885 \qquad \gamma_s := 96.9 \frac{lbf}{ft^3} \qquad \gamma_w := 9.807 \frac{kN}{m^3}$$

7. The volume of sand, which is used to determine the volume of biodiesel, is determined within each range increment using the End Area Method:

Setup 4

$$V_{s3} := d_3 \cdot \frac{L1_3 + 2L2_3 + 2L3_3 + 2L4_3 + L5_3}{2}$$

	1
1	29161.86
2	1586.64
3	6557.16
4	2238.66
5	5579.52
6	5760.6
7	5674.74
8	5641.74
9	4857.6
10	5079.06
11	4090.14
12	930.48
13	414.36
14	269.46
15	124.62
16	9.36

$V_{s3} = \quad in^3$

Setup 4

$$V_{s4} := \frac{L1_4 + L2_4}{2} \cdot d1_4 + \frac{L2_4 + L3_4}{2} \cdot d2_4$$

	1
1	6501.85
2	330
3	1246.95
4	1379.8
5	1031.32
6	3905.06
7	5554.19
8	2979.83
9	1843.6
10	1739.69
11	1635.84
12	1519.52
13	1209.22
14	824.23
15	510
16	278.9

$V_{s4} = \quad in^3$

8. The weight of biodiesel is determined as follows:

Setup 3

$$W_{bd3} := V_{s3} \cdot \gamma_s \cdot BdContent3_{ave}$$

$$W_{bd3} = 78.37\ lbf$$

Setup 4

$$W_{bd4} := V_{s4} \cdot \gamma_s \cdot BdContent4_{ave}$$

$$W_{bd4} = 55.956\ lbf$$

9. The volume of residual biodiesel retained in the sand is determined as follows:

Setup 3

$$V_{residual3} := \frac{W_{bd3}}{SG_{bd} \cdot \gamma_w}$$

$V_{residual3} = 10.611\ gal$

$V_{residual3} = 40.166\ L$

Setup 4

$$V_{residual4} := \frac{W_{bd4}}{SG_{bd} \cdot \gamma_w}$$

$V_{residual4} = 7.576\ gal$

$V_{residual4} = 28.679\ L$

10. Based on the total volume of residual biodiesel, the residual biodiesel as a percent of the total pore volume of the affected zone is determined:

Area of Box: $Area := 5\ ft \cdot 5\ ft$

Setup 3

$depth3 := 24\ in$ $\quad V3_t := Area \cdot depth3$

$PV3 := n \cdot V3_t$ $\quad PV3 = 20.76\ ft^3$

$\frac{V_{residual3}}{PV3} = 6.833\ \%$

Setup 4

$depth4 := 13\ in$ $\quad V4_t := Area \cdot depth4$

$PV4 := n \cdot V4_t$ $\quad PV4 = 11.245\ ft^3$

$\frac{V_{residual4}}{PV4} = 9.006\ \%$